Synthetic Applications of Polar Transition Metal Metallocenes

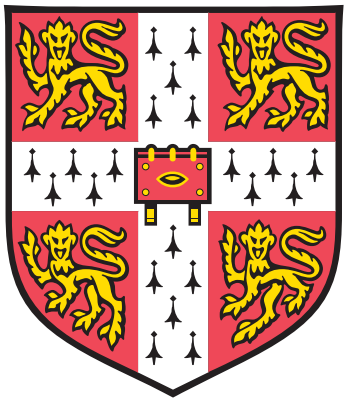

Francesca A. Stokes

Jesus College

University of Cambridge

This dissertation is submitted for the degree of *Doctor of Philosophy*

September 2013

EPSRC

Engineering and Physical Sciences
Research Council

"*Pour yourself a drink, put on some lipstick, and pull yourself together.*"

- Elizabeth Taylor

Declaration

This Dissertation is submitted to the Academic Division Student Registry in partial fulfilment of the requirements for the qualification of Doctor of Philosophy at the University of Cambridge. Research presented herein was carried out by the author at the University Chemical Laboratories between October 2009 and March 3013. Except where specific reference is made to the contrary, it is original work and contains nothing that is the outcome of collaboration. Neither the whole, nor any part of this work has been submitted before for a degree in any other institution. This thesis does not exceed 60,000 words.

Acknowledgements

I wish to thank those
Who made this work possible
In haiku format.

My supervisors
Dom Wright and Andy Wheatley
For time and guidance

Also to Rob Less
For all his help and advice
Friendship is magic!

I am grateful to
All technical services -
For their expertise.

Thanks to the teams at
NMR spectroscopy
And elemental.

For assistance with
X-ray crystallography
Doctors John Davies

And Aggi Steiner.
DFT calculations
Were performed by both

Professor Kloo and
Dr Vincent. Thanks to both.
SQUID measurements were

Undertaken by
Dr Eichhöfer. I am
Extremely grateful.

Thanks are due to the
EPSRC as they
funded my research.

To everyone in
Lab 301for making
My time here so fun

In particular
Hayley, Phil and Spud, for cake,
Shuffling and Guess Who?

To all my great friends
Above all Dave, HJ and
JessthebestBerry

My BFF Rose
For always making me laugh
Your face is so great

Thanks to my parents
And my sister Erica
Always there for me

Christopher Elsmore
For patience, support and love
Thank you most of all.

Abstract

Since the sandwich structure of ferrocene was elucidated in 1952, metallocenes have generated a vast amount of interest. Transition metal metallocenes have previously been shown to be suitable precursors in the syntheses of novel organometallic and metallo-organic complexes, although the use of metal halide starting materials for organometallic synthesis is much more common due to their being readily commercially available and generally easier to handle than the extremely air- and moisture-sensitive metallocene alternatives.

In this project, the polar transition metal metallocenes Cp_2V, Cp_2Cr, Cp_2Mn and Cp_2Ni were employed as precursors in the synthesis of fourteen novel metal-containing complexes, in several cases generating products which could not have been obtained using metal halide starting materials.

Chapter 1 presents an overview of previous work in the area of inorganic synthesis utilising transition metal metallocene precursors. The history of the metallocenes is discussed, along with the developments within areas relevant to this project. Chapter 2 outlines the techniques utilised during this investigation, including NMR spectroscopy, single crystal X-ray diffraction and SQUID magnetometry, whilst Chapter 3 presents the preparative procedures used and the characterisation of the subsequent products.

In Chapter 4, the reactions of manganocene with some simple amido and phosphido ligands containing one or more acidic protons are discussed. Three novel manganese dimers are presented, including a highly unusual phosphine/phosphide complex. Chapter 5 focuses on the reactions of the metallocene precursors with a range of amidinate and guanidinate ligands, to give six novel metal-containing complexes. The research presented in this chapter is also concerned with establishing the degree of inter-metal bonding, if any, present within the complexes synthesised. Chapter 6 features five novel complexes obtained following the reactions of metallocenes with redox-active ligands, an area which has not been widely explored previously.

The implications of the work presented within this project and the potential applications of the complexes obtained are discussed in Chapter 7, with general conclusions as to the value of this research presented. Chapter 8 focuses on ideas for future work, and the rationale behind them.

Abbreviations

COSHH - Control of Substances Hazardous to Health
PPE - Personal Protective Equipment
M - Molar
mmol - Millimoles
mL - Millilitres
mg - Milligrams
K - Kelvin
° C - Degrees Celsius
Me - Methyl
Et - Ethyl
i-Pr - *iso*-Propyl
Ph - Phenyl
Ar - Aryl
Bn - Benzyl
Ac - Acetyl
Cy - Cyclohexyl
Cp - The cyclopentadienyl anion $C_5H_5^-$
Cp* - The pentamethylcyclopentadienyl anion $C_5Me_5^-$
hppH - 1,3,4,6,7,8-Hexahydro-2*H*-pyrimido[1,2-*a*]pyrimidine
hpp$^-$ - The anion of 1,3,4,6,7,8-hexahydro-2*H*-pyrimido[1,2-*a*]pyrimidine
quin - Quinoline
DPhF - *N,N*′-Diphenylformamidinate
dipp - Diisopropylphenyl
pm - Pyrimidine
saoH_2 - Salicylaldoxime or 2-hydrobenzaldehyde oxime
sao- The doubly deprotonated form of salicylaldoxime or 2-hydrobenzaldehyde oxime
salophen - N,N′-*o*-Phenylene-*bis*(salicylideneiminato) dianion
dan - Diaminonaphthalene
salen - *N,N*′-Ethylenebis(salicylimine)
acac - Acetylacetonate
BTC - 1,3,5-Benzenetricarboxylate
n-Bu - *normal*-Butyl
t-Bu - *tertiary*-Butyl
M - General metal ion
R - General alkyl group
E - General main group element

THF - Tetrahydrofuran
TMEDA - *N,N,N′,N′*-Tetramethylethane-1,2-diamine
PMDETA - *N,N,N′,N′,N″*-Pentamethyldiethylenetriamine
DMF - Dimethylformamide
IR - Infrared
cm^{-1} - Wavenumber
NMR - Nuclear Magnetic Resonance
δ - Chemical shift
ppm - Parts per million
MHz - Megahertz
s - Singlet
d - Doublet
t - Triplet
q - Quartet
m - Multiplet
br -Broad
CSD - Cambridge Structural Database
M - Molecular weight of asymmetric unit
a, b, c - Unit cell dimensions
α, β, γ - Unit cell angles
T - Temperature
λ - Wavelength
V - Unit cell volume
μ - Linear absorption coefficient
Z - Number of formula units per unit cell
ρ_{calcd} - Calculated density
e - Electron
R - R-factor (unweighted)
$\omega R2$ - R-factor (weighted)
S - Goodness of Fit
θ - Angle of data collection
SMM - Single Molecule Magnet
S - Spin
TIP - Temperature Independent Paramagnetism
DFT - Density Functional Theory
MO - Molecular Orbital
AIM - Atoms in Molecules H-F - Hartree-Fock

B3LYP - Becke, 3-parameter, Lee-Yang-Parr hybrid functional
SQUID - Superconducting Quantum Interference Device
μ_B - Bohr magnetons

Contents

List of Tables

List of Figures

List of Schemes

Chapter 1

Introduction

1.1 Historical Background

1.1.1 The Discovery of Ferrocene

The history of dicyclopentadienyl transition metal chemistry began with the discovery of dicyclopentadienyl iron by Kealy and Pauson in 1951.[1] Using $FeCl_3$ and the Grignard reagent CpMgBr they were able to isolate orange crystals, shown by elemental analysis to have the formula $C_{10}H_{10}Fe$, which they assigned the σ-bonded structure **1.1** seen in Figure 1.1.

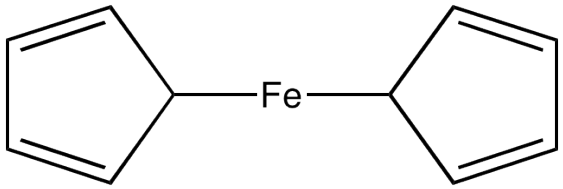

Figure 1.1: The dicyclopentadienyl iron structure postulated by Kealy and Pauson, **1.1**.

They attributed the remarkable stability of this compound to the aromatic nature of the cyclopentadienyl ligand, noting that there would be important contributions from the resonance form seen in Figure 1.2.

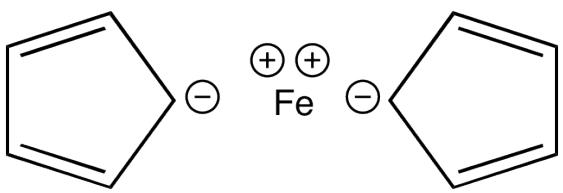

Figure 1.2: The resonance form of dicyclopentadienyl iron, which was argued to be responsible for its unusual stability.

The correct structure of this compound was elucidated soon afterwards in two independent publications; one by Fischer and Pfab,[2] the other by Wilkinson *et al.*,[3] in 1952. Both groups reached the conclusion that the compound adopted a 'Doppelkegel' or 'sandwich' structure, **1.2**, although through different means - Fischer relied on preliminary X-ray data which showed the centrosymmetric arrangement of the molecule, whereas Wilkinson referred to the diamagnetic nature of the compound and the presence of only one C−H stretching frequency in the IR spectrum.

The structure was soon confirmed beyond all doubt by two crystallographic studies.[4;5] The two cyclopentadienyl rings may be orientated in two extremes to give either an eclipsed (D_{5h}) or staggered (D_{5d}) conformation. The energy of rotation is small ($\sim$4 kJ mol^{-1}),[6] so the ground state of ferrocene may show either conformation.

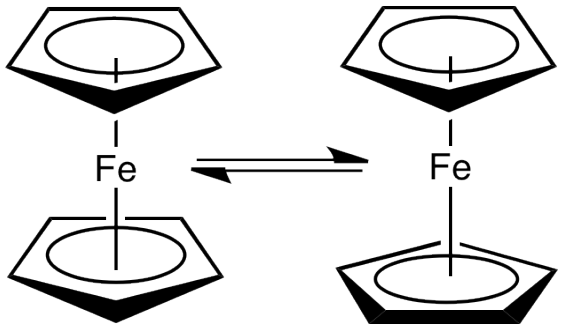

Figure 1.3: The correct structure of dicyclopentadienyl iron, as elucidated in 1952, **1.2** *left*, eclipsed and *right*, staggered.

The bonding pattern within this compound is largely covalent, combining the donation of ligand electron density to the metal with 'back-donation' from the metal to the ligand. The involvement of the metal d orbitals is key, and results in ferrocene and other simple metallocenes conforming to rigid electronic constraints, with their bonding orbitals filled according to the '18-electron rule' which confers the greatest electronic stability to ferrocene with its 18-electron count. The name ferrocene was suggested after it was shown that the compound was aromatic and readily underwent Friedel-Crafts acylation at the cyclopentadienyl rings, as the 'ene' ending implied aromatic character.[7]

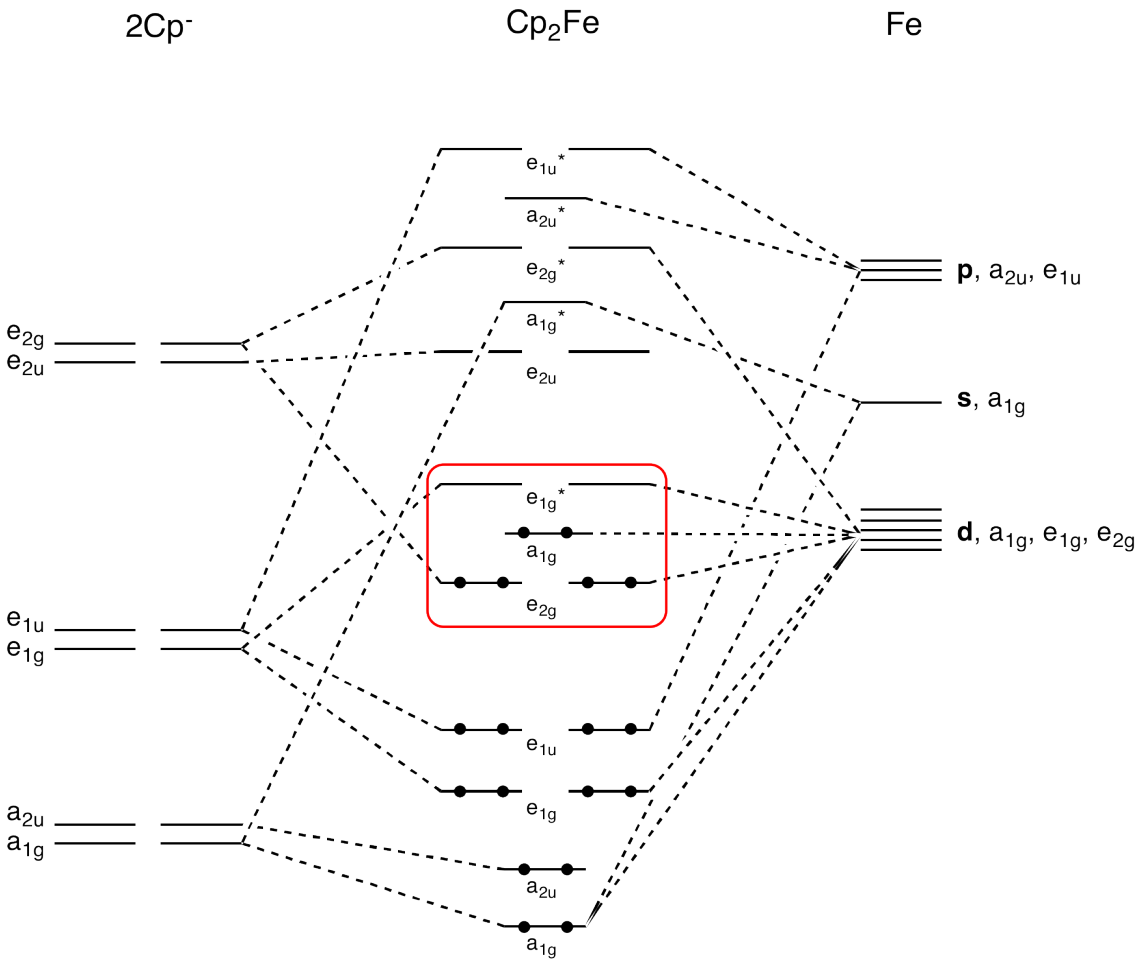

Figure 1.4: MO diagram for ferrocene, assuming D_{5d} symmetry.

The MO energy level diagram shown in Figure 1.4 is relevant to all of the first-row transition metal metallocenes, although the electron configuration shown is that of ferrocene. Within ferrocene all of the bonding orbitals are filled, along with the non-bonding a_{1g} state, with no electrons forced to populate the higher energy anti-bonding orbitals. This is not the case for nickelocene, which has two electrons in the two degenerate e_{1g}* orbitals. Hence, nickelocene is easily oxidised, and many reactions involving nickelocene will involve the loss or modification of a cyclopentadienyl ring ligand in order to conform to the 18-electron rule and give a more stable product. Vanadocene, chromocene and manganocene are all electron-deficient in comparison to ferrocene (see Table 1.1), with the bonding orbitals not entirely filled, making these metallocenes highly reactive and given to bonding with other species in order to reach a stable 18-electron configuration.

Metallocene	Cp_2V	Cp_2Cr	Cp_2Mn	Cp_2Fe	Cp_2Ni
Colour	purple	red	brown	orange	green
Number of d Electrons	15	16	17	18	20
Number of Unpaired Electrons	3	2	5	0	2
Spin-Only Magnetic Moment (μ_B)	3.87	2.83	5.92	0	2.83

Table 1.1: Some key properties of relevant metallocenes.

1.1.2 The Development of Metallocene Chemistry

After ferrocene had been fully characterised, there was a great deal of interest in producing analogues using other transition metals. Between 1952 and 1954 there were reports of bis-cyclopentadienyl compounds for a large number of transition metals from both Fischer and Wilkinson, with the research interests also expanding into cyclopentadienyl complexes of the f- and p-block elements, and of course into probing the chemistry of these new compounds.

The stability of ferrocene was shown to be rather unique amongst the metallocenes, with the newly synthesised analogues proving to be extremely sensitive to both oxygen and water due to their unfavourable electron counts. The metallocenes utilised in this project, namely vanadocene (Cp_2V), nickelocene (Cp_2Ni), manganocene (Cp_2Mn) and chromocene (Cp_2Cr), also differ from ferrocene in terms of their polarity. The bonding between the cyclopentadienyl anion and the metal in ferrocene is considered to be of largely covalent character, which cannot be said of the other first-row transition metal metallocenes. The ionic component of this bonding strongly affects the reactivity patterns of the metallocenes, manganocene in particular,[8] and has previously been exploited in syntheses which use these reagents as precursors to a broad range of organometallic and metallo-organic complexes.

1.2 Reactivity of Transition Metal Metallocenes

There are several advantages to using metallocenes as precursors to more complex metal-containing structures. Chief amongst these are the organically-soluble nature of the metallocenes, and their ability to transfer 2-oxidation state ions intact without oxidation or reduction of the metal centres taking place, which can occur when using transition metal salts as precursors. Research using metallocenes as precursors has revealed certain reactivity pathways and patterns which continue to direct current studies, and which allow for the development of informed synthetic strategies. Several of the more common of these reaction pathways are discussed below.

1.2.1 Nucleophilic Addition at the Metal Centre

Weak nucleophiles can be added to the transition metal centre following the reaction pathway seen in Scheme 1.1, in which the nucleophile (R^-) simply adds onto the metal without ligand displacement.

$$Cp_2M + R^- \longrightarrow Cp_2MR^-$$

Scheme 1.1: Nucleophilic addition at a transition metal centre.

Using $R^- = Cp^-$, this approach has led to the formation of ion-separated and ion-paired complexes containing the $[Cp_3Mn]^-$ ion. For example, Bond *et al.* showed in 2001 that an extended graphite-like lattice is formed with K^+ counterions, consisting of six-membered K_3Mn_3 ring units linked by cyclopentadienyl ligands (Figure 1.5).[9]

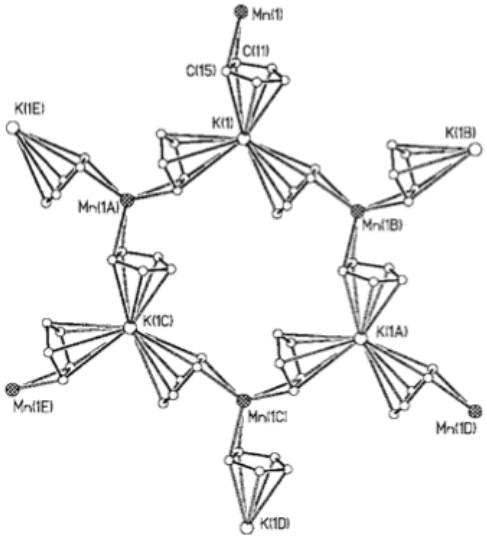

Figure 1.5: The sheet structure of $[(\eta^2{-}Cp)_3MnK \cdot 1.5\,THF]$, **1.3**, viewed along the *c*-axis. Only part of one sheet is shown. H-atoms and THF ligands have been omitted for clarity.[9]

As in graphite, the sheets lay staggered with respect to each other, with the Mn^{II} cations coincident with the centroid of the $[(\eta^2{-}Cp)_3MnK]$ units of the adjacent layers. This structure is similar to that of the Pb^{II} complex $[(Cp)_2(Cp^{THF})PbNa \cdot 0.5THF]$ ($Cp^{THF} = C_5H_4CH_2C_4H_7O$),[10] a p-block metallocene structure which also exists as a graphite-like lattice, although in this case the hexanuclear Pb_3Na_3 rings result from the intramolecular coordination of the Cp-bonded ether functionality to Na^+ cations rather than the η^5-Cp bonding of the

three cyclopentadienyl ligands to the K^+ cations seen in $[(\eta^2{-}Cp)_3MnK \cdot 1.5\,THF]$. The reactivity of the transition metal metallocenes in comparison to that of their p-block counterparts will be discussed further in Section 1.2.4

The structure $[(\eta^2{-}Cp)_3MnK \cdot 1.5\,THF]$ was the first reported example of a transition metal tris-cyclopentadienide anion, and the first to contain a paramagnetic metal, d^5 Mn^{II}. This suggested that this reactivity pattern of nucleophilic addition at the metal centre was an overlooked aspect of transition metal metallocene chemistry, and one which could be investigated and developed during the course of the current research into the potential synthetic applications of these materials.

1.2.2 Nucleophilic Substitution of Cyclopentadienyl

When stronger organic nucleophiles are reacted with metallocenes, the result is often displacement of one or more Cp^- ligands rather than the simple addition of the nucleophile to the metal centre (Scheme 1.2).

$$Cp_2M + R^- \xrightarrow[\text{-}Cp^-]{} RMCp \xrightarrow[\text{-}Cp^-]{R^-} R_2M$$

Scheme 1.2: Nucleophilic substitution of the cyclopentadienyl ligand.

A relevant example of metallocenes undergoing this type of reactivity is seen in the reaction of manganocene with Li(hpp), Scheme 1.3.[11]

$$2\,Cp_2Mn \xrightarrow[\text{-}2CpLi]{2Li(hpp)} [CpMn(hpp)]_2 \xrightarrow[\text{-}2CpLi]{4Li(hpp)} [(hpp)_3MnLi]_2$$

Scheme 1.3: The stepwise nucleophilic substitution reaction of manganocene with Li(hpp).

In the first step of this reaction, Cp_2Mn reacts with one equivalent of Li(hpp) to give the neutral centrosymmetric dimer $[CpMn(hpp)]_2$ (Compound **1.4**) seen in Figure 1.6.

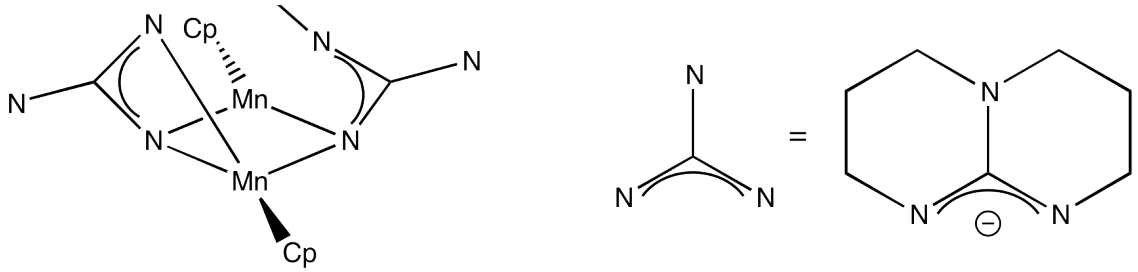

Figure 1.6: The structure of $[CpMn(hpp)_2]$, **1.4**.

In **1.4** the Mn^{II} ions are bridged by one of the N centres of each hpp^- ligand and are terminally coordinated by η^5-Cp ligands. The $[Mn_2N_2]$ diamond core features relatively long Mn−N bonds due to the strain imposed by the chelating ligands, and this, coupled with the fact that the Mn−Cp bond is still highly polar, allows for further reaction of this complex. With the addition of another two equivalents of Li(hpp), the remaining Cp^- is displaced to give a dimeric manganate cage compound, $[LiMn(hpp)_3]_2$ (Compound **1.5**) seen in Figure 1.7.

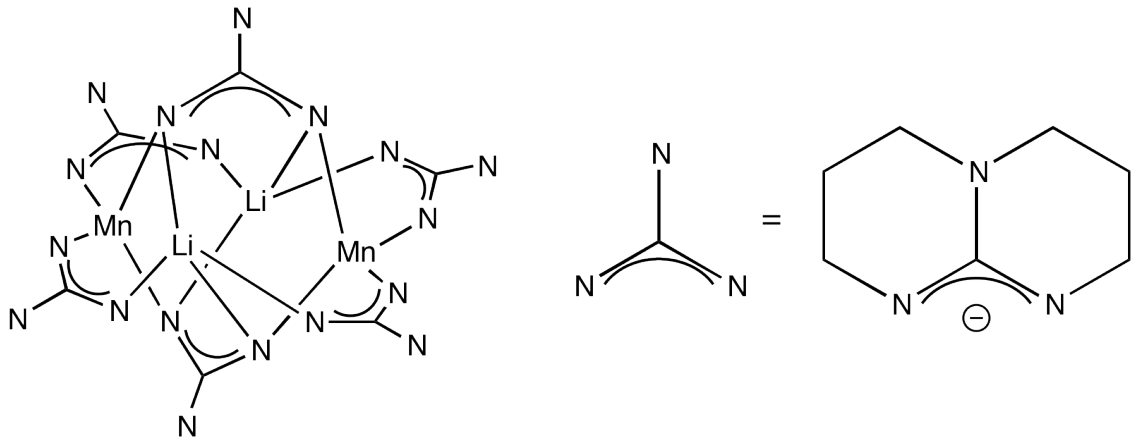

Figure 1.7: The structure of $[LiMn(hpp)_3]_2$, **1.5**.

This compound is of particular interest as the majority of known manganate compounds contain ion-separated manganate ions, such as the complexes $[Li(THF)_4]^+$-$[(CH_2{=}CH{-}CH_2)_3Mn]^-$[12] and $[Mg(THF)_6]^{2+}[(Cp)_{3-x}(CpMe)_xMn]^-$ (where x = 1 or 2; CpMe = C_5H_4Me).[9;13] Of the known ion-paired species, only one other molecular arrangement is known, that of the tris-amido complex $[\{(Me_3Si)_2N\}Mn\{\mu{-}N(SiMe_3)_2\}Li \cdot THF]$.[14] Two-dimensional ion-paired networks also exist, such as the 'graphite-like' $[(\eta^2{-}Cp)_3MnK \cdot 1.5\,THF]$[9] discussed in Section 1.2.1, but these represent a very different type of ion-paired complex in which the manganate anions associate into infinite hexagonal sheets *via* μ-Cp bridges.

The cage dimer of $[LiMn(hpp)_3]_2$ consists of a butterfly-shaped Mn_2Li_2 metal core held together by six bridging hpp^- ligands. There are two observed ligand-metal coordination modes, with four ligands using an η^1:η^1-mode around the equator of the dimer and the two remaining ligands situated above and below the Mn_2Li_2 ring using a μ:μ-bonding mode, so that each metal ion is held in a pseudo-tetrahedral geometry. Preliminary magnetic studies suggest that both $[CpMn(hpp)]_2$ and $[LiMn(hpp)_3]_2$ exhibit temperature-dependant paramagnetism.

This study illustrates several relevant research strands within the area of polar metallocenes, such as the synthesis of polynuclear transition metal complexes, the use of nitrogen donor ligands in reaction with transition metal metallocenes, and the development of potentially interesting magnetic materials. It is also relevant to the current project as it demonstrates that with the use of lithiated ligands with transition metallocenes, CpLi is formed as a side product. This can act as a driving force for the reactions, as CpLi is an ionic polymer with a large enthalpy of formation. This reactivity pattern is exploited extensively throughout this project, with lithiated ligands employed to shift reaction equilibria to the right through the formation of polymeric CpLi.

1.2.3 Reaction with Organic Acids

The reactions of metallocenes with organic acids often proceed according to the pathway seen in Scheme 1.4, if the organic acid RH is sufficiently acidic.

$$Cp_2M + RH \xrightarrow[\text{-CpH}]{} RMCp \xrightarrow[\text{-CpH}]{RH} R_2M$$

Scheme 1.4: Reaction of metallocenes with organic acids.

The reaction of the metallocenes with organic acids stems from the polarity of the Cp−metal bonds, which allows the anionic cyclopentadienyl ligand to behave as a base. Indeed, the reactivity of manganocene, the most polar of these systems, has been compared with that of strong organometallic bases such as the commercially available Bu_2Mg.[15] This type of metallocene behaviour can be observed in the reaction between manganocene and 8-aminoquinoline reported by Alvarez *et al.* in 2001.[16] Here, the manganocene deprotonated the ligand to give a centrosymmetric dimer (Compound **1.6**) in which each Mn centre was bonded to a terminal η^5-Cp ligand [Mn···$Cp_{centroid}$ 2.18 Å] and also to a μ-NH centre, forming a core Mn_2N_2

ring unit which adopted a diamond shape. The manganese centres were further stabilised by the formation of longer bonds to the N centres within the quinoline ligand [Mn(1)−N(1) 2.219(2) Å].

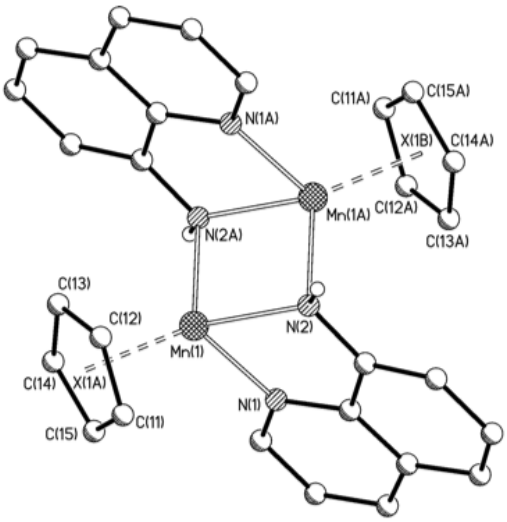

Figure 1.8: The crystal structure of the dimer $[CpMn(\mu-8-HNquin)]_2$, **1.6**. H-atoms, except those attached to N, have been omitted for clarity.[16]

The extent of deprotonation is also largely dependent on the strength of the organic acid. In the example $[CpMn(\mu-8-HNquin)]_2$ manganocene was able to singly-deprotonate the 8-aminoquinoline ligand but not to doubly-deprotonate it, so one cyclopentadienyl unit remained coordinated to each manganese centre. In other reported cases, double deprotonation of amino groups occurs - some relevant examples of this type are discussed in Section 1.3.3. The example of $[CpMn(\mu-8-HNquin)]_2$ is particularly germane as it uses a bicyclic nitrogen-based ligand with structural features in common with many of the ligands employed throughout the current project.

The attempted reaction of manganocene with $(BnNHCH_2)_2$, a weak organic acid, illustrates the limited range of these reactions of organic acids with metallocenes. The result is simple complexation rather than deprotonation to give $[(\eta^1-Cp)(\eta^5-Cp)Mn(BnNHCH_2)_2]$ (Compound **1.7**) seen in Figure 1.9.

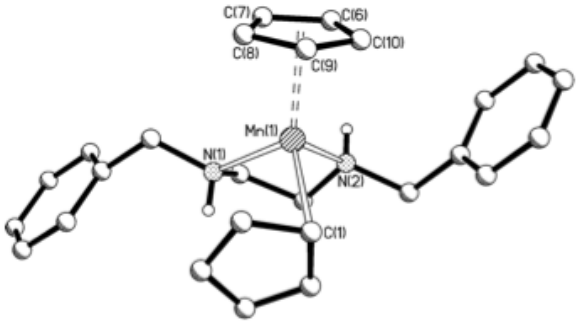

Figure 1.9: Structure of $[(\eta^1{-}\mathrm{Cp})(\eta^5{-}\mathrm{Cp})\mathrm{Mn}(\mathrm{BnNHCH_2})_2]$, **1.7**. H-atoms, except those attached to N, have been omitted for clarity.[16]

The structure of **1.7** is quite strained due to the steric bulk of the ligand employed, which forces the cyclopentadienyl ligands to adopt η^1- and η^5- bonding modes and causes asymmetric coordination of the two N centres, with the Mn−N bond lengths differing by *ca.* 0.35 Å. This type of reaction has the potential to be developed within the scope of the current project, as such strained metal-bonded acids may potentially react further on heating or upon the use of an external base to give polymetallic species.

This ability of the transition metal metallocenes to deprotonate organic acids allows for the design of one-step syntheses of structurally complex molecules and clusters. This chemistry is efficient and potentially high yielding as the simplicity of the reactions limits the number of possible side products formed as a result of the involvement of other reagents.

1.2.4 Comparison with the p-Block Metallocenes

The reactivity of the non-ferrocene transition metal metallocenes is often more directly comparable to their p-block counterparts, as these also tend to be highly polar and capable of undergoing various transformations when reacted with suitable ligands.[17] However, the p-block metallocenes of groups 13 – 15 differ from the transition metal analogues in that there is little involvement of the high energy metal d orbitals in the bonding, which leads to less restricted electronic demands and so to greater structural diversity.[18] Indeed, electron counting in these main group metallocene compounds is often little more than a formality, as the coordination of the π-bonded cyclopentadienyl ligands tends to be weak and electronically variable as different hapticities can be adopted, as shown in Figure 1.10.[17]

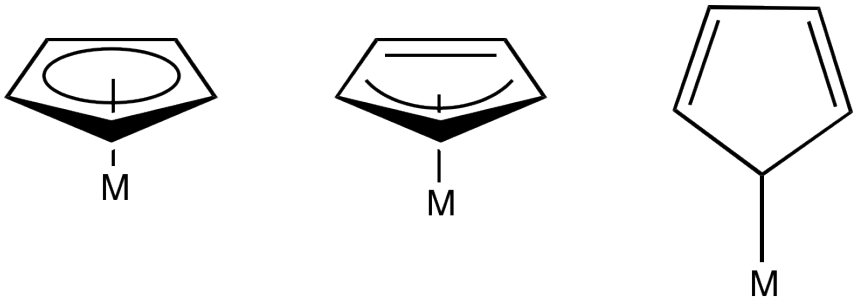

Figure 1.10: The cyclopentadienyl ligand bonding to a metal in η^5-, η^3- and η^1-modes.

The p-block metals are also comparable to the d-block metals in terms of their electronegativities, a consequence of the 'd-block contraction' of atomic radii across the periodic table, leading to a covalent component of their bonding which is not seen in the s-block metallocenes.[19] A review of the p-block metallocenes by Beswick *et al.* draws these comparisons and highlights some of the structures obtained to date with the p-block metallocenes, which are of interest to this project as they share some key characteristics with the transition metal metallocenes being deployed herein as synthetic precursors.[17]

The nucleophilic addition of cyclopentadienyl to the metal centre of stannocene or plumbocene on reaction with CpNa shows a very similar reactivity pattern to manganocene in the example seen in Figure 1.5, with the result in each case being the formation of a $[Cp_3M]^-$ ion. With the Group 14 metals, a 'loose-contact' ion-paired complex is formed with the three cyclopentadienyl ligands coordinating η^5- with a trigonal planar geometry.[20]

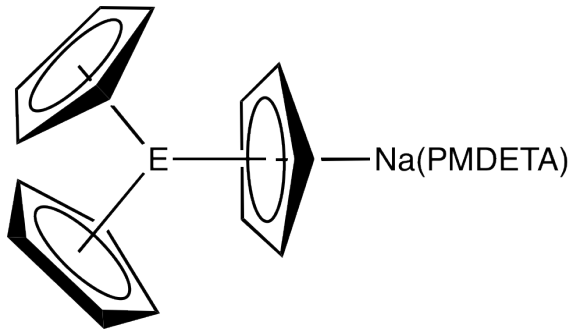

Figure 1.11: The structure of $[Cp_2E(\mu{-}Cp)Na \cdot PMDETA]$, **1.8**, where E = Sn, Pb.

One area in which p-block metallocenes differ from their transition metal counterparts is in the prevalence of oxidative addition reactions. In these, both the oxidation state and the coordination number of the metal are increased. Oxidative addition reactions are common amongst transition metal complexes, particularly within catalytic cycles.[21] However, as previously mentioned, one of the advantages of using transition metal metallocenes as precursors is their ability to transfer ions in their +2 oxidation state intact,[22;23] a fact often taken into account when designing a synthesis involving them. p-Block elements tend to have two available oxidation states, the *n* oxidation state which involves both the s and p valence orbitals, and the *n*-2 oxidation state, which involves only the p electrons, with the s electrons existing as a lone pair (the 'inert pair effect').[24] This latter state tends to predominate at the bottom of the periodic table due to the increasing dominance of relativistic effects on s/p separation. Products that contain transition metal centres may have a wider range of accessible oxidation states due to their d electrons, and it is not always straightforward to predict which states will dominate.

1.3 Metallocenes as Precursors to Complexes with Multiple Metal Centres

1.3.1 Metal-Metal Bonding in the d-Block

Metal-metal bonding is a feature of many organometallic complexes, and is common amongst the low oxidation state metals of the early d-block.[25]

The M−M bonded species may exist as discrete clusters or as extended solid-state compounds, although the presence of bridging ligands can make determination of the character and strength of direct M−M bonds difficult. An example of this difficulty from main group chemistry can be seen in the controversy surrounding Robinson's claim in 1997 to have made the first complex containing a Ga≡Ga triple bond[26] (Compound **1.9**) seen in Figure 1.12, which was widely debated and refuted by some leading figures in the field of inorganic chemistry.

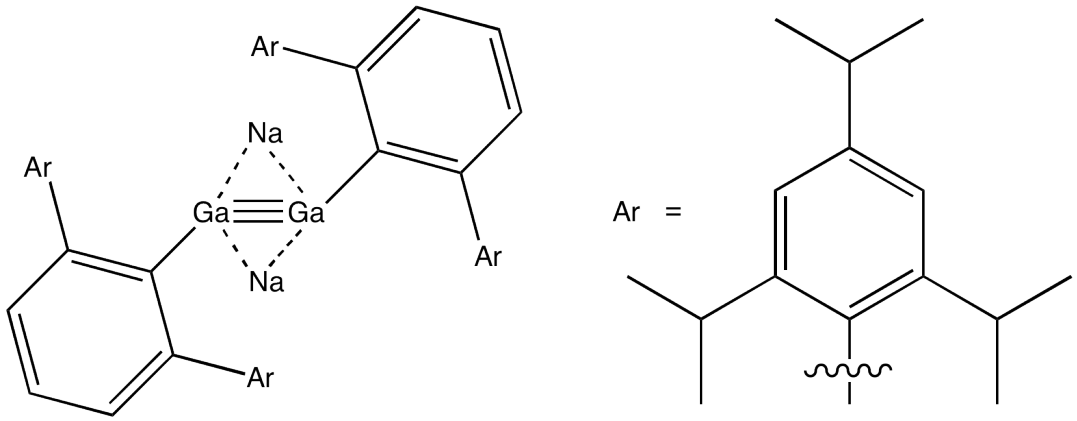

Figure 1.12: The first reported Ga≡Ga triply-bonded compound, $Na_2[\{(i\text{–}Pr_3C_6H_2)_2C_6H_3\}GaGa\{C_6H_3(i\text{–}Pr_3C_6H_2)_2\}]$, **1.9**.

The claim to have synthesised a compound containing a Ga≡Ga triple bond was remarkable considering that no examples of Group 13 triple bonds existed and indeed, no molecule containing a discrete Ga=Ga double bond was known. The 'gallyne' $Na_2[RGaGaR]$ (R = $(i\text{–}Pr_3C_6H_2)_2C_6H_3$) Ga···Ga distance of 2.319 Å was the shortest in the literature. Robinson and his group emphasised that the *trans*-bent orientation of the molecule had been predicted by several theoretical studies to be the favoured configuration for triply-bonded compounds and was therefore a viable model.[27] This was opposed by Power, who asserted that MO theory pointed to a double bond resonance structure, in which a lone pair can reside on either gallium centre.[28] This theory was supported by the synthesis and characterisation of a related tin-based system using the same terphenyl ligand as Robinson's group, which also displayed *trans*-bent geometry and a formal Sn–Sn bond order of 1.5.[28] Cotton used DFT calculations to show that the short Ga···Ga distance could arise from a doubly-bonded structure in which the sodium ions found on either side of the Ga=Ga bond play a part in drawing together the phenyl rings of the terphenyl ligand, leading to an overall shortening of the bond.[29] Robinson dismissed this and produced further data to support his claim,[30] and the discussion devolved into a somewhat less civil discourse.

There is still no definite consensus on the bonding within **1.9**, although current opinion seems to favour the double bond model.[31] The heated debate surrounding this structure did succeed in raising interesting questions as to what exactly constitutes a bond and how they can best be defined and measured, questions which are still relevant today, particularly within organometallic and coordination chemistry.

Measuring the M−M force constants and the stability of d-block metal complexes indicates that M−M bonds become stronger down a group,[32] in contrast to the trend observed within the p-block wherein generally homoatomic bonds become weaker down a group.[25] M−M bonded compounds are much more common amongst the 4d and 5d metals, which have more radially expanded d orbitals available for bonding than their smaller, more contracted 3d counterparts.

Recent research focused on the formation of multiple bonds between 3d transition metals has led to the observation of Cr−Cr quintuply-bonded species.[33] Single, double and triple bonds amongst the transition metals are commonplace,[34] with quadruple bonds more rare but observed particularly for Cr,[35] Mo,[36] W[37] and Re[38] species. There is competition within complexes between metal-ligand bonding and metal-metal bonding, with orbitals involved in the former often unavailable for involvement in the latter. Quintuply-bonded species tend to be of the type ML_2, with ten electrons participating in the bonding between the metal centres in a $\sigma^2\pi^4\delta^4$ configuration (as opposed to $\sigma^2\pi^4\delta^2$ for quadruply-bonded examples). The MO diagrams of both a typical M−M quadruply-bonded ML_4 complex and a quintuply-bonded ML_2 complex can be seen in Figure 1.13.

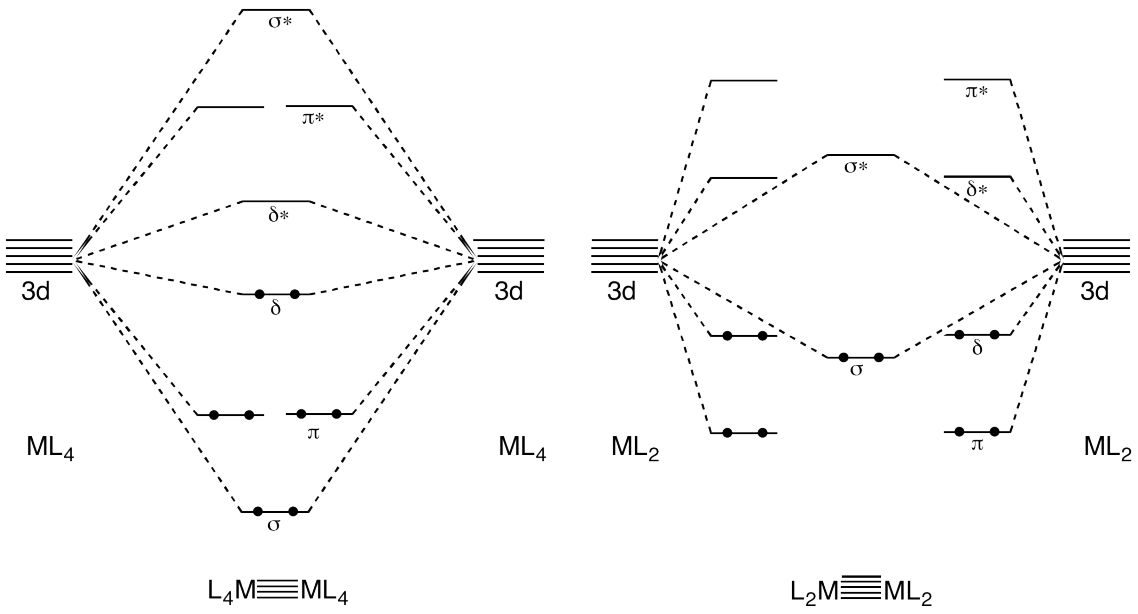

Figure 1.13: *Left*, MO diagram of a typical quadruply-bonded metal complex; *right*, MO diagram of a typical quintuply-bonded transition metal complex.

In the quintuply-bonded species, the σ-bond present is the result of the end-on combination of the two metal $d_z{}^2$ atomic orbitals. The π-bonds are generated by the combination of the two d_{xz} and the two d_{yz} orbitals from each metal, whilst the δ-bonds come from the combination of the two $d_{x^2-y^2}$ and the two d_{xy} orbitals, as shown in Figure 1.14. The quadruply-bonded complex only utilises one δ-bonding orbital as opposed to the two involved in the formation of the quintuple bond, with the ligands involved in the latter enabling the proximity necessary for the overlap of the radially-contracted δ orbitals.

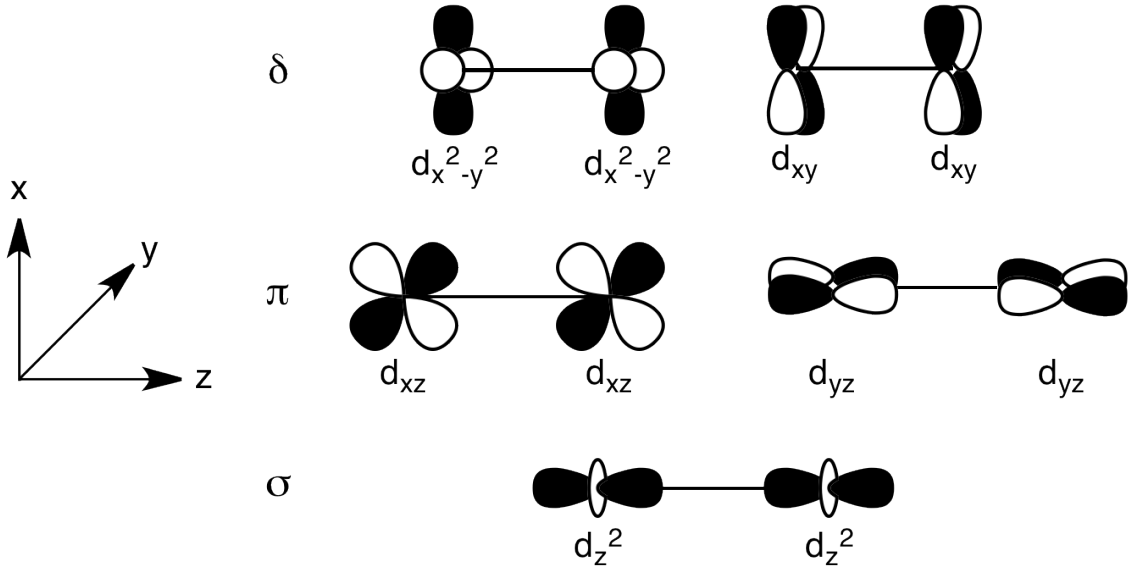

Figure 1.14: The metal orbitals involved in the formation of a quintuple M−M bond.

Calculations have shown that the π-bonding orbitals in the quintuply-bonded species are the lowest in energy, followed by the σ-bonding orbital and the two δ-bonding orbitals, making the LUMO the δ^* orbitals. For Cr(I), the two d^5 metal centres contribute a total of ten electrons to fill all of the bonding orbitals, giving a formal bond order of 5 as can be seen in **1.10** (Figure 1.15).

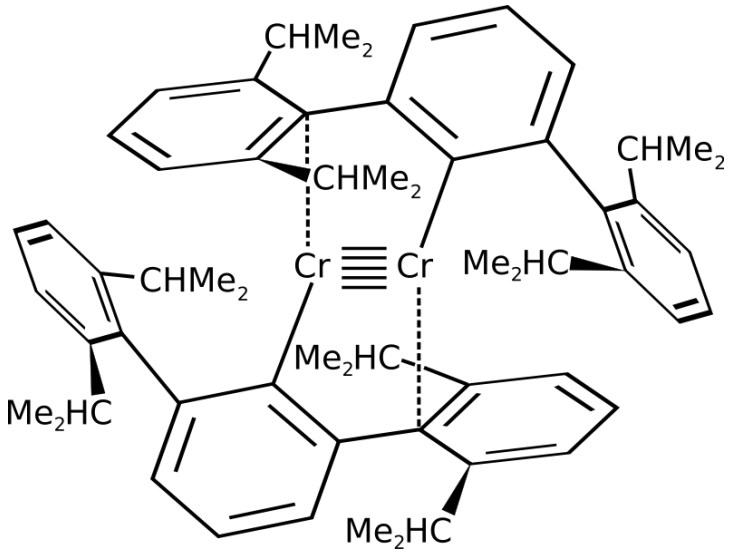

Figure 1.15: The structure of the Cr−Cr quintuply bonded complex $[(CrC_6H_3{-}2,6{-}dipp_2)_2]$, **1.10**.[33]

The $[(CrC_6H_3{-}2,6{-}dipp_2)_2]$ species shown in Figure 1.15 was the first reported compound to feature fivefold bonding.[33] This compound is stabilised by the bulky terphenyl ligands, which weakly interact with the metal centres causing a slight weakening of the quintuple bond. Since this compound was reported, several groups have focused on synthesising materials containing the shortest recorded metal-metal bonds, shaving the record from 1.80 Å in 2007[39] to 1.74 Å in 2008[40] and most recently to 1.73 Å in 2010.[41] All of these species were quintuply-bonded chromium dimers utilising various bulky ligands for stabilisation. In order to obtain these compounds, dimetal species were reduced using potassium graphite (C_8K), adding valence electrons to the metal centres so that they could then participate in this type of bonding. Ligand choice is also extremely important, with the most suitable ligands being those that act to push the metal centres closer together, creating a short inter-metal distance. However, although ligands which facilitate a short inter-metal distance do promote multiple bonding by improving inter-metal orbital overlap, they can also complicate the situation by giving compounds the appearance of multiple bonding, as in the digallium complex **1.9** discussed previously.

The studies of these quintuply-bonded complexes is still very new, with expectations being that these materials will be useful precursors in the search for novel, previously unattainable compounds, in particular compounds which feature unusual magnetic behaviour. One of the aims of this research project was to synthesise materials with multiple bonds between the metal centres using metallocenes as reagents, to show their suitability and versatility within this field.

1.3.2 Paddlewheel Complexes

Paddlewheel or 'Chinese-lantern' complexes are those which contain two metal centres bridged by four ligands. This structural motif $[M_2L_4]$ is very common within coordination chemistry.[34]

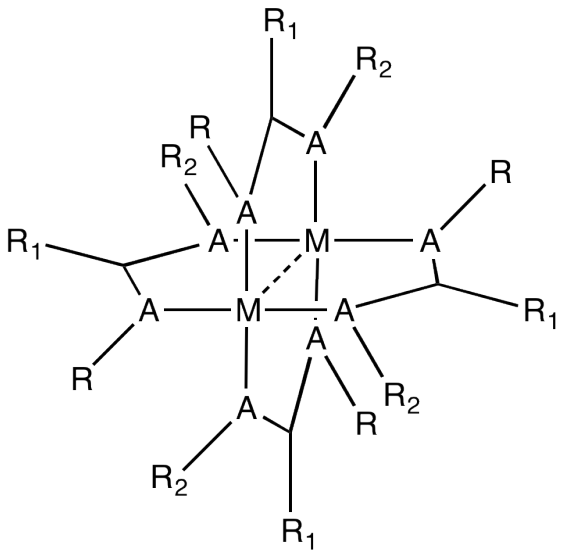

Figure 1.16: A typical paddlewheel structure of the general formula M_2L_4, where A = any donor atom, commonly O, N, P or S.

The amidinate and guanidinate ligands used within this project have been established as suitable candidates for the formation of paddlewheel-type structures, as they are capable of stabilising the low oxidation states likely to be encountered within these materials, contain nitrogen centres ideally situated for bridging, and can easily be adapted through substitution of the R groups to tune the sterics and electronics of the overall system. Neutral amidines have been employed as ligands in a broad range of coordination complexes,[42] whilst the anionic amidinates and guanidinates have become increasingly popular choices for the stabilisation of both main group and transition metal complexes.[43] Coles and Jordan successfully utilised amidinate ligands in the synthesis of aluminium-based ethylene polymerization catalysts,[44] showcasing the versatility of these ligands and the potential for structural control that they present through judicious substitution of the amidinate R groups.[45]

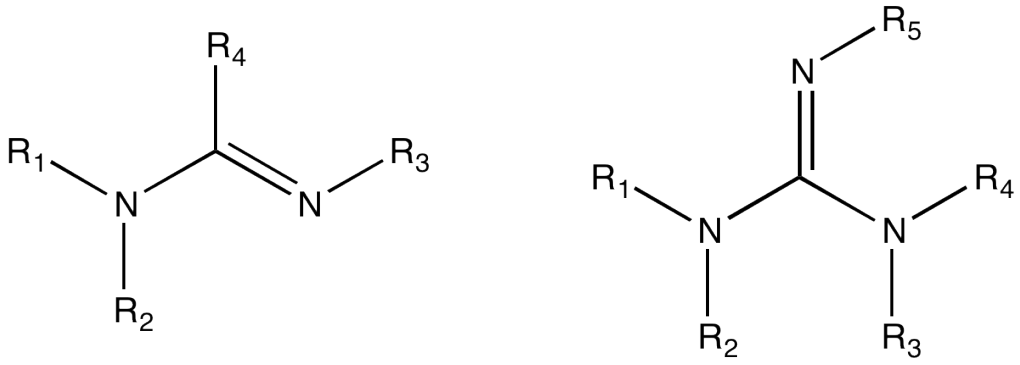

Figure 1.17: *Left*, The general structure of an amidine; *right*, the general structure of a guanidine.

There have been several examples of amidinate- and guanidinate-based paddlewheel structures in recent literature that influenced the direction of this project. One area of interest was that of the use of sterically-undemanding amidinate ligands to form 'open' paddlewheel arrangements, something which had already undergone some preliminary investigation within the Wheatley group. Unpublished work from the Wheatley group reports the synthesis of two novel compounds containing transition metals and *N,N′*-dimethylformamidinate, which was repeated and expanded upon during the course of this work. The first species was a classic paddlewheel of the type M_2L_4 obtained from the reaction of Cp_2Ni with the lithiated anion of *N,N′*-dimethylformamidine (Compound **1.11**) as seen in Figure 1.18.[46]

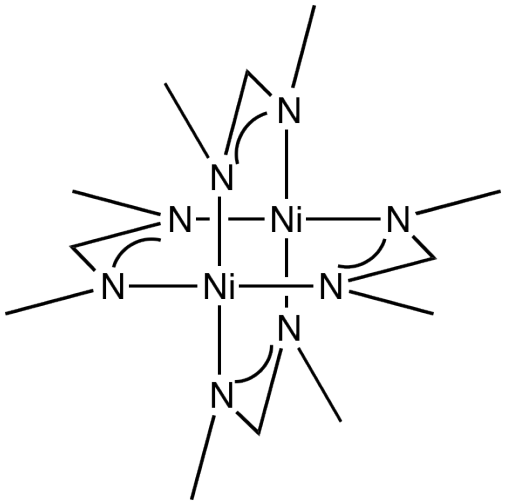

Figure 1.18: The structure of Ni_2(*N,N′*−dimethylformamidinate)$_4$, **1.11**.

The observed structure of **1.11** featured the desired 'open' arrangement, leaving the metal centres relatively exposed and accessible, as the ligand methyl groups are not sterically bulky and so are able to stabilise the metal centres without

blocking them entirely and restricting further reaction. This was seen as a promising result, and one which deserved to be investigated further. In particular, the precise nature of the bonding within this species could be probed using theoretical methods, something which is discussed at length in Chapter 5, Section 5.3.2.

A repeat of the previous reaction using Cp_2Mn in place of Cp_2Ni was found to give a complex containing a $Mn_4(\mu_4{-}O)$ core (Figure 5.2),[46] in spite of attempts to keep oxygen out of the system.

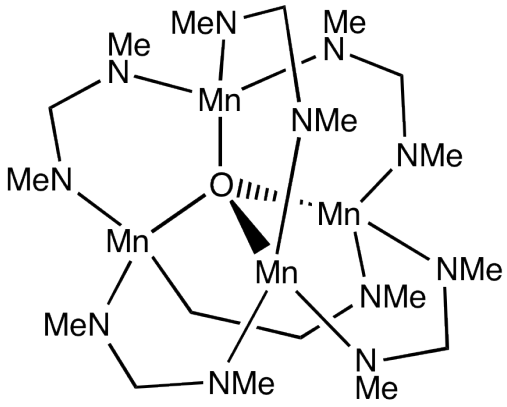

Figure 1.19: The structure of $Mn_4O(N,N'{-}$dimethylformamidinate$)_6$, **1.12**.

The observed structure **1.12** was of interest as the presence of oxygen, likely from trace amounts of O_2 or H_2O that entered the reaction at some point, did not cause decomposition but instead oxygen became incorporated into the product structure, maintaining the +2 oxidation state of the metal centres. The encapsulation of an oxide without decomposition has been observed previously for organometallic complexes,[47] for example in the carboxylation reaction between Cp^*Zn and CO_2 in which the isolated product is the zinc oxocarboxylate $[Zn_4(\mu_4\text{-}O)(O_2CCp^*)_6]$ featuring a tetrahedral $[Zn_4O]^{6+}$ core.[48] Within such complexes both octahedral $\mu_6{-}O$ and tetrahedral $\mu_4{-}O$ core structures are observed.[49]

The structure obtained of **1.12** was analogous to one first reported by Cotton *et al.* in 1997, $Mn_4O(DPhF)_6$,[50] which also featured a tetrahedron of manganese centres surrounding the oxygen core and bridged by the substantially bulkier *N,N'*-diphenylformamidinate. The synthesis of $Mn_4O(DPhF)_6$ involved layering the reaction solution with moist but oxygen-free hexanes, suggesting that the source of the interstitial $\mu_4{-}O$ in $Mn_4O(N,N'{-}$dimethylformamidinate$)_6$ is likely to be trace H_2O rather than atmospheric O_2, which would probably in fact be destructive to the molecule, causing oxidation and/or decomposition. Within organometallic

chemistry, O_2 has been successfully introduced into molecular complexes to give peroxides,[51] superoxides[52] and metal oxides,[53] although this is generally performed in a controlled manner to prevent unwanted decomposition.[54] It was decided to perform similar experiments to that which led to the isolation of **1.12** in the current project in order to obtain further analysis, and to fit these results into a broader narrative relating to the reactivity of several transition metal metallocenes with a variety of amidinate and guanidinate ligands.

A further feature of transition metal paddlewheel complexes which this project aimed to explore is their ability to trap small molecules and unstable fragments, as seen in the X-ray crystallographic structure of $[V_2(hpp)_4]$, Figure 1.20.[22]

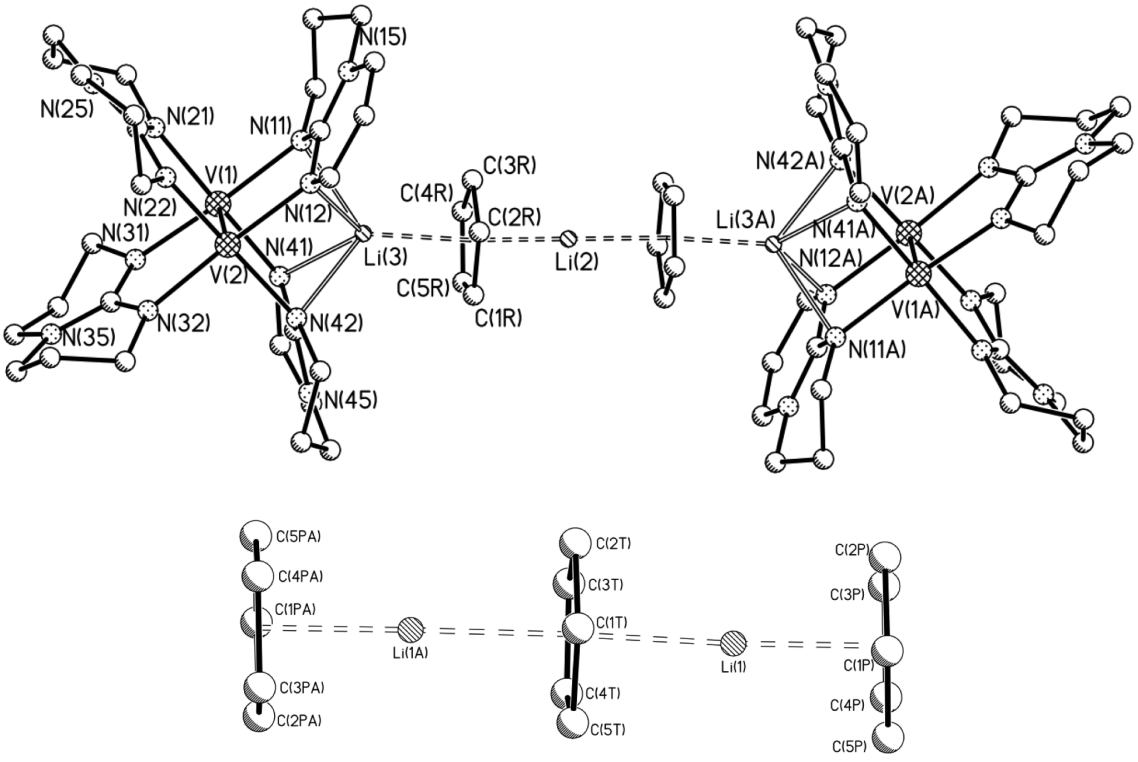

Figure 1.20: The crystal structure of $[\{V_2(hpp)_4\}Li(\mu{-}Cp)Li\{V_2(hpp)_4\}]^+$-$[(\eta^5\text{-}Cp)Li(\mu{-}Cp)Li(\eta^5\text{-}Cp)]^-$, **1.13**. *Above*, the centrosymmetric cation; *below*, the centrosymmetric anion of **1.13** (showing one orientation of the disordered central cyclopentadienyl ligand). H-atoms and lattice-bound THF molecules omitted for clarity.[22]

The formally V≡V species $[\{V_2(hpp)_4\}Li(\mu{-}Cp)Li\{V_2(hpp)_4\}]^+[(\eta^5\text{-}Cp)Li(\mu{-}Cp)Li(\eta^5\text{-}Cp)]^-$ is observed to trap charged oligomeric fragments of the $(CpLi)_\infty$ parent lattice[55] in the solid state, in a manner which is highly unusual. Indeed, there is only one precedent, the crystal structure $[(THF)Li(\mu{-}Cp^{Ar})Li(\mu{-}Cp^{Ar})Li(THF)]^+$-$[(\eta^5{-}Cp^{Ar})_2Li]^-$ ($Cp^{Ar} = 3,5{-}(Me_2C_6H_3)_5C_5$)[56] which contains a similar $[Li(\mu{-}Cp)$-$Li(\mu{-}Cp)Li]^+$ core but is significantly different in composition, containing no other metal species and relying on 'superbulky' cyclopentadienyl ligands rather than nitrogen donor atoms to stabilise the alkali metal ions. These multidecker cations and anions have provoked attention and interest in recent years,[57] due to the novel bonding arrangements observed,[19] and the scarcity of structures containing unsubstituted and unsolvated cyclopentadienyl-alkali metal 'supersandwiches'.[19;58] The ability of $[V_2(hpp)_4]$ to stabilise the cation $[Cp_2Li_3]^+$ by acting as a bulky ligand coordinating the terminal Li^+ ions became a factor in the design of several syntheses undertaken within the current project as it was hoped that this area could be developed and expanded upon.

1.3.3 Polynuclear Transition Metal Clusters

Metal clusters may be defined as molecular complexes with metal-metal bonds that form triangular or larger closed structures, a definition that excludes polymetallic complexes held together by bridging ligands rather than by metal-metal bonding.[25] Transition metal metallocenes are ideal starting materials for the formation of clusters, with recent research within the area directed towards creating clusters using Cp_2M reagents (in particular manganocene) with N- or P- donor ligands.

Manganese carboxylate clusters have been widely studied in recent years as there has been interest in their magnetic properties, and their potential applications as molecule-based magnetic materials, either as precursors or in their own right.[59] However, relatively few nitrogen- or phosphorus-based clusters of manganese have been synthesised or studied. One interesting example of an amido/imido Mn(II) cluster, $[(\eta^5{-}Cp)Mn\{2{-}NH(4,6{-}Me_2pm)\} \cdot Mn\{2{-}N(4,6{-}Me_2pm)\}]_4$, was published by Alvarez *et al.* in 2001[15] and was synthesised using Cp_2Mn as a starting material and a pyrimidine ligand which could be both doubly- and singly-deprotonated by the cyclopentadienyl of the manganocene to give a heteroleptic cage with the structure seen in Figure 1.21. This example is of particular relevance to this project as the synthesis utilised the polar nature of the metallocene and the ability of the cyclopentadienyl ligand to behave as a base.

The structure of $[(\eta^5{-}\mathrm{Cp})\mathrm{Mn}\{2{-}\mathrm{NH}(4,6{-}\mathrm{Me_2pm})\} \cdot \mathrm{Mn}\{2{-}\mathrm{N}(4,6{-}\mathrm{Me_2pm})\}]_4$ is perhaps best regarded as a co-complex of four monomer units of Mn(II) imido ($\mathrm{Mn}\{2{-}\mathrm{N}(4,6{-}\mathrm{Me_2pm})\}$) and four of organo/amido ($(\eta{-}\mathrm{Cp})\mathrm{Mn}\{2{-}\mathrm{NH}(4,6{-}\mathrm{Me_2pm})\}$), giving the highest nuclearity imido or amido manganese cage to be structurally characterised. This study is not only interesting due to the novel structure formed or for the use of the basicity of manganocene to facilitate the synthesis thereof, but also for its investigation into the magnetic properties of this polynuclear cluster. The magnetic properties of the products of reactions utilising transition metal metallocenes was a further area into which this research project aimed to expand, due to the current surge of interest into single-molecule magnets, discussed at length in Section 1.3.5.

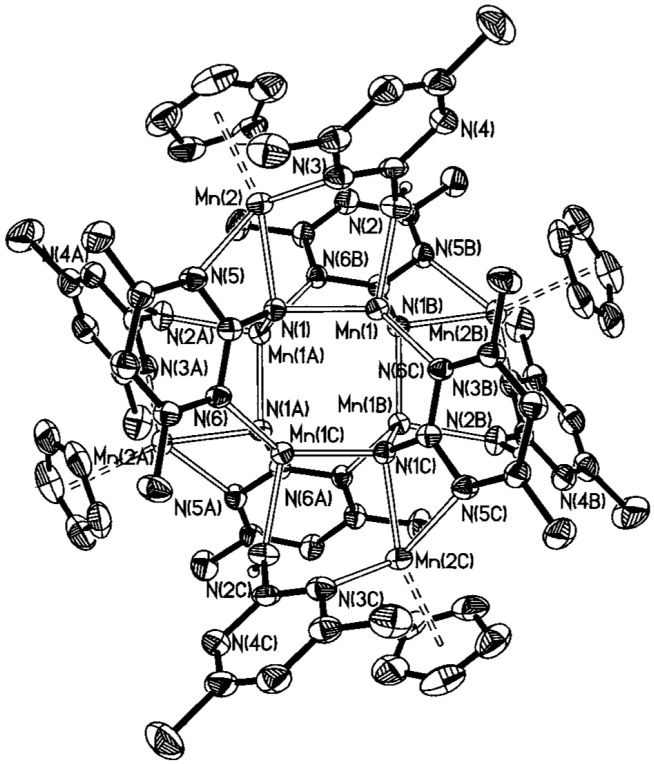

Figure 1.21: The crystal structure of the cage $[(\eta^5{-}\mathrm{Cp})\mathrm{Mn}\{2{-}\mathrm{NH}(4,6{-}\mathrm{Me_2pm})\} \cdot \mathrm{Mn}\{2{-}\mathrm{N}(4,6{-}\mathrm{Me_2pm})\}]_4$, **1.14**. Thermal ellipsoids are drawn at the 40% probability level. H-atoms, except those attached to N, and lattice-bound THF atoms have been omitted for clarity.[15]

Variable-temperature magnetic studies on the cluster $[(\eta^5{-}\mathrm{Cp})\mathrm{Mn}\{2{-}\mathrm{NH}(4,6{-}\mathrm{Me_2pm})\} \cdot \mathrm{Mn}\{2{-}\mathrm{N}(4,6{-}\mathrm{Me_2pm})\}]_4$ showed an unusual evolution of effective magnetic moment with temperature, possibly due to exchange interactions between imido- and amido-bridged Mn(II) ions although single-ion effects are also likely to

play a part. Cyclopentadienyl is a strong-field ligand which could cause a change in spin state of the CpMn units of this aggregate,[60] and zero-field splitting may occur as it is known to in manganocenes.[61] The fact that this structure exhibited novel magnetic behaviour was encouraging, as it suggested that further research into the synthesis of metallocene-derived transition metal complexes and clusters could yield other magnetic materials, with potentially useful applications.

A similar synthetic method was also employed in the generation of a class of cages featuring Mn_8 cores and bridging nitrogen-based ligands.[16] This study showed that in order for double deprotonation of the amino group to occur, the organic substituents had to contain several N atoms in order to stabilise the resultant negative charge. Using this information, it was shown that acidic 2-amino-pyrimidines could be doubly-deprotonated even in the presence of electron-donating MeO and Me ring substituents, whereas the less acidic 2-aminopyridines and related aromatic amines were only singly-deprotonated, as was the case with the 8-aminoquinoline ligand discussed in Section 1.2.3.

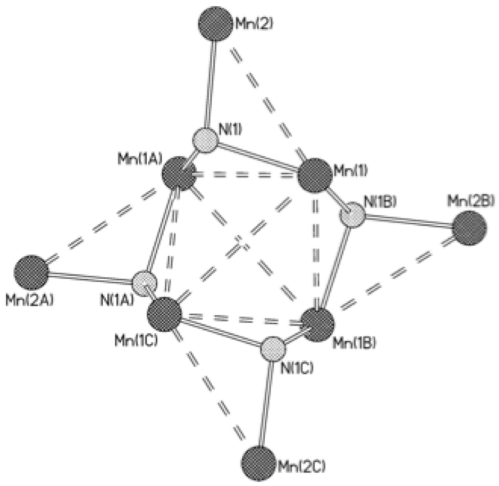

Figure 1.22: The core structure of the manganese amido/imido cages with the general formula $[(CpMnNHR)(MnNR)]_4$ (where R = 4,6-Me_2pm, 4-MeO-6-Mepm or 4,6-$(MeO)_2$-pm; pm = pyrimidinyl) showing the Mn_8 arrangement and the shortest Mn···Mn contacts (dashed lines).[16]

The synthesis of the cage structures with the general formula $[(CpMnNHR)(MnNR)]_4$ involved the addition of the ligand to manganocene at -78° C, gradual warming and storage at room temperature to yield crystals of the appropriate products. No further studies were attempted as to the effect of temperature on these reactions, such

as whether refluxing the reaction solution resulted in more complete deprotonation of the less acidic ligands and the isolation of different products. This area was of interest at the outset of this project and several of the reactions described herein were attempted at various temperatures in order to obtain complete data about said reactions, and to assess whether simple alterations to the reaction conditions would affect the product(s) obtained in any way.

1.3.4 Metallocene Reactivity with Non-Innocent Ligands

The terms 'innocent' and 'non-innocent' (or 'suspect') with regard to ligands were first introduced by Jørgensen in 1966.[62] Ligands which are considered 'non-innocent' are those which are redox-active and can render the oxidation state of a metal to which they are coordinated ambiguous. This most common examples of this class of ligand are those based on 1,2-disubstituted benzene rings such as catechols and diamines, the redox behaviour of which can be seen in Figure 1.23.

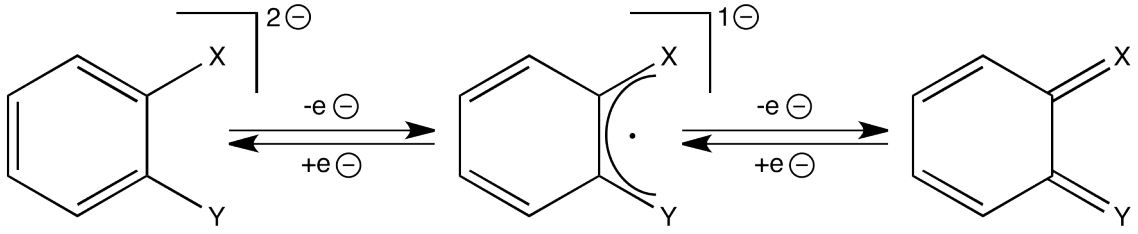

Figure 1.23: The redox series for various non-innocent 1,2-disubstituted benzene ligands. X and Y are donor atoms such as O, N or S.

Complexes containing such ligands have been of interest in transition metal coordination chemistry since the 1960s, when various complexes with 'non-innocent' ligands were reported, beginning with planar dithiolates of nickel, palladium and platinum.[63] This was soon followed by characterisation of metal complexes containing oxygen[64] and nitrogen[65] ligand analogues, the latter being of particular relevance to this work as investigating the reactivity of transition metal metallocenes with nitrogen-based non-innocent ligands was a primary aim of this project.

Compound **1.15** is a planar nickel complex containing two chelating 1,2-benzenediamine ligands (Figure 1.24), and was first reported by Balch and Holm in 1966.[65] As can be seen Figure 1.24, three possible structures were discussed, with the electronic structure of B proposed by the authors as the most likely arrangement.[65] This was fully confirmed by Herebian *et al.* in 2002-3 using computational methods including DFT calculations.[66–68]

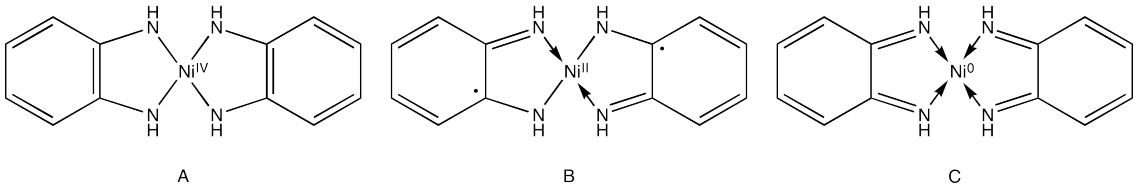

Figure 1.24: The three postulated structures of $[Ni(C_6H_4(NH)_2)_2]$, **1.15**.

1.15 was synthesised using a nickel halide salt and 1,2-benzenediamine in aqueous ammonia. There have been few reported compounds synthesised using redox-active ligands and transition metals which exclude oxygen and moisture, with the majority of interesting examples confined to the main group elements.[69;70] One particularly interesting example is seen in the reaction shown in Figure 1.25, where reaction with the base $Sn(NMe_2)_2$ and *n*-BuLi leads to oxidative dehydrocoupling and rearrangement into the triazolyl anion.[71]

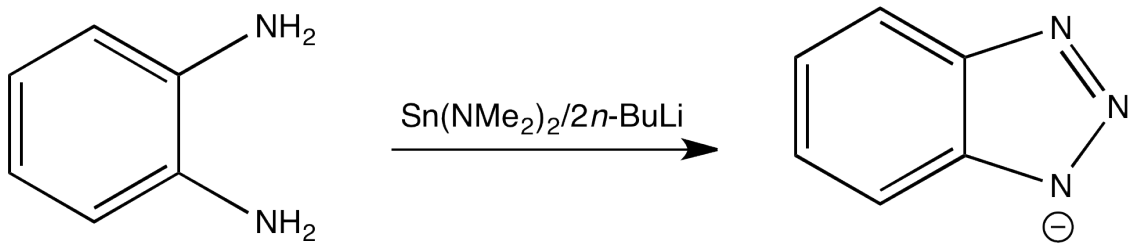

Figure 1.25: The reaction of 1,2-benzenediamine using $Sn(NMe_2)_2$.[71]

This project aimed to develop this field by conducting preliminary investigations into the reactions of transition metal metallocenes with nitrogen-based redox-active ligands, with the goal of producing and characterising novel higher- or mixed-oxidation state molecular arrangements.

1.3.5 Single-Molecule Magnets

Single-molecule magnets are a class of metallo-organic compounds that exhibit magnetic hysteresis of purely molecular origin below a certain temperature (the blocking temperature).[72] In contrast to conventional bulk magnets and molecule-based magnets, it is not necessary for there to be any collective long-range ordering of magnetic moments for this behaviour to be observed. As the smallest possible magnetic devices, they have potential applications in a range of areas including thin films for technological devices,[73] magnetic refrigeration, quantum computing and information storage.[74] The latter of these is particularly exciting, making use of the fact that SMMs represent a macroscopic quantum system in which spin flips

could be detected and used to store information.[72] This would greatly increase the storage capacity of hard disks and improve computing methods significantly.

In order to behave as SMMs, each molecule must have a large enough magnetic moment (so a large spin ground state, S) and magnetic anisotropy to function as a magnet. The majority of characterised SMMs are manganese-based, with the most thoroughly studied being "Mn_{12}" systems, the archetype of which is "Mn_{12}-acetate", $[Mn_{12}O_{12}(OAc)_{16}(H_2O)_4] \cdot 4\,H_2O \cdot 2\,AcOH$.[75] This dodecanuclear structure features a central $Mn^{IV}{}_4O_4$ cubane unit surrounded by a ring of eight Mn^{III} centres connected by bridging oxo ligands, giving an overall disc-shaped geometry. This has an S = 10 ground state[76] and a blocking temperature of 3 K, below which it exhibits a magnetisation half-life of more than two months.[77]

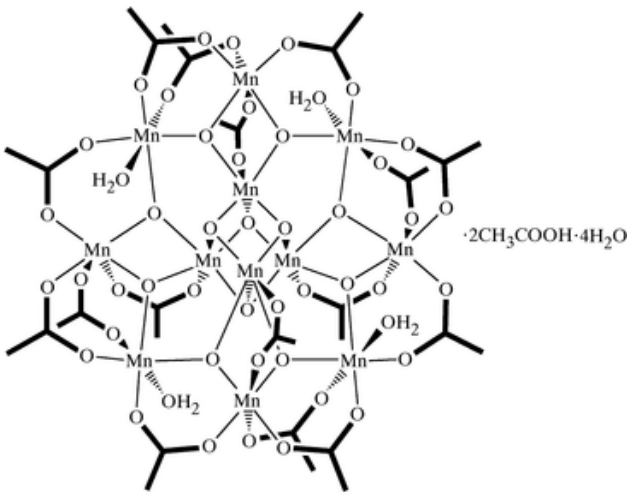

Figure 1.26: The structure of the single-molecule magnet $[Mn_{12}O_{12}(OAc)_{16}(H_2O)_4] \cdot 4\,H_2O \cdot 2\,AcOH$, **1.16**.[78]

Another common type of SMM is the "Mn_4" system, examples of which contain a planar $Mn^{III}{}_2Mn^{II}{}_2$ diamond core and have an S = 9 ground state.[79] More recently, an "Mn_6" complex containing six Mn(III) ions (Compound **1.17**) has been reported with an S = 12 ground state and the largest recorded energy barrier to magnetisation, 86.4 K (Figure 1.27).[80] A high energy barrier is desirable as this ensures that the material remains magnetised for longer.

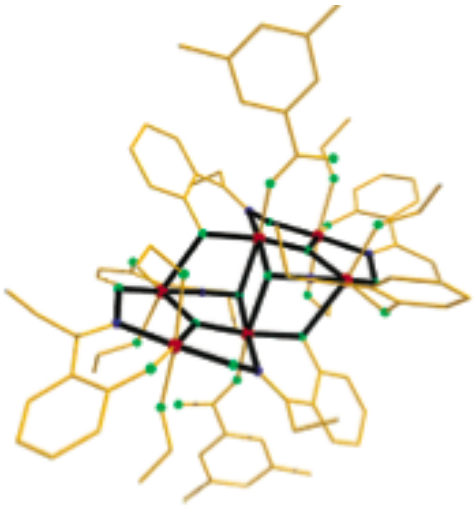

Figure 1.27: The structure of the "Mn_6" SMM with the largest recorded energy barrier to magnetisation, $[Mn_6O_2(sao)_6(O_2CPh)_2 \cdot 4\,EtOH]$, **1.17**, with the core shown in black. Mn = red, O = green, N = blue.[74]

As these studies show, manganese-based clusters are an extremely promising research area within the field of single-molecule magnetism. Following on from the successes of the Wright group in synthesising polynuclear manganese cluster compounds,[16] this project aimed to generate other novel manganese-based magnetic materials, alongside other transition metal complexes that may also exhibit unusual magnetic behaviour, and test their variable-temperature magnetic response.

1.4 Aims of this Project

The aims of this project can now be set into context.

- To synthesise and characterise a range of transition metal-containing complexes and materials using transition metal metallocenes as starting materials.
- To develop the synthetic chemistry of the transition metal metallocenes, using their known reactivity patterns and versatility to design novel reaction pathways, and to fully investigate the properties of any resulting materials.
- To investigate the reactivity of transition metal metallocenes with nitrogen-based redox-active ligands.
- To study the variable-temperature magnetic behaviour of products formed, where relevant.
- To study any inter-metal bonding interactions (in particular any multiple bonds) of products formed where relevant, including by computational methods.

Chapter 2

General Experimental Techniques

2.1 COSHH Considerations

Throughout the course of this project, hazardous chemicals were regularly handled and used. In order to minimise the risk of dangerous spillages or inhalation of potentially harmful materials, all synthetic operations were carried out inside a fume hood. Appropriate PPE was employed, including a laboratory coat, safety glasses and nitrile gloves. Risk assessments were carried out prior to the use of any chemical, and any glassware contaminated with phosphorus-containing compounds with an unpleasant odour was soaked in 1:1 bleach/water before being washed up.

2.2 Inert Atmosphere Techniques

All syntheses and manipulations described in this project were carried out under oxygen-free, anhydrous conditions due to the extremely air- and moisture-sensitive nature of the compounds involved. In particular, two pieces of specialist equipment were employed - a vacuum and inert gas double-manifold (used inside a fume hood), and a glovebox for the storage and handling of air-sensitive materials.

Synthetic operations were carried out in accordance with known air-sensitive techniques. Reactions were performed in Schlenk tubes, previously dried in a glassware oven at 80° C, which were then evacuated to less than 0.1 Torr three times whilst being heated thoroughly using a heat gun. Dry argon or nitrogen from the house supply was used to fill the tubes between evacuations. Liquid reagents were added to reactions under a positive pressure of inert gas *via* syringes, which were first purged with dry nitrogen several times. Solid reagents were weighed inside the glovebox into Schlenk tubes before being connected to the vacuum manifold

or, if the reagents themselves were not air-sensitive, added to reactions against a positive pressure of inert gas. The removal of solvent from reactions was carried out using the vacuum manifold. Filtrations were performed using filter sticks of the appropriate porosity, which were placed in Schlenk tubes and capped before being attached to the manifold and evacuated as described above. The prepared filter stick was then inserted into the Schlenk containing material to be filtered, and the connected glassware inverted. The receiving Schlenk was placed under vacuum to enable filtration. Crystallisations were carried out within the Schlenk tubes, either at room temperature, +5° C or -30° C.

The glovebox employed was from Saffron Scientific Instruments, and was used frequently for the storage and manipulation of both starting materials and products. Apparatus was introduced to the glovebox *via* the port, which was then sealed to atmosphere and evacuated for 10 minutes before being filled with dry nitrogen. This was repeated twice more, then the gloves were evacuated and refilled three times before the box was used. The oxygen level inside the box was monitored using an NTRON MICROX O_2 Analyser, with measures taken to ensure that this stayed below 2 ppm. The atmosphere inside the glovebox was continually recirculated through columns containing a copper catalyst, which was regularly reformed using 25% H_2 in N_2 whilst heating to 200° C.

2.3 Starting Materials and Solvents

Reagents obtained from the Sigma-Aldrich chemical company were of the highest available purity and were used as received. Other reagents were synthesised in house, either prior to this project or by myself (see Chapter 3, Section 3.1). Liquid reagents were distilled prior to use and stored over molecular sieves (pore size 4 Å), or were obtained in Aldrich SureSeal^{TM} bottles, in which case the liquid was removed using a dry syringe with inert gas used to refill the container and prevent the formation of a vacuum. Solid reagents were either stored in the glovebox and used directly, or if they were not air-sensitive, were placed under vacuum immediately prior to use. Any solvents used were freshly distilled and stored over sodium or sodium-potassium amalgam. Deuterated THF and toluene were stored inside the glovebox over sodium or potassium mirrors, whilst other deuterated NMR solvents were bought from Aldrich in 0.75 mL ampoules and used as received.

2.4 Melting Point Determination

Melting point determination was carried out using Griffin melting point apparatus. Approximately 3 mg of the sample was added to a melting point tube inside the glovebox, which was then sealed with vacuum grease and Parafilm^{TM} before being removed and analysed.

2.5 Elemental Analyses

Elemental Analyses were performed on an Exeter Analytical CE-440 Elemental Analyzer, which determined the percentage by mass of carbon, hydrogen and nitrogen in the characterised products. All samples were prepared inside the glovebox to prevent oxidation and degradation, using pre-weighed aluminium boats. Approximately 2 mg of product was placed inside the boats, which were then sealed and accurately weighed prior to analysis.

2.6 Infrared Spectroscopy

Infrared Spectroscopy was performed using a PerkinElmer Spectrum RX I FT-IR Spectrometer. For solid samples, a mull was made inside the glovebox using Nujol dried over sodium wire. This was applied to NaCl plates, the edges of which were then wrapped in Parafilm^{TM} to prevent oxidation of the sample. Liquid reagents and samples were applied directly to the NaCl plates.

2.7 Nuclear Magnetic Resonance Spectroscopy

^{1}H, ^{13}C, ^{31}P and ^{7}Li NMR spectra were recorded using a Bruker DRX 500 FT-NMR spectrometer at 300 K (500.05 MHz for ^{1}H, 125.8 MHz for ^{13}C, 162.0 MHz for ^{31}P and 194.4 MHz for ^{7}Li). The chemical shifts were internally referenced against the deuterated solvents used for ^{1}H and ^{13}C NMR, whilst 85% H_3PO_4 in D_2O and 1M LiOH in D_2O were used as references for ^{31}P and ^{7}Li NMR respectively. Air- and moisture- sensitive NMR samples were prepared in the glovebox under an inert atmosphere of N_2, with the tubes capped using a Young's tap seal to ensure effective protection against oxidation. In some cases, the presence of paramagnetic metal centres made obtaining NMR data difficult, as they cause peak broadening and affect nuclear relaxation times, therefore rendering integration less accurate.

2.8 Single-Crystal X-Ray Diffraction Studies

Single-crystal X-ray diffraction was the principle technique used to structurally characterise the solid products obtained throughout this project. Crystals were grown under an inert atmosphere in sealed Schlenk tubes until they reached an appropriate size for crystallography (ideally larger than 0.1 mm in all dimensions) whereupon they were removed under a positive pressure of inert gas and placed on a slide. A Nonius Kappa CCD diffractometer, equipped with an Oxford Cryostream cooling device was employed throughout. Crystals were mounted using perfluorohydrocarbon oil which freezes at low temperature and protects the crystals from oxidation.[81] The SHELX-97 program[82] was used to solve the structures, locating the heavy atoms by direct methods and refining by full-matrix least-squares on F^2, with non-hydrogen atoms being treated anisotropically and hydrogen atoms being added in calculated positions and allowed to ride on their parent atom. Specific details as to the handling of crystallographic disorder in individual structures is discussed within the relevant sections of Chapter 3, Experimental Procedures and Results.

2.9 Magnetic Measurements

Magnetic measurements were performed on a SQUID magnetometer (Quantum Design, model MPMS-XL-5), both in Cambridge and in Germany. For the measurements undertaken in Cambridge, gelatine capsules were used as sample containers, with a small amount of cotton wool used to keep the powdered sample from shifting. The very small diamagnetic contribution of the gelatine capsule and high temperature sample holder had a negligible contribution to the overall magnetisation, which was dominated by the sample. Further measurements were carried out by Dr Andreas Eichhöfer at the Karlsruhe Institut für Technologie (KIT), where samples were placed in a quartz tube held between quartz rods during measurements. Specific experimental details regarding magnetic measurements are discussed within the relevant chapters.

2.10 Theoretical Calculations

Theoretical calculations were carried out by Lars Kloo at the KTH Royal Institute of Technology in Stockholm, Sweden. Calculations were performed using the Gaussian09 program package using quantum mechanical methods at Hartree-Fock (HF), density-functional (BLYP) and hybrid density-functional (B3PW91, B3LYP,

B3LYP*, O3LYP and cam-B3LYP) levels. Lighter elements used 6-311G-type basis sets supplemented with diffuse and polarisation functions. Transition metals were described by an effective-core potential of Los Alamos type. In some cases larger basis sets were used for more complete calculations - specific experimental details are discussed within the relevant chapters.

Chapter 3

Experimental Procedures and Results

3.1 Synthesis of Starting Materials

This section describes the syntheses of any starting materials that were not available commercially. The metallocenes were synthesised according to modified literature procedures.[83] *N,N′*-Dimethylformamidine was synthesised according to literature procedure,[84] and the purity confirmed with ^{1}H NMR.

3.1.1 Synthesis of Cp_2Mn

9.2 g (0.40 mol) sodium was cut up and stirred in approximately 100 mL of THF. To this, 33 mL (0.40 mol) freshly cracked cyclopentadiene was added dropwise at -78° C and the resulting pale orange solution left to stir overnight. This solution was cooled to -78° C and 25 g (0.20 mol) $MnCl_2$ added against a positive flow of inert gas. The reaction was heated under reflux at 80° C for 4 hours before the solvent was removed and the pale brown solid sublimed at approximately 100° C to yield 14.2 g (24%) orange-brown crystals of Cp_2Mn. In later syntheses, NaH (9.6 g, 0.40 mol) was used rather than solid sodium, and a slight excess of cyclopentadiene (37 mL, 0.43 mol) was also added. These modifications made the first step of the reaction considerably quicker and produced yields of Cp_2Mn of 50 – 70%.

3.1.2 Synthesis of Cp_2V and Cp_2Cr

9.2 g (0.40 mol) sodium was cut up and stirred in approximately 100 mL of THF. To this, 33 mL (0.40 mol) freshly cracked cyclopentadiene was added dropwise at -78° C and the resulting pale orange solution left to stir overnight. The THF solvent was removed and the resulting white solid redissolved in DME. The resulting beige solution was then cooled to -78° C and reacted with either VCl_3 (15.7 g, 0.10 mol) or $CrCl_3$ (15.8 g, 0.10 mol). The reaction was left to stir overnight before the solvent was removed and the solid sublimed in portions at 100°– 140° C, giving dark purple crystals of Cp_2V and red crystals of Cp_2Cr. The yields were of the order of 30 – 40% based on the halides. Use of NaH (9.6 g, 0.40 mol) and an excess of cyclopentadiene (37 mL, 0.43 mol) made the first step of reaction considerably quicker and increased the yields of the metallocenes to 60 – 70%, based on the halides.

3.1.3 Purification of Cp_2Ni

Cp_2Ni was obtained from the Part II teaching laboratory and sublimed at 120° C, giving dark green crystals in a 60 – 70% yield.

3.1.4 Synthesis of *N,N′*-Dimethylformamidine

23.5 mL methylamine (33% wt in EtOH, 0.25 mol) and 20.8 mL triethyl orthoformate (0.13 mol) were combined and 7.15 mL glacial acetic acid (0.12 mol) was added dropwise. The resulting solution was refluxed overnight to give a yellow liquid. This was distilled under vacuum at 60°– 70° C yielding a colourless viscous liquid.

Yield - 7.5 mL, 68%

^{1}H NMR (500.05 MHz, THF−d_8), δ (ppm) - 7.58 (1H, s, br, N*H*), 6.35 (1H, s, br, NC*H*N), 2.49 (6H, s, N*Me*)

^{13}C NMR (125.8 MHz, THF−d_8), δ (ppm) - 162.9 (N*C*HN), 18.9 (H_3CN)

3.2 Experimental Procedures and Results for Chapter 4

3.2.1 Synthesis of $[(\eta^2\text{- Cp})Mn(BnNHC_2H_4NBn)]_2$, 4.1

N,N′-Dibenzylethylenediamine (0.13 mL, 0.55 mmol) was stirred in approximately 5 mL of THF. *n*−BuLi (0.35 mL, 1.6 mol L^{-1} in hexanes, 0.55 mmol) was syringed into this solution dropwise under inert gas at -78° C, and the pale yellow suspension allowed to warm to room temperature. This was then syringed dropwise under inert gas into a solution of Cp_2Mn (100 mg, 0.55 mmol) in approximately 5 mL THF cooled to -78° C before being allowed to warm to room temperature. The solution was stirred overnight, then filtered warm *in vacuo* using a filter stick and stored at -30° C, affording pale green crystals in a dark red solution after one day.

Yield - 40 mg, 20% with respect to Cp_2Mn

Melting Point - 205 – 209° C

Elemental Analysis - found C 69.6, H 6.8, N 7.7, calcd. for $C_{26}H_{52}Mn_2P_4$ C 70.2, H 6.7, N 7.8

Crystal Data for **4.1** - $C_{46}H_{56}Mn_2N_4O$, M = 790.83, monoclinic, space group C2/c, a = 15.4673(3), b = 9.1372(2), c = 29.1960(6) Å, α = 90°, β = 94.480(1)°, γ = 90°, V = 4113.60(15) Å^3, Z = 4, ρ_{calcd} = 1.277 g cm^{-3}, Mo-Kα radiation, λ = 0.71073 Å, μ = 0.653 mm^{-1}, T = 180(2) K. 15150 data (4610 unique, R_{int} = 0.0418, $\theta < 27.46°$) were collected. *wR2* = 0.1415, conventional R = 0.0451 on F values of 3158 reflections with $F^2 > 2\sigma(F^2)$, S = 1.056, 237 parameters. Residual electron density extrema ±1.269 eÅ^{-3}. Nitrogen bonded H-atoms were directly located by Fourier synthesis and refined isotropically. The THF solvent molecule was disordered. For the refinement, a single isotropic displacement parameter was assigned to the O and C atoms of this group.

3.2.2 Synthesis of $[(\eta^5\text{- Cp})Mn(EtNHC_2H_4NEt)]_2$, 4.2

N,N′-Diethylethylenediamine (0.08 mL, 0.55 mmol) was stirred in approximately 5 mL of THF. *n*−BuLi (0.35 mL, 1.6 mol L^{-1} in hexanes, 0.55 mmol) was syringed into this solution dropwise under inert gas at -78° C, and the pale yellow suspension

allowed to warm to room temperature. This was then syringed dropwise under inert gas into a solution of Cp_2Mn (100 mg, 0.55 mmol) in approximately 5mL THF cooled to -78° C before being allowed to warm to room temperature. The solution was stirred overnight, then filtered warm *in vacuo* using a filter stick and stored at -30° C, affording pale green crystals in a dark red solution after one day.

Yield - 8 mg, 6% with respect to Cp_2Mn

Melting Point - 249 – 252° C

Elemental Analysis - Correct C, H, N analysis could not be obtained despite repeated attempts.

Crystal Data for **4.2** - $C_{30}H_{56}Mn_2N_4O_2$, $M = 614.67$, monoclinic, space group $P2_1/c$, $a = 10.9178(2)$, $b = 16.4668(4)$, $c = 9.2536(3)$ Å, $\alpha = 90°$, $\beta = 91.024(2)°$, $\gamma = 90°$, $V = 1663.36(7)$ Å^3, $Z = 2$, $\rho_{calcd} = 1.227$ g cm^{-3}, Mo-Kα radiation, $\lambda = 0.71073$ Å, $\mu = 0.789$ mm^{-1}, $T = 180(2)$ K. 16246 data (3629 unique, $R_{int} = 0.0328$, $\theta < 27.10°$) were collected. $wR2 = 0.1642$, conventional $R = 0.0513$ on F values of 2912 reflections with $F^2 > 2\sigma(F^2)$, $S = 1.086$, 174 parameters. Residual electron density extrema ±0.688 eÅ^{-3}. Nitrogen bonded H-atoms were directly located by Fourier synthesis and refined isotropically.

3.2.3 Synthesis of $[(t\text{–BuPH}_2)(\eta^5\text{- Cp})\text{Mn}\{\mu\text{–}(t\text{–BuPH})\}]_2$, 4.3

Cp_2Mn (102 mg, 0.55 mmol) was dissolved in 3 mL THF and cooled to -78° C. t–$BuPH_2$ (0.07 mL, 0.55 mmol) was added *via* syringe and the reaction vessel warmed to room temperature. After stirring overnight, the resulting yellow-brown solution was stored at -30° C, affording yellow crystals of **4.3**. These crystals rapidly decomposed under prolonged vacuum, releasing t–$BuPH_2$. In order to preserve their integrity, they were carefully isolated using only a brief reduction in pressure (approximately 10 seconds) before being stored under argon. The crystals obtained using this technique gave satisfactory chemical analysis (C, H, P), in contrast to samples placed under vacuum for a prolonged period during isolation.

Yield - 101 mg, 31% with respect to Cp_2Mn

Melting Point - 169 – 171° C

^{1}H NMR (500.05 MHz, THF−d_8), δ (ppm) - 4.20 (10H, s, Cp), 3.76 (2H, dm, br, P*H*, $^{1}J_{H\text{-}P}$ = 301 Hz), 3.21 (4H, d, br, PH_2, $^{1}J_{H\text{-}P}$ = 313 Hz), 2.80 (10H, d, free PH_2, $^{1}J_{H\text{-}P}$ = 185 Hz), 1.53 (18H, d, HPCMe_3, $^{3}J_{H\text{-}P}$ = 9 Hz), 1.16 (45H, d, free H_2PCMe_3, $^{3}J_{H\text{-}P}$ = 11 Hz), 1.07 (18H, d, H_2PCMe_3, $^{3}J_{H\text{-}P}$ = 1Hz)

^{13}C NMR (125.8 MHz, THF−d_8), δ (ppm) - 76.2 (Cp), 33.7 (HPCMe_3), 32.8 (d, free H_2PCMe_3, $^{2}J_{C\text{-}P}$ = 12 Hz), 31.9 (H_2PCMe_3)

^{31}P NMR (162.0 MHz, THF−d_8), δ (ppm) - 237.1 (d, *P*H, $^{1}J_{P\text{-}H}$ = 301 Hz), 75.2 (t, *P*H_2, $^{1}J_{P\text{-}H}$ = 313 Hz), -80.1 (br, free H_2*P*CMe_3)

^{31}P{H} NMR (162.0 MHz, THF−d_8), δ (ppm) - 241.6 (s, *P*H_2), 79.7 (s, H_2*P*CMe_3), -75.7 (br, free H_2*P*CMe_3)

Elemental Analysis - found C 52.0, H 8.8, P 19.7, calcd. for $C_{26}H_{52}P_4Mn_2$ C 52.2, H 8.8, P 20.7

Infrared Spectroscopy (Nujol mull) - 2397, 2328, 2234 cm^{-1} (PH and bound PH_2 symmetric and asymmetric); (after 1 minute air exposure) 2290 cm^{-1} (free PH_2)

Crystal Data for **4.3** - $C_{26}H_{52}P_4Mn_2$, M = 598.44, tetragonal, space group P 4_32_12, a = 9.1287(1), b = 9.1287(1), c = 35.7743(3) Å, α = 90°, β = 90°, γ = 90°, V = 2981.19(3) Å^3, Z = 4, ρ_{calcd} = 1.333 g cm^{-3}, Mo-Kα radiation, λ = 0.71073 Å, μ = 1.075 mm^{-1}, T = 180(2) K. 13256 data (2515 unique, R_{int} = 0.0264, θ < 24.69°) were collected. *wR2* = 0.0546, conventional R = 0.0186 on F values of 2485 reflections with $F^2 > 2\sigma(F^2)$, S = 1.242, 162 parameters. Residual electron density extrema ±0.263 eÅ^{-3}. Phosphorus bonded H-atoms (H1, H21, H22) were directly located by Fourier synthesis and refined isotropically.

3.3 Experimental Procedures and Results for Chapter 5

3.3.1 Synthesis of $Mn_4O(N,N'-dimethylformamidine)_6$, 5.1

N,N'-Dimethylformamidine (0.33 mL, 4.5 mmol) was stirred in approximately 5 mL THF. *t*−BuLi (2.7 mL, 1.7 mol L^{-1} in hexanes, 4.5 mmol) was syringed into this suspension dropwise under Ar at -78° C, and the yellow suspension allowed to warm to room temperature. The resultant white solution was then cooled again to -78° C and a solution of Cp_2Mn (278 mg, 1.5 mmol) in approximately 5 mL THF was syringed in dropwise. The solution was allowed to warm to room temperature before being stirred overnight. It was heated under reflux for 10 minutes, then filtered *in vacuo* and stored at -30° C. This afforded colourless crystals of **5.1** in a bright pink solution.

Yield - 97 mg, 33% with respect to Cp_2Mn

Melting Point - 228 – 230° C

^{1}H NMR (500.05 MHz, DMSO−d_6), δ (ppm) - 5.32 (1H, s, br, NC*H*N), 1.22 (6H, s, N*Me*)

^{13}C NMR (125.8 MHz, DMSO−d_6), δ (ppm) - 130.3 (N*C*HN), 29.2 (H_3CN)

Elemental Analysis - Correct C, H, N analysis could not be obtained despite repeated attempts.

Crystal Data **5.1** - $C_{18}H_{42}Mn_4N_{12}O$, M = 662.40, monoclinic, space group C2/c, a = 19.629(4), b = 11.044(2), c = 27.210(5) Å, α = 90°, β = 93.36(3)°, γ = 90°, V = 5889(2) Å^3, Z = 8, ρ_{calcd} = 1.494 g cm^{-3}, Mo-Kα radiation, λ = 0.71073 Å, μ= 1.709 mm^{-1}, T = 180(2) K. 22895 data (5188 unique, R_{int} = 0.0371, θ < 25.02°) were collected. *wR2* = 0.0861, conventional R = 0.0301 on F values of 2736 reflections with $F^2 > 2\sigma(F^2)$, S = 1.029, 316 parameters. Residual electron density extrema ±0.282 eÅ^{-3}. Nitrogen bonded H-atoms were directly located by Fourier synthesis and refined isotropically.

3.3.2 Synthesis of $Ni_2(CH_3NCHNCH_3)_4$, 5.2

N,N′-Dimethylformamidine (0.33 mL, 4.5 mmol) was stirred in approximately 5 mL THF. *t*−BuLi (2.7 mL, 1.7 mol L^{-1} in hexanes, 4.5 mmol) was syringed into this suspension dropwise under Ar at -78° C, and the yellow suspension allowed to warm to room temperature. The resultant white solution was then cooled again to -78° C and a solution of Cp_2Ni (283 mg, 1.5 mmol) in approximately 5 mL THF was syringed in dropwise. The solution was allowed to warm to room temperature before being stirred overnight. It was heated under reflux for 10 minutes, then filtered *in vacuo* and stored at -30° C. This afforded brown crystals of **5.2**.

Yield - 200 mg, 33% with respect to Cp_2Ni

^{1}H NMR (500.05 MHz, THF−d_8), δ (ppm) - 5.74 (1H, s, NC*H*N), 2.79 (6H, s, N*Me*)

^{13}C NMR (125.8 MHz, THF−d_8), δ (ppm) - 164.4 (N*C*HN), 40.5 (N*Me*)

Elemental Analysis - Correct C, H, N analysis could not be obtained despite repeated attempts.

Crystal Data **5.2** - $C_{12}H_{28}Ni_2N_8$, M = 401.84, monoclinic, space group $P2_1/c$, a = 8.4174(7), b = 7.3216(3), c = 14.7973(4) Å, α = 90°, β = 106.898(2)°, γ = 90°, V = 872.57(8) Å^3, Z = 2, ρ_{calcd} = 1.529 g cm^{-3}, Mo-Kα radiation, λ = 0.71073 Å, μ= 2.167 mm^{-1}, T = 180(2) K. 22026 data (1987 unique, R_{int} = 0.078, θ < 27.48°) were collected. *wR2* = 0.0848, conventional R = 0.0376 on F values of 1795 reflections with $F^2 > 2\sigma(F^2)$, S = 1.131, 105 parameters. Residual electron density extrema ±0.398 eÅ^{-3}. The crystals grew as non-merohedral twins. The program TwinRotMat[85] was used to determine the appropriate twin law and generate an HKLF5 file which was used for further refinement cycles. The R values, K values, esds and general background noise were all substantially improved indicating the correct TWIN assignment.

3.3.3 Synthesis of $Cr_2(CH_3NCHNCH_3)_4$, 5.3

N,N′-Dimethylformamidine (0.13 mL, 1.65 mmol) was added to 5 mL of THF. *n*−BuLi (1.0 mL, 1.6 mol L^{-1} in hexanes, 1.65 mmol) was syringed into this solution dropwise under Ar at -78° C, and the yellow suspension allowed to warm to room

temperature. The resultant white suspension was then returned to -78° C. A solution of Cp_2Cr (100 mg, 0.55 mmol) in 5 mL THF was syringed in dropwise before the system was allowed to warm to room temperature. The solution was stirred overnight, heated under reflux for 10 minutes, then filtered *in vacuo* and stored at -30° C. This afforded yellow crystals of **5.3**.

Yield - 15 mg, 15% with respect to Cp_2Cr

Melting Point - Did not melt, sublimed around 300° C

^{1}H NMR (500.05 MHz, THF$-d_8$), δ (ppm) - 8.01 (4H, s, NC*H*N), 3.01 (24H, s, H_3CN)

^{13}C NMR (125.8 MHz, THF$-d_8$), δ (ppm) - 167.1 (N*C*HN), 38.7 (H_3CN)

Elemental Analysis - Correct C, H, N analysis could not be obtained despite repeated attempts.

Crystal Data **5.3** - $C_{12}H_{28}Cr_2N_8$, M = 388.42, monoclinic, space group $P2_1/c$, a = 8.4194(3), b = 7.4038(2), c = 15.0492(6) Å, α = 90°, β = 106.888(1)°, γ = 90°, V = 900.94(5) Å^3, Z = 2, ρ_{calcd} = 1.432 g cm^{-3}, Mo-Kα radiation, λ = 0.71073 Å, μ= 1.215 mm^{-1}, T = 180(2) K. 6533 data (2045 unique, R_{int} = 0.038, $\theta < 27.44°$) were collected. *wR2* = 0.0882, conventional R = 0.0319 on F values of 1665 reflections with $F^2 > 2\sigma(F^2)$, S = 1.028, 106 parameters. Residual electron density extrema ±0.314 eÅ^{-3}.

3.3.4 Synthesis of $Li_2[Mn\{NC(N(CH_3)_2)_2\}_4 \cdot 3\,THF]$, 5.4

1,1,3,3-Tetramethylguanidine (0.48 mL, 4.5 mmol) was stirred in approximately 5 mL THF. *t*−BuLi (2.7 mL, 1.7 mol L^{-1} in hexanes, 4.5 mmol) was syringed into this suspension dropwise under Ar at -78° C, and the yellow suspension allowed to warm to room temperature. The resultant white solution was then cooled again to -78° C and a solution of Cp_2Mn (278 mg, 1.5 mmol) in approximately 5 mL THF was syringed in dropwise. The solution was allowed to warm to room temperature before being stirred overnight before being filtered *in vacuo* and stored at -30° C. This afforded brown crystals of **5.4**.

Yield - 50 mg, 5% with respect to Cp_2Mn

^{1}H NMR (500.05 MHz, THF−d_8), δ (ppm) - 2.63 (48H, s, N*Me*)

^{13}C NMR (125.8 MHz, THF−d_8), δ (ppm) - 103.4 (*C*N_3), 37.49 (*NMe*)

Elemental Analysis - Correct C, H, N analysis could not be obtained despite repeated attempts.

Crystal Data **5.4** - $C_{32}H_{72}Li_2MnN_{12}O_3$, M = 741.84, tetragonal, space group P 4(2) bc, a = 25.5067(2), b = 25.5067(2), c = 13.2394(2) Å, α = 90°, β = 90°, γ = 90°, V = 8613.44(16) Å^3, Z = 8, ρ_{calcd} = 1.144 g cm^{-3}, Mo-Kα radiation, λ = 0.71073 Å, μ= 0.350 mm^{-1}, T = 150(2) K. 12577 data (9680 unique, R_{int} = 0.0728, $\theta < 30.77°$) were collected. $wR2$ = 0.118, conventional R = 0.048 on F values of 9680 reflections with $F^2 > 2\sigma(F^2)$, S = 1.029, 467 parameters. Residual electron density extrema ±0.554 eÅ^{-3}.

3.3.5 Synthesis of $Ni_2(hpp)_4$, 5.5

1,3,4,6,7,8-hexahydro-2*H*-pyrimido[1,2-*a*]pyrimidine (hppH, 150 mg, 1.10 mmol) was stirred in approximately 5 mL of THF. *n*−BuLi (0.7 mL, 1.6 mol L^{-1} in hexanes, 1.10 mmol) was syringed into this solution dropwise under N_2 at -78° C, and the reaction mixture was allowed to warm to room temperature.The resultant white suspension was then added dropwise to a solution of Cp_2Ni (100 mg, 0.55 mmol) in 5 mL THF at -78° C before the system was allowed to warm to room temperature. The solution was stirred overnight, filtered warm and stored at -30° C, affording dark purple crystals of **5.5**.

Yield - 28 mg, 16% with respect to Cp_2Ni

Melting Point - 228 – 324° C

^{1}H NMR (500.05 MHz, THF−d_8), δ (ppm) - 3.32 (16H, t, $^3J_{H\text{-}H}$ = 5.98 Hz, NCH_2), 2.63 (16H, t, $^3J_{H\text{-}H}$ = 5.98 Hz, NCH_2), 1.56 (16H, quin, $^3J_{H\text{-}H}$ = 5.98 Hz, $CH_2CH_2CH_2$)

^{13}C NMR (125.8 MHz, THF−d_8), δ (ppm) - 155 (*C*N_3), 49.3 (N*C*H_2), 46.7

(NCH_2), 25.6 ($CH_2CH_2CH_2$)

Elemental Analysis - found C 50.1, H 7.2, N 24.3, calcd. for $C_{28}H_{48}N_{12}Ni_2$ C 50.2, H 7.2, N 25.0

Crystal Data **5.5** - $C_{28}H_{48}N_{12}Ni_2$, M = 670.20, triclinic, space group P -1, a = 9.6812(6), b = 11.1600(7), c = 14.355(2) Å, α = 98.997(3)°, β = 95.812(3)°, γ = 102.941(3)°, V = 1477.9(2) Å^3, Z = 2, ρ_{calcd} = 1.506 g cm^{-3}, Mo-Kα radiation, λ = 0.71069 Å, μ= 1.316 mm^{-1}, T = 180(2) K. 14243 data (5841 unique, R_{int} = 0.0325, $\theta < 27.60°$) were collected. *wR2* = 0.1037, conventional R = 0.0399 on F values of 4763 reflections with $F^2 > 2\sigma(F^2)$, S = 1.042, 379 parameters. Residual electron density extrema ±0.692 eÅ^{-3}.

3.3.6 Synthesis of $[Cr_2\{HNC(NPh)_2\}_4](Li\cdot 2\,THF)_4(LiCp)_2$, 5.6

1,3-Diphenylguanidine (0.34 g, 1.65 mmol) was stirred in approximately 5 mL of THF. $n-$BuLi (1.6 mL, 1.6 mol L^{-1} in hexanes, 1.65 mmol) was syringed into this solution dropwise under Ar at -78° C, and the reaction mixture was allowed to warm to room temperature. The resultant white suspension was then returned to -78° C. A solution of Cp_2Cr (100 mg, 0.55 mmol) in 5 mL THF was syringed in dropwise before the system was allowed to warm to room temperature. The solution was stirred overnight, heated under reflux for 10 minutes, then filtered *in vacuo* and stored at -30° C. This afforded orange crystals of $[\{Cr_2(HNC(NPh)_2)_4\}(Li\cdot 2\,THF)_4(LiCp)_2]$.

Yield - 50 mg, 11% with respect to Cp_2Cr

^{1}H NMR (500.05 MHz, THF$-d_8$), δ (ppm) - 6.93 (16H, t, Ph), 6.81 (16H, t, Ph), 6.02 (8H, d, Ph) 4.765.00 (10H, m, br, Cp), 3.58 (16H, m, THF CH_2O), 1.75 (16H, m, THF CH_2)), NH not observed.

^{13}C NMR (125.8 MHz, THF$-d_8$), δ (ppm) - 150.9 (CN_3), 128.9 (m-Ph), 126.5 (o-Ph), 123.1(p-Ph) 122.1 (NC), 118.6 (Cp), 67.5 (THF CH_2O, 25.6 (THF CH_2)

Elemental Analysis - found C 67.5, H 5.3, N 12.0, calcd. for $C_{74}H_{78}Cr_2Li_6N_{12}O_3$ (**5.6** - 5 THF solvent molecules) 67.4, H, 5.2, N, 12.7

Crystal Data for **5.6** - $C_{94}H_{118}Cr_2Li_6N_{12}O_8$, M = 1689.64, monoclinic, space group $P2_1/n$, a = 13.3034(2), b = 26.0736(3), c = 13.4077(2) Å, α = 90°, β = 92.383(1)°, γ = 90°, V = 4646.7(1) Å^3, Z = 2, ρ_{calcd} = 1.208 g cm^{-3}, Mo-Kα radiation, λ = 0.71073 Å, μ = 0.294 mm^{-1}, T = 180(2) K. 34121 data (6673 unique, R_{int} = 0.036, $\theta < 25.35°$) were collected. *wR2* = 0.1666, conventional R = 0.0723 on F values of 6673 reflections with $F^2 > 2\sigma(F^2)$, S = 1.139, 542 parameters. Residual electron density extrema ±0.448 eÅ^{-3}.

3.4 Experimental Procedures and Results for Chapter 6

3.4.1 Synthesis of $Mn_6(LH_2)_6(\mu_6{-}O) \cdot 4\,THF$, 6.1

Freshly sublimed 1,2-diaminobenzene (60 mg, 0.55 mmol) was dissolved in 5 mL of THF. n−BuLi (0.7 mL, 1.6 mol L^{-1} in hexanes, 1.10 mmol) was syringed into this solution dropwise under N_2 at -78° C, and the solution allowed to warm to room temperature. A solution of Cp_2Mn (100 mg, 0.55 mmol) in 5 mL THF was cooled to -78° C and the lithiated ligand solution syringed in dropwise. The resulting dark solution was allowed to warm to room temperature. This solution was stirred overnight, then filtered warm *in vacuo* and stored at room temperature, affording pink crystals of **6.1** in a dark pink solution.

Yield - 45 mg, 39% with respect to Cp_2Mn

^{1}H NMR (500.05 MHz, DMSO−d_6), δ (ppm) - 6.46 (12H, m, br, HNC*H*), 6.34 (12H, m, br, HNCHC*H*) 4.35 (12H, s, br, N*H*) 3.58 (m, THF CH_2O), 1.74 (m, THF CH_2)

^{13}C NMR (125.8 MHz, THF−d_8), δ (ppm) - 134.9 (HN*C*), 117.2 (HNCCH*C*H), 114.5 (HNC*C*H), 67.0 (THF *C*H$_2$O), 25.1 (THF *C*H$_2$)

Elemental Analysis - found C 47.9, H 4.7, N 10.7, calcd. for $C_{68}H_{100}MnN_{12}O_9$ C 49.6, H 4.5, N 13.4

Crystal Data for **6.1** - $C_{68}H_{100}Mn_6N_{12}O_9$, M = 1559.24, monoclinic, space group $P2_1/c$, a = 13.2698(2), b = 16.7091(3), c = 16.7888(3) Å, α = 90°, β = 101.780(1)°,

$\gamma = 90°$, $V = 3644.12(11)$ Å^3, $Z = 2$, $\rho_{calcd} = 1.421$ g cm^{-3}, Mo-Kα radiation, $\lambda = 0.71070$ Å, $\mu = 0.070$ mm^{-1}, $T = 180(2)$ K. 32704 data (6640 unique, $R_{int} = 0.0677$, $\theta < 25.35°$) were collected. *wR2* = 0.1318, conventional $R = 0.0458$ on F values of 4771 reflections with $F^2 > 2\sigma(F^2)$, $S = 1.000$, 439 parameters. Residual electron density extrema ±0.386 eÅ^{-3}. Nitrogen bonded H-atoms were directly located by Fourier synthesis and refined isotropically. There was disorder within the THF solvent molecules. For the refinement, a single isotropic displacement parameter was assigned to the O and C atoms.

3.4.2 Synthesis of (η^5−Cp)(LH_2)VV(LH_2)(Li · 4 THF), 6.2

Freshly sublimed 1,2-diaminobenzene (60 mg, 0.55 mmol) was dissolved in 5 mL of THF. *n*−BuLi (0.7 mL, 1.6 mol L^{-1} in hexanes, 1.10 mmol) was syringed into this solution dropwise under N_2 at -78° C, and the solution allowed to warm to room temperature. A solution of Cp_2V (100 mg, 0.55 mmol) in 5 mL THF was cooled to -78° C and the lithiated ligand solution syringed in dropwise. The resulting dark solution was allowed to warm to room temperature. This solution was stirred overnight, then filtered warm *in vacuo* and stored at room temperature, affording green crystals of **6.2** in a dark green solution, in an 8% yield with respect to Cp_2V. When the crystal structure was obtained, the synthesis was adapted to reflect the stoichiometry observed, with 90 mg (0.83 mmol) of 1,2-diaminobenzene and 1 mL *n*−BuLi (1.6 mol L^{-1} in hexanes, 1.65 mmol) used instead. This increased the yield significantly.

Yield - 75 mg, 36% with respect to Cp_2V

^{1}H NMR (500.05 MHz, DMSO−d_6), δ (ppm) - 6.47 (6H, m, HNC*H*), 6.34 (6H, m, HNCHC*H*), 5.30 (5H, s, C_5H_5), 4.36 (6H, s, N*H*), 3.58 (16H, m, THF CH_2O), 1.74 (16H, m, THF CH_2)

^{13}C NMR (125.8 MHz, THF−d_8), δ (ppm) - 135.0 (HN*C*), 117.3 (HNCCH*C*H), 114.6 (HNC*C*H), 103.1 (*C*$_5$H$_5$), 67.1 (THF *C*H$_2$O, 25.2 (THF *C*H$_2$)

Elemental Analysis - found C 57.7, H 7.0, N 11.0, calcd. for $C_{39}H_{55}LiN_6O_4V_2$ C 60.0, H 7.1, N 10.8

Crystal Data for **6.2** - $C_{39}H_{55}LiN_6O_4V_2$, $M = 780.71$, monoclinic, space group $P2_1/c$, $a = 15.3041(1)$, $b = 20.2762(3)$, $c = 13.8669(2)$ Å, $\alpha = 90°$, $\beta = 114.35(3)°$,

$\gamma = 90°$, $V = 3920(1)$ Å^3, $Z = 4$, $\rho_{calcd} = 1.323$ g cm^{-3}, Mo-Kα radiation, $\lambda = 0.71073$ Å, $\mu = 0.524$ mm^{-1}, $T = 180(2)$ K. 34260 data (11221 unique, $R_{int} = 0.0405$, $\theta < 29.98°$) were collected. $wR2 = 0.1719$, conventional $R = 0.0489$ on F values of 7794 reflections with $F^2 > 2\sigma(F^2)$, $S = 1.085$, 483 parameters. Residual electron density extrema ± 1.292 eÅ^{-3}. Several restraints were employed - simu 0.01 0.01 3.8 C26 C27 C25 C24 O1, simu 0.01 0.01 3.8 C35 O3 C34 C33 C32, DFIX 31.000 N1 H1N N2 H2N N5 H5N N6 H6N.

3.4.3 Synthesis of $[Ni_6\{C_6H_4(NH)_2\}_6][Ni_6\{C_6H_4(NH)_2\}_3\{C_6H_4(NH)(N)\}_3(Li \cdot THF)][2(Li \cdot 4\,THF)]$, 6.3

Freshly sublimed 1,2-diaminobenzene (60 mg, 0.55 mmol) was dissolved in 5 mL of THF. $n-$BuLi (0.7 mL, 1.6 mol L^{-1} in hexanes, 1.10 mmol) was syringed into this solution dropwise under N_2 at -78° C, and the solution allowed to warm to room temperature. A solution of Cp_2Ni (100 mg, 0.55 mmol) in 5 mL THF was cooled to -78° C and the lithiated ligand solution added to this dropwise by syringe. The resulting dark solution was allowed to warm to room temperature. It was stirred overnight before being filtered warm *in vacuo*. Storage at room temperature afforded highly air-sensitive purple crystals of **6.3** in a dark solution.

Yield - 60 mg, 67% with respect to Cp_2Ni

Melting Point - does not melt up to 360° C

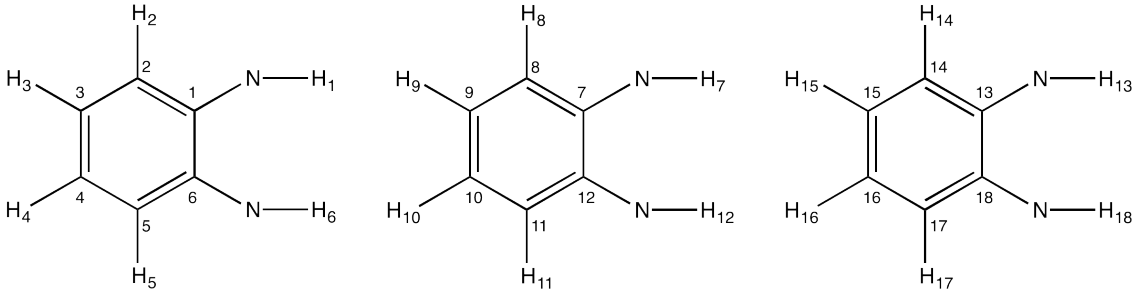

Figure 3.1: The labelling scheme for the three distinct ring systems of **6.3**.

^{1}H NMR (500.05 MHz, DMSO$-$d$_6$), δ (ppm) - 6.45 (6H, d, $^3J_{H\text{-}H} = 7.58$ Hz, $H2$), 6.34-6.28 (12H, m, H3-5), 6.32 (6H, d, $^3J_{H\text{-}H} = 7.58$ Hz, $H8$), 6.14 (6H, t, $^3J_{H\text{-}H} = 7.58$ Hz, $H10$), 6.08, (6H, t, $^3J_{H\text{-}H} = 7.58$ Hz, $H15$), 5.76 (6H, t, $^3J_{H\text{-}H} = 7.58$ Hz,

*H*9), 5.65 (6H, d, $^{3}J_{H\text{-}H}$ = 7.58 Hz, *H*17), 5.55 (6H, t, $^{3}J_{H\text{-}H}$ = 7.58 Hz, *H*16), 5.51 (6H, d, $^{3}J_{H\text{-}H}$ = 7.58 Hz, *H*11), 5.45 (6H, d, $^{3}J_{H\text{-}H}$ = 7.58 Hz, *H*14), 3.59 (84H, m, THF CH_2O), 1.75 (84H, m, THF CH_2), 0.63 (6H, s, *H*7), 0.58 (6H, s, *H*1), 0.43 (6H, s, *H*6), 0.29 (6H, s, *H*13), -0.05 (6H, s, *H*12), -2.10 (6H, s, *H*18)

^{13}C NMR (125.8 MHz, DMSO−d_6), δ (ppm) - 159.4 (*C*18), 158.9 (*C*7), 152.5 (*C*6), 151.0 (*C*1), 147.9 (*C*12), 146.7 (*C*13), 119.6 (*C*10), 119.6 (*C*15), 119.3 (*C*3, 4), 117.2 (*C*8, 17), 116.6 (*C*5), 116.5 (*C*2), 111.3 (*C*14), 110.5 (*C*11), 109.3 (*C*9), 109.0 (*C*16), 67.1 (THF *C*H_2O), 25.2 (THF *C*H_2)

^{7}Li NMR (194.4 MHz, DMSO−d_6), δ (ppm) - 3.20 (s, 2Li), -1.21 (s, 3Li)

Elemental Analysis - found C 51.3, H 6.0, N 12.2, calcd. for $C_{128}H_{181}N_{24}O_{14}Ni_{12}Li_3$ C 51.2, H 6.1, N 11.2

Crystal Data for **6.3** - $C_{64}H_{96.5}N_{12}O_7Ni_6Li_{1.5}$, M = 1508.70, monoclinic, space group $P2_1$, a = 13.2275(3), b = 17.0537(7), c = 16.5692(6) Å, α = 90°, β = 95.948(3)°, γ = 90°, V = 3717.5(2) Å^3, Z = 2, ρ_{calcd} = 1.348 g cm^{-3}, Mo-Kα radiation, λ = 0.68890 Å, μ = 1.543 mm^{-1}, T = 293(2) K. 27906 data (10066 unique, R_{int} = 0.1137, θ < 22.75°) were collected. *wR2* = 0.3641, conventional R = 0.1434 on F values of 4604 reflections with $F^2 > 2\sigma(F^2)$, S = 1.817, 396 parameters. Residual electron density extrema ±1.338 eÅ^{-3}. Ni atoms were refined anistropically, all other atoms isotropically using similar U restraints. Ligands and THF molecules were refined with similar distance restraints. Hydrogen atoms were not included in the refinement.

3.4.4 Synthesis of $[C_{10}H_6(NH)_2]_3V(Li \cdot 2\,THF)_3$, 6.4

1,8-Diaminonaphthalene (87 mg, 0.55 mmol) was dissolved in 5 mL of THF. *n*−BuLi (0.7 mL, 1.6 mol L^{-1} in hexanes, 1.10 mmol) was syringed into this solution dropwise under N_2 at -78° C. A solution of Cp_2V (100 mg, 0.55 mmol) in 5 mL THF was cooled to -78° C and the ligand solution added to this dropwise by syringe. The resulting dark yellow solution was allowed to warm to room temperature. It was stirred overnight before being filtered warm *in vacuo*. Storage at 5° C afforded highly air-sensitive brown crystals in a dark solution.

Yield - 30 mg, 6 % with respect to Cp_2V

Melting Point - 161 – 164° C

^{1}H NMR (500.05 MHz, DMSO−d_6), δ (ppm) - 6.35 (6H, t, $^{3}J_{H\text{-}H}$ = 7.64 Hz, *m*-C*H*), 5.74 (6H, d, $^{3}J_{H\text{-}H}$ = 7.72 Hz, *p*-C*H*), 5.42 (6H, d, $^{3}J_{H\text{-}H}$ = 7.65 Hz, *o*-C*H*), 3.60 (m, THF CH_2O), 1.76 (m, THF CH_2), N*H* not observed)

^{13}C NMR (125.8 MHz, THF−d_8), δ (ppm) - 154.5 (HN*C*), 145.3 (CH*C*CH), 131.3 (CH*C*HCH), 131.2 (NHC*C*CNH), 110.0 (HNC*C*H), 109.9 (CH*C*HC), 72.3 (THF *C*H_2O), 30.4 (THF *C*H_2)

Elemental Analysis - found C 66.8, H 7.9, N 8.4, calcd. for $C_{62}H_{82}Li_3N_6O_8V$ C 66.7, H 7.5, N 8.6

Crystal Data for **6.4** - $C_{62}H_{82}Li_3N_6O_8V$, M = 1111.10, monoclinic, space group C2/c, a = 25.7117(6), b = 14.1550(4), c = 18.9518(6) Å, α = 90°, β = 119.140(1)°, γ = 90°, V = 6024.5(3) Å^3, Z = 4, ρ_{calcd} = 1.225 g cm^{-3}, Mo-Kα radiation, λ = 0.71073 Å, μ = 0.222 mm^{-1}, T = 150(2) K. 21086 data (6087 unique, R_{int} = 0.0640, $\theta < 26.38°$) were collected. *wR2* = 0.2060, conventional R = 0.0686 on F values of 3812 reflections with $F^2 > 2\sigma(F^2)$, S = 1.096, 351 parameters. Residual electron density extrema ±0.683 eÅ^{-3}. Nitrogen bonded H-atoms were directly located by Fourier synthesis and refined isotropically. The THF solvate molecule was disordered. For the refinement, this was modelled as two 1/2 weight molecules with bond length constraints and a common isotropic displacement parameter for the C and O atoms.

3.4.5 Synthesis of $\{[C_{10}H_6(NH)_2]_2Ni\}(Li \cdot 2\,THF)_2$, 6.5

1,8-Diaminonaphthalene (87 mg, 0.55 mmol) was dissolved in 5 mL of THF. *n*−BuLi (0.7 mL, 1.6 mol L^{-1} in hexanes, 1.10 mmol) was syringed into this solution dropwise under N_2 at -78° C. A solution of Cp_2Ni (100 mg, 0.55 mmol) in 5 mL toluene was cooled to -78° C and the ligand solution added to this dropwise by syringe. The resulting dark red solution was allowed to warm to room temperature. It was stirred overnight before being filtered warm *in vacuo*. Storage at -30° C afforded highly air-sensitive orange-red crystals in a dark red solution.

Yield - 125 mg, 34% with respect to Cp_2Ni

Melting Point - did not melt up to 360° C

^{1}H NMR (500.05 MHz, DMSO−d_6), δ (ppm) - 6.12 (4H, t, $^{3}J_{H\text{-}H}$ = 7.61 Hz, *m*-C*H*), 5.41 (4H, d, $^{3}J_{H\text{-}H}$ = 7.36 Hz, *p*-C*H*), 5.26 (4H, d, $^{3}J_{H\text{-}H}$ = 7.54 Hz, *o*-C*H*), 3.58 (16H, m, THF CH_2O), 1.74 (16H, m, THF CH_2), 1.36 (4H, m, N*H*)

^{13}C NMR (125.8 MHz, THF−d_8), δ (ppm) - 155.6 (HN*C*), 140.4 (CH*C*CH), 126.4 (CH*C*HCH), 117.3 (NHC*C*CNH), 102.5 (HNC*C*H), 101.8 (CH*C*HC), 67.5 (THF *C*H_2O), 25.6 (THF *C*H_2)

Elemental Analysis - found C 64.3, H 7.2, N 8.7, calcd. for $C_{36}H_{48}Li_2N_4NiO_4$ (loss of lattice solvent) C 64.2, H 7.2, N 8.3

Crystal Data for **6.5** - $C_{47}H_{64}Li_2N_4NiO_5$, M = 837.61, trigonal, space group P-3, a = 20.0120(6), b = 20.0120(6), c = 8.1348(2) Å, α = 90°, β = 90°, γ = 120°, V = 2821.36(14) Å^3, Z = 3, ρ_{calcd} = 1.451 g cm^{-3}, Mo-Kα radiation, λ = 0.71070 Å, μ = 1.054 mm^{-1}, T = 120(2) K. 20818 data (5366 unique, R_{int} = 0.0556, θ < 30.00°) were collected. *wR2* = 0.1399, conventional R = 0.0478 on F values of 2478 reflections with $F^2 > 2\sigma(F^2)$, S = 0.704, 234 parameters. Residual electron density extrema ±0.715 eÅ^{-3}. Nitrogen bonded H-atoms were directly located by Fourier synthesis and refined isotropically. The THF and toluene solvate molecules were disordered. For the refinement, these were modelled with bond length constraints and common isotropic displacement parameters for the C and O atoms.

Chapter 4

Studies of the Formation of Manganese(II) Complexes Containing Amido and Phosphido Ligands

4.1 Publications Resulting from this Work

F. A. Stokes, R. J. Less, J. Haywood, R. L. Melen, R. I. Thompson, A. E. H Wheatley and D. S. Wright, "Structure and Bonding of the Manganese(II) Phosphide Complex (t−BuPH$_2$)(η^5−Cp)Mn\{μ−(t−BuPH)\}$_2$Mn(η^5−Cp)(t−BuPH$_2$)", *Organometallics*, 2012, **31**, 23.

4.2 Introduction

Manganocene (Cp_2Mn) is the most polar of the first-row transition metal metallocenes, and is therefore most capable of deprotonating organic acids, with the labile cyclopentadienyl ligand acting as a Brønsted base (Chapter 1, Section 1.2.3). The work presented within this chapter aimed to utilise this reactivity to design efficient syntheses of novel compounds, probing the limits of manganocene basicity and establishing appropriate conditions for these reactions to occur. Amido and phosphido complexes of metals have attracted attention as potential precursors to heterometallic arrangements,[86] so for these early studies simple N- and P- donor ligands possessing one or more acidic protons were selected to react with manganocene.

4.3 Results and Discussion

4.3.1 $[(\eta^2\text{- Cp})Mn(BnNHC_2H_4NBn)]_2$, 4.1

The reagent *N,N′*-dibenzylethylenediamine was selected for reaction with manganocene due to its simple structure and potential ability to bridge metal centres. This ligand contains two nitrogen donor atoms, whilst the C_2H_4 unit confers some element of flexibility. The benzyl groups add bulk and provide additional potential metal coordination sites in the form of the aromatic rings. The reaction between manganocene and this ligand had been attempted previously within the Wright group, but no deprotonation by the manganocene took place, with the reaction instead yielding the simple complexation product $[(\eta^1{-}Cp)(\eta^5{-}Cp)Mn(BnNHCH_2)_2]$.[16] This product was observed to have quite a strained conformation due to the bulky nature of the ligand, so it was decided that this reaction should be repeated using *n*-butyllithium to initially deprotonate the ligand before reacting the mono-lithiate with the manganocene (Scheme 4.1).

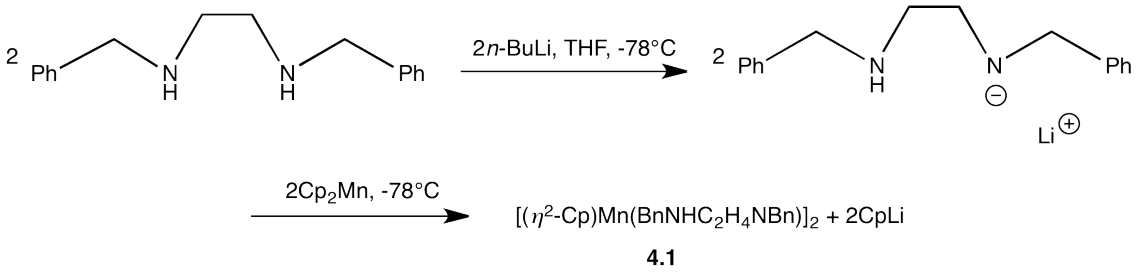

Scheme 4.1: Reaction scheme illustrating the synthetic method employed in the generation of $[(\eta^2\text{- Cp})Mn(BnNHC_2H_4NBn)]_2$, **4.1**.

It was anticipated that the reaction might progress further, with double deprotonation occurring upon complexation with the manganese. However, this was not the case. The sole isolated product, **4.1**, was structurally similar to that obtained from the previously known reaction of manganocene with 8-aminoquinoline, where single deprotonation occurred giving a product with two bridging ligands and two coordinated Cp ligands. The structure of $[CpMn(\mu{-}8{-}HNquin)]_2$ (Compound **1.6**) is discussed in Chapter 1, Section 1.2.3 (Figure 1.8). Crystals of **4.1** were isolated as green blocks in a red solution in a 20% yield (with respect to Cp_2Mn) from the reaction of *N,N′*-dibenzylethylenediamine with *n*-BuLi followed by *in situ* reaction in THF with Cp_2Mn and crystallisation at -30° C. Unfortunately, **4.1** proved too insoluble for satisfactory ^1H or ^{13}C NMR spectra to be obtained. However, **4.1** was characterised using elemental analysis (C, H, N) and single-crystal X-ray diffraction.

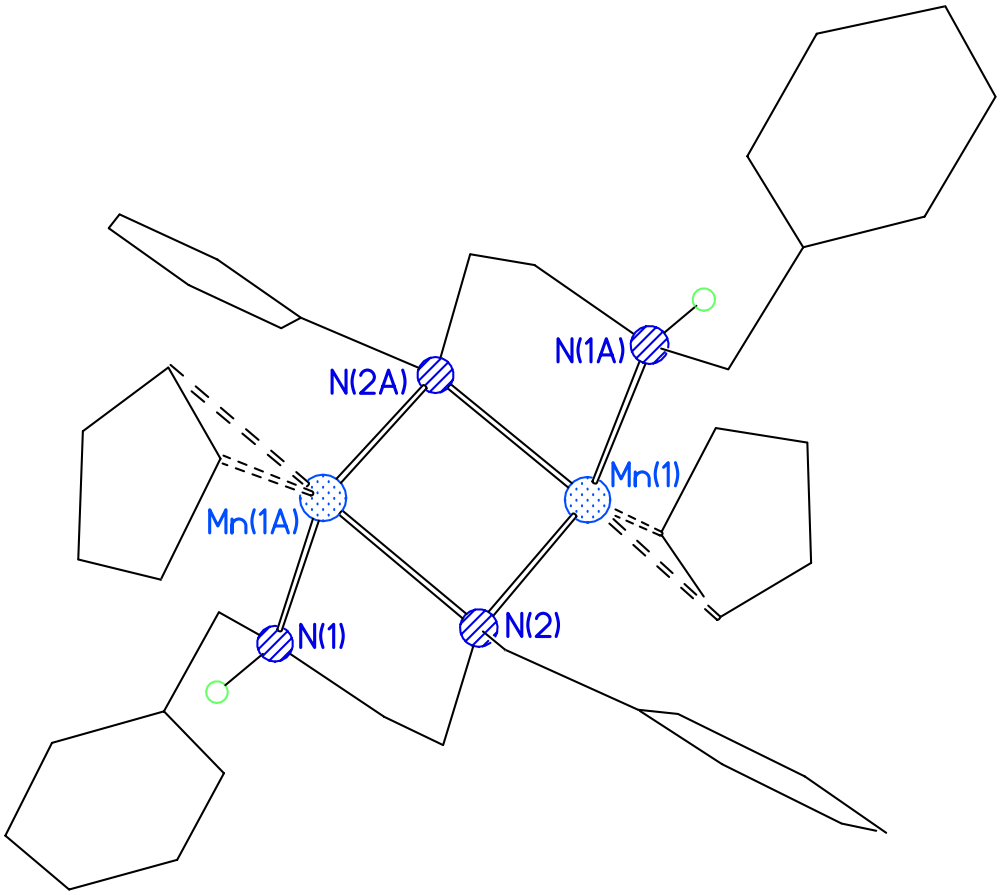

Figure 4.1: The crystal structure of $[(\eta^2\text{-Cp})\text{Mn}(\text{BnNHC}_2\text{H}_4\text{NBn})]_2$, **4.1**. H-atoms, except those attached to N, and one lattice THF molecule omitted for clarity.

Atoms	**Distance (Å)**
Mn(1)···Mn(1A)	2.9582(5)
Mn−C(17/18)	2.412(3) – 2.437(3)
Mn−C(19/20/21)	2.629(3) – 2.771(3)
Mn···$C_{centroid}$	2.2991(3)
Mn(1)−N(2)	2.122(2)
Mn(1A)−N(1)	2.228(2)
Mn(1A)−N(2)	2.203(2)
N(1)−H(1)	0.95(3)
	Angle (°)
Mn(1)−N(2)−Mn(1A)	86.28(7)
Mn(1)−Mn(1A)−N(1)	95.98(6)

Table 4.1: Selected bond lengths and angles for **4.1**.

4.1 is a centrosymmetric dimer in the solid state, in which each Mn centre is bonded to a terminal η^2-Cp ligand [Mn(II)···$Cp_{centroid}$ = 2.2991(3) Å] and is further bonded to a nitrogen donor atom to give a diamond-shaped Mn_2N_2 core featuring average Mn−N bond distances of 2.122(2) Å (Figure 4.1). The structure of **4.1** is consistent with the previously reported literature examples of products formed by the reaction of manganocene with weak organic acids, as discussed in Chapter 1, Section 1.2.3.[16] Each manganese centre is stabilised by a bond to the remaining protonated nitrogen of the ligand [Mn(1)−N(1) 2.227(3) Å]. The aromatic groups are too distant from the Mn centres to form a π-bond, with the rings orientated so as to twist away from the core of the molecule, presumably to minimise steric repulsion. The Mn···Mn separation in this complex is 2.9582(5) Å, which is comparable to that of 2.944(1) Å seen in $[CpMn(\mu-8-HNquin)]_2$.[16] The Cambridge Crystallographic Database reports Mn···Mn separations within similar Mn_2N_2 dimers as usually being significantly shorter than this (2.39 – 2.64 Å),* so it seems unlikely that there is any degree of Mn−Mn bonding in **4.1**.

The formation of **4.1** illustrates the point that the outcomes of reactions of Cp_2Mn and other polar metallocenes with organic acids greatly depend on the acidity of the element−H bonds involved.

4.3.2 $[(\eta^5\text{-}Cp)Mn(EtNHC_2H_4NEt)]_2$, 4.2

The *N,N′*-diethylethylenediamine ligand has a similar structure to the ligand used in the synthesis of **4.1**, with the flexible C_2H_4 moiety and the two nitrogen centres, which can potentially act as donors to two metal centres. The terminal ethyl groups are relatively sterically undemanding, but without any added aromatic functionality that may coordinate the metal centres. It was hoped that significantly altering the nature of the ligands used would affect the solubility of any products formed, potentially avoiding the solubility issues encountered with **4.1** which resulted in the inability to collect suitable NMR data on the product. The synthetic strategy employed was the same as that used in the synthesis of **4.1**, in that it was anticipated that the ligand lacked protons of the requisite acidity to be deprotonated by manganocene, thus *n*−BuLi was used to deprotonate the ligand prior to the reaction with Cp_2Mn (Scheme 4.2).

*Based on a search of the CSD (March 2013), returning 121 results

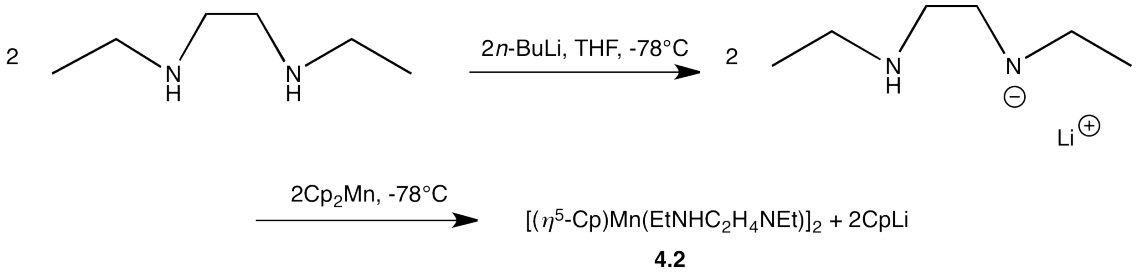

Scheme 4.2: Reaction scheme illustrating the synthetic method employed in the generation of $[(\eta^5\text{-Cp})\text{Mn}(\text{EtNHC}_2\text{H}_4\text{NEt})]_2$, **4.2**.

Crystals of **4.2** were isolated as pale green blocks in a red solution in a 6% yield (with respect to Cp_2Mn) from the reaction of *N,N′*-diethylethylenediamine with *n*-BuLi followed by *in situ* reaction in THF with Cp_2Mn and crystallisation at -30° C. Unfortunately, like **4.1**, **4.2** proved to be too insoluble for satisfactory ^{1}H or ^{13}C NMR spectra to be obtained. However, **4.2** was characterised using single-crystal X-ray diffraction. The product formed from the reaction of manganocene with lithiated *N,N′*-diethylethylenediamine is similar to **4.1**, with two ligands bridging two manganese centres, each of which is still coordinated to a cyclopentadienyl ligand (Figure 4.2), although in the case of **4.2** this ligand is η^5 coordinated. In **4.1**, the Mn−C(Cp) bond distances fell into two distinct categories separated by approximately 0.2 Å, whereas in **4.2** this is not evident, with the Mn−C(Cp) bond distances exhibiting only the small variations expected with η^5 coordination (0.08 Å). This structural difference is likely due to sterics, with the bulkier benzyl ligand present in **4.1** preventing the cyclopentadienyl ligands from coordinating to the metal in an η^5 fashion.

The structure of **4.2** is also comparable to that of $[\text{CpMn}(\mu\text{−8−HNquin})]_2$ (Compound **1.6**) in which single deprotonation of the 8-aminoquinoline ligand had occurred to give a centrosymmetric manganese dimer containing two of the aminoquinoline ligands and two undisplaced cyclopentadienyl ligands. **4.2** is a centrosymmetric dimer in the solid state, within which each Mn centre is bonded to a terminal η^2-Cp ligand [Mn(II)···$\text{Cp}_{\text{centroid}}$ = 2.254 Å] and is further bonded to a nitrogen donor to give a diamond-shaped Mn_2N_2 core featuring average Mn−N bond distances of 2.171(2) Å (Figure 4.2). The structure of **4.2** is consistent with the previously reported literature examples of products formed by the reaction of manganocene with weak organic acids, as discussed in Chapter 1, Section 1.2.3.[16]

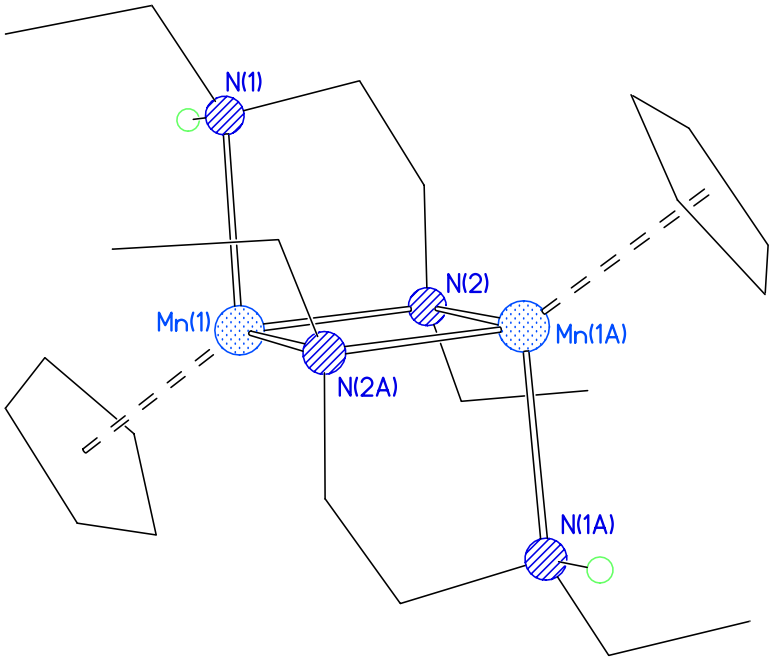

Figure 4.2: The crystal structure of $[(\eta^5\text{-}\,Cp)Mn(EtNHC_2H_4NEt)]_2$, **4.2**. H-atoms, except those attached to N, and one lattice THF molecule omitted for clarity.

Atoms	**Distance (Å)**
Mn(1)−Mn(1A)	2.9720(5)
Mn−C(Cp)	2.501(4) – 2.581(4)
Mn···$C_{centroid}$	2.2539(4)
Mn(1)−N(2)	2.139(2)
Mn(1A)−N(1)	2.282(3)
Mn(1A)−N(2)	2.171(2)
N(1)−H(1)	0.93(3)
	Angle (°)
Mn(1)−N(2)−Mn(1A)	87.18(8)
Mn(1)−Mn(1A)−N(1)	97.75(7)

Table 4.2: Selected bond lengths and angles for **4.2**.

Each manganese centre in **4.2** is stabilised by a bond to the remaining protonated nitrogen of the ligand [Mn(1)−N(1) 2.282(3) Å]. Both of the Mn−N bond lengths are shorter than their equivalents in **4.1** although the Mn···Mn distance of 2.9720(5) Å is similar to that of 2.9582(5) Å seen in the analogous compound, once more longer than is usually seen for this type of Mn_2N_2 compound. Therefore it can be considered unlikely that **4.2** contains any Mn−Mn bonding.

As with **4.1**, the formation of **4.2** gives further information as to the reactivity of manganocene with regard to its ability to deprotonate organic acids. The relevant protons of the *N,N′*-diethylethylenediamine ligands employed in the synthesis of **4.2** are likely to be of a very similar acidity to those in the related ligand *N,N′*-dibenzylethylenediamine, so the formation of a structurally analogous product on reaction with manganocene is unsurprising. This further demonstrates the limitations of manganocene as a Brønsted base, and the necessity of the selection of a sufficiently acidic ligand for deprotonation to occur.

4.3.3 $[(t\text{−}BuPH_2)(\eta^5\text{-}Cp)Mn\{\mu\text{−}(t\text{−}BuPH)\}]_2$, 4.3

The ability of manganocene to behave as a Brønsted base toward weak organic acids, as discussed in Chapter 1, Section 1.2.3, informed the synthetic strategy employed in this reaction. *t*-Butylphosphine was reacted in a 1:1 ratio with manganocene (Scheme 4.3), in the expectation that the primary phosphine would undergo bis-deprotonation and an extended structure would be formed. The pyrimidines utilised in the construction of the amido/imido cage structures (Chapter 1, Section 1.3.3) underwent both mono- and bis-deprotonation by manganocene, and it was anticipated that an analogous situation might occur with the use of primary phosphine reagents. Despite the advances in the field of Mn(II) amide synthesis very little is known about their phosphide analogues,[87;88] with no reactions of primary phosphines with the polar metallocenes having previously been explored, which made this synthetic approach particularly appealing. Crystals of **4.3** were isolated as yellow blocks in a brown solution in a 31% yield (with respect to Cp_2Mn) from the reaction of t−$BuPH_2$ with Cp_2Mn in THF and crystallisation at -30° C. **4.3** was characterised using ^1H, ^{13}C and ^{31}P NMR spectroscopy, elemental analysis (C, H, N), IR spectroscopy, and by single-crystal X-ray diffraction.

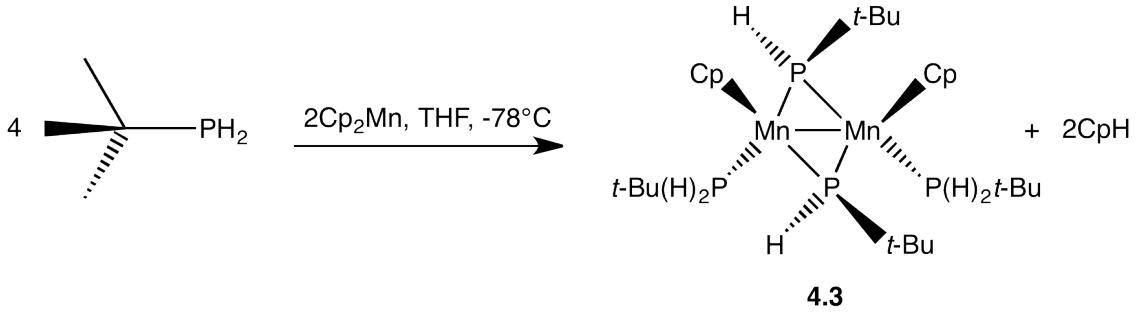

4.3

Scheme 4.3: Reaction scheme illustrating the synthetic method employed in the generation of $[(t{-}\mathrm{BuPH_2})(\eta^5\text{-}\mathrm{Cp})\mathrm{Mn}\{\mu{-}(t{-}\mathrm{BuPH})\}]_2$, **4.3**.

Compound **4.3** proved to be unstable under vacuum, readily losing $t{-}\mathrm{BuPH_2}$, and was also relatively insoluble in hydrocarbon media. ^{1}H, ^{13}C and ^{31}P NMR studies in THF$-\mathrm{d_8}$ (Figures 4.3, 4.4, 4.5 and 4.6) were consistent with the compound being diamagnetic, with sharp resonances observed for Cp at δ 4.20 and 76.2 ppm, respectively. In the ^{1}H NMR spectra, two doublets featuring $^{3}\mathrm{J_{H\text{-}P}}$ coupling at δ 1.53 and 1.07 indicated the presence of two distinct t-butyl environments, with $^{13}\mathrm{C}\{^{1}\mathrm{H}\}$ NMR spectroscopy reinforcing this view by revealing t-butyl signals at δ 33.7 and 31.9 ppm. The ^{1}H NMR spectrum also suggested that the two phosphine/phosphide environments observed in the crystal structure determined later persisted in solution, with the associated hydrogen atoms observed at δ 3.76 ppm (1H, $^{1}\mathrm{J_{H\text{-}P}}$ = 301 Hz) and 3.21 ppm (2H, $^{1}\mathrm{J_{H\text{-}P}}$ = 313 Hz), although both the ^{1}H and the ^{31}P NMR spectra showed the presence of significant amounts of free ($t{-}\mathrm{BuPH_2}$). This was established by comparison of the signals observed in the NMR spectra of **4.3** with those of the phosphine starting material $t{-}\mathrm{BuPH_2}$.

The free $t{-}\mathrm{BuPH_2}$ observed in the NMR spectra of **4.3** may have been the result of some unavoidable hydrolysis of the bridging $t{-}$BuPH groups, although the quantity present suggested that some of the coordinated neutral $t{-}\mathrm{BuPH_2}$ was being displaced in solution by THF. This was consistent with the observed lability of the ligands in **4.3** under vacuum. The proximity in the ^{1}H NMR spectrum of **4.3** of the t-butyl signal at δ 1.07 ppm to that of free phosphine (δ 1.16 ppm) allowed the assignment of the former as the bonded $t{-}\mathrm{BuPH_2}$ ligand in **4.3**. In addition, the low-field shift of the t-butyl signal from the phosphide ligand was consistent with previous studies.[86;89] The presence of free phosphine was reiterated by ^{31}P NMR spectroscopy, with a broad signal observed at δ -75.7 ppm agreeing well with that noted in a reference $t{-}\mathrm{BuPH_2}$ spectrum. A doublet at δ 241.6 ppm ($^{1}\mathrm{J_{H\text{-}P}}$ = 301 Hz) and a triplet at δ 79.7 ppm ($^{1}\mathrm{J_{H\text{-}P}}$= 313 Hz) unambiguously established the presence of both mono-deprotonated phosphide and coordinated phosphine in **4.3**.

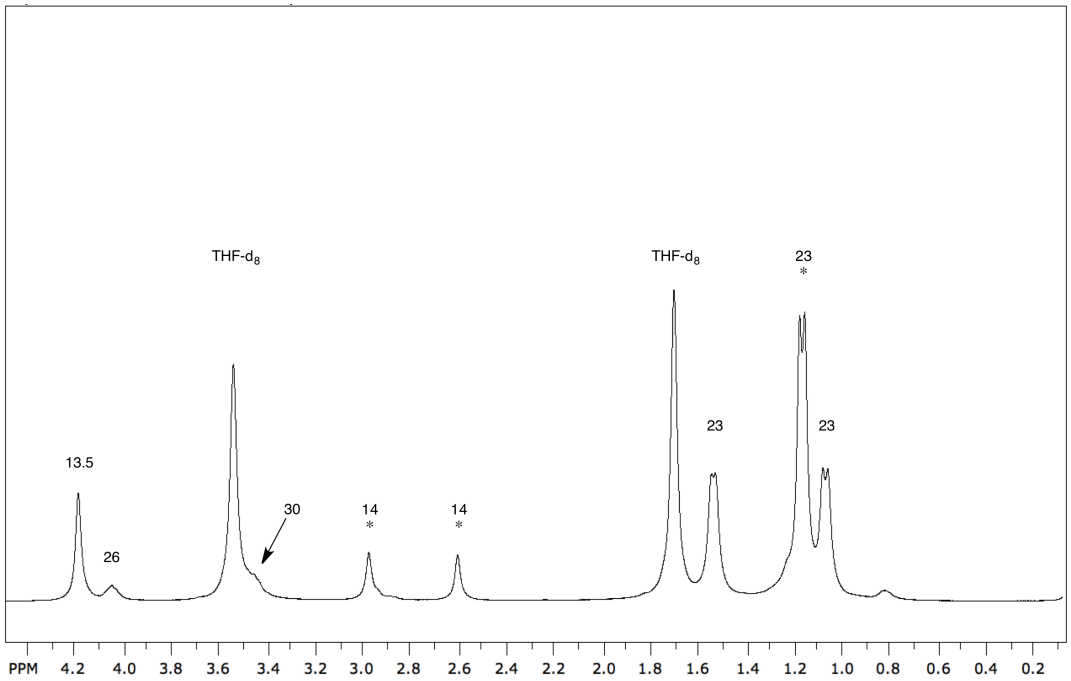

Figure 4.3: ^{1}H NMR spectrum of **4.3** (* denotes free phosphine). Numbers indicate peak widths at half height (Hz). No other peaks were visible between δ -100 and +200 ppm.

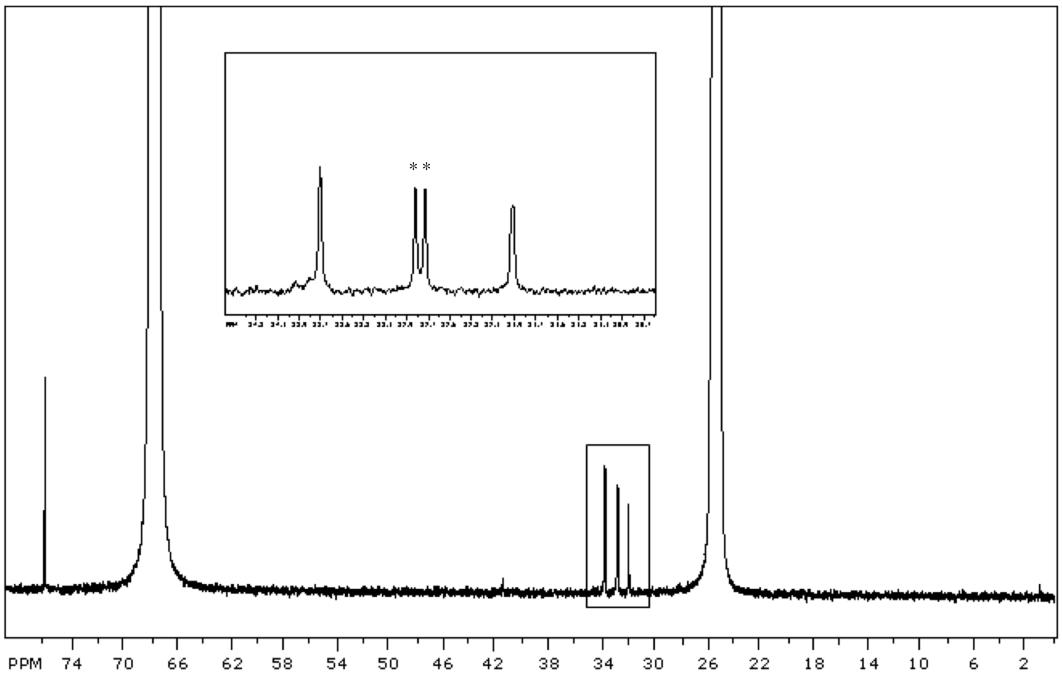

Figure 4.4: ^{13}C{^{1}H} NMR spectrum of **4.3** (* denotes free phosphine). *Inset*, expansion of the boxed aliphatic region.

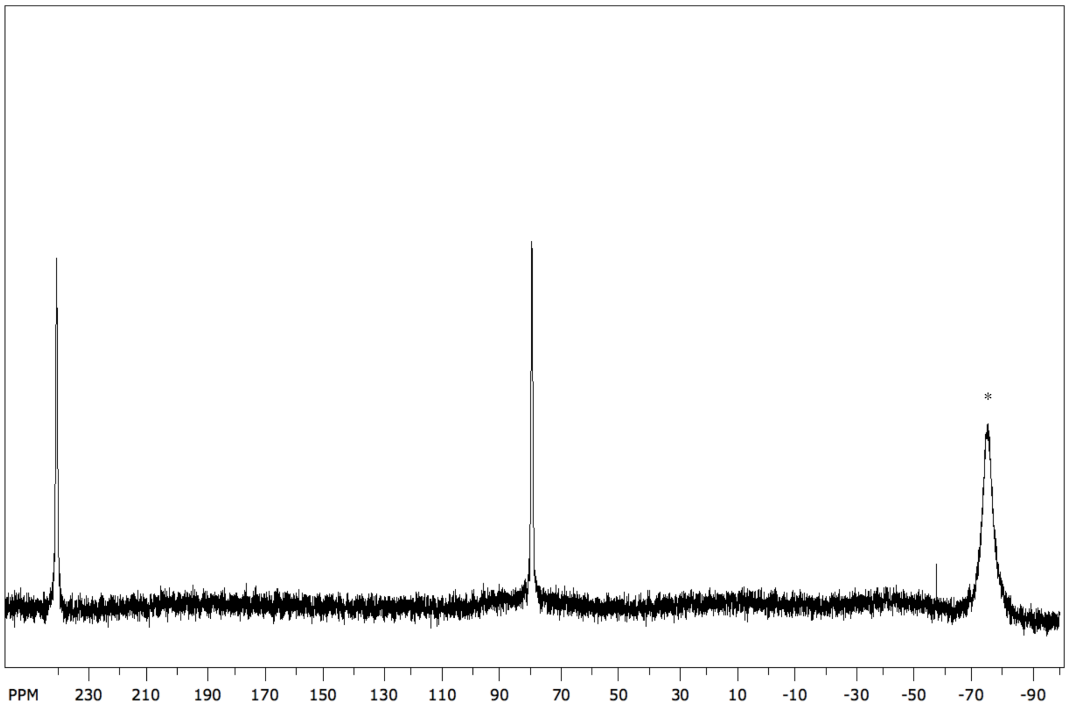

Figure 4.5: ^{31}P NMR spectrum of **4.3** (* denotes free phosphine).

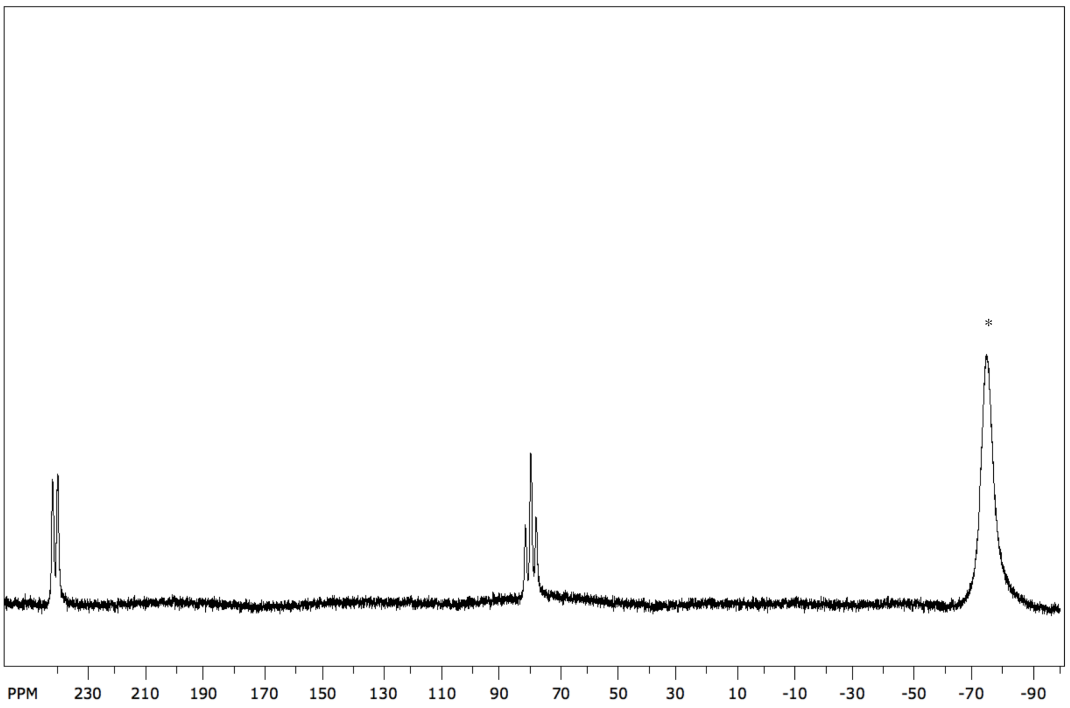

Figure 4.6: ^{31}P{^{1}H}NMR spectrum of **4.3** (* denotes free phosphine).

Full NMR assignments are given in Chapter 3, Section 3.2.3.

IR spectroscopy was undertaken on **4.3**, and the data obtained reinforced the NMR spectroscopic observation of two phosphorus-based ligands, phosphide and phosphine, resulting from the incomplete deprotonation of $t-BuPH_2$ at room temperature. Three P−H stretching modes were noted, at 2397, 2328 and 2234 cm^{-1}, which were replaced by a band at 2290 cm^{-1} upon air exposure (the P−H stretch for the free phosphine starting material is observed at 2288 cm^{-1}).

Attempts were made to induce further reaction, including heating the reaction mixture to reflux before storage at -30° C, and redissolving isolated crystals of **4.3** in THF and reacting them with a further equivalent of *n*-BuLi, however no other products were obtained under these conditions and no further reactions appeared to occur. **4.3** was not recovered from these reactions.

The crystal structure of **4.3** is unexpected in that the 1:1 Cp_2Mn-to-phosphine ratio employed in the reaction supplied sufficient Brønsted base to mono-deprotonate all of the phosphine present. However, NMR spectroscopy and X-ray crystallography reveal an incomplete reaction, in which half of the available phosphine is mono-deprotonated to give the secondary phosphide bridging ligands, whilst the remaining phosphine simply coordinates to the manganese centre with an average Mn−P distance of 2.1937(4) Å, resulting in a diamagnetic Mn(II) phosphide dimer based on a metallocyclic $Mn_2(phosphide)_2$ core (Figure 4.7). For both the bridging phosphides and the coordinated phosphine, H-atoms were observable in the Fourier difference map.

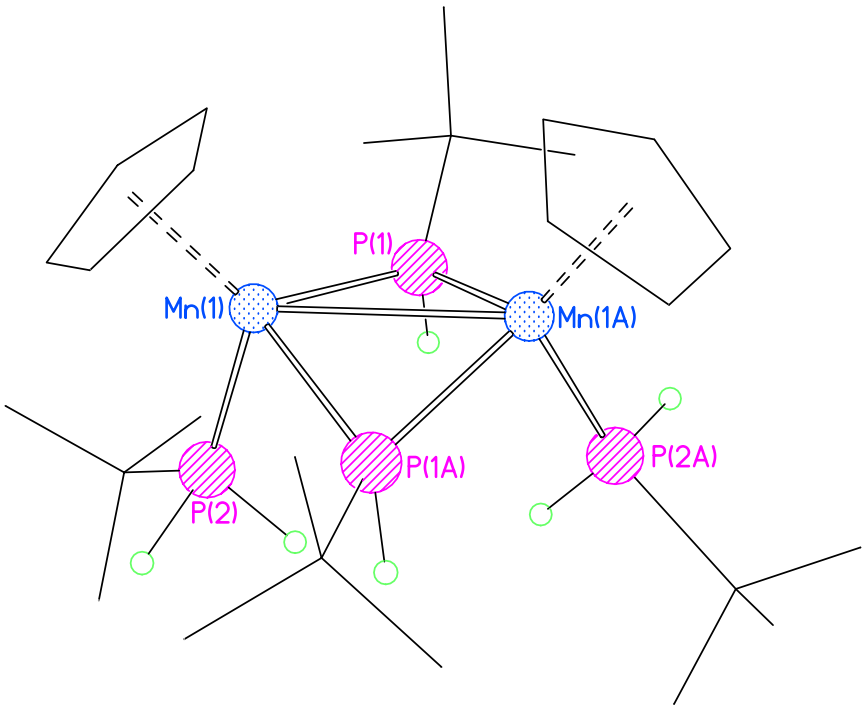

Figure 4.7: The crystal structure of $[(t\text{–BuPH}_2)(\eta^5\text{-Cp})\text{Mn}\{\mu\text{–}(t\text{–BuPH})\}]_2$, **4.3**. H-atoms, except those attached to P, omitted for clarity.

Atoms	**Distance (Å)**
Mn(1)–Mn(1A)	2.8717(4)
Mn–C(Cp)	2.117(2) – 2.178(2)
Mn···$C_{centroid}$	1.7835(2)
Mn(1)–P(1)	2.2218(5)
Mn(1)–P(1A)	2.2500(4)
Mn(1)–P(2)	2.1937(4)
P(1)–H	1.285(19)
P(2)–H	1.29(2) – 1.34(2)
	Angle (°)
P(1)–Mn(1)–P(1A)	90.50(2)
Mn(1)–P(1)–Mn(1A)	79.91(2)

Table 4.3: Selected bond lengths and angles for **4.3**.

In the solid state the core of the structure of **4.3** is folded along the inter-metal axis, giving a 'butterfly' configuration that can be seen in the crystal structure of the molecule (Figure 4.7). The phosphide ligands in the metallocyclic core are relatively *syn*-arranged, such that the sterically undemanding phosphido hydrogen centres project *endo* to the pocket described by the core metallocycle, while the *t*-butyl units are *exo* oriented. The two η^5-cyclopentadienyl ligands that are retained within the dimer are situated in a *syn* fashion with respect to the phosphide *t*-butyl components, allowing the metal-coordinating secondary phosphines to occupy relatively sterically uncongested positions on the same face of the molecule as the phosphide hydrogen atoms. The contrasting actions of the phosphide and phosphine ligands (bridging *vs* terminal) are reflected in the relative metal-phosphorus bond lengths; the short bridging Mn−P(phosphide) (mean 2.24 Å) nevertheless being extended relative to terminal Mn−P(phosphine) (mean 2.19 Å).

The crystallographically verified structure of **4.3** is unique, there being no closely analogous examples of Mn(II) phosphides reported in the literature.[90;91] Silyl phosphide and aryl phosphide Mn(II) complexes are known, but **4.3** represents one of a very limited number of Mn(II) complexes incorporating aliphatic phosphide ligands.[92] The related THF-complexed silyl phosphide dimer $[(Me_3Si)_2PMn(\mu-(Me_3Si)_2P)]_2$ also shares the tendency of **4.3** to lose solvating molecules *in vacuo*.[93]

Of the few salient literature examples of phosphide-bridged dimanganese systems, only the Mn(I) carbonyl complexes *trans*−$(CO)_4Mn\{\mu-P(H)Ph\}_2Mn(CO)_4$,[94] *trans*−$(CO)_4Mn\{\mu-P(H)Ph\}(\mu-Br)Mn(CO)_4$[95] and *trans*−$(CO)_4Mn\{\mu-P(H)Ph\}\{\mu-P(COMe)Ph\}Mn(CO)_4$[96] reveal bridging *sec*-phosphides (Figure 4.8). Within this family of Mn(I) *sec*-phosphides the Mn−P bonds range from 2.346(6) – 2.415(1) Å and are significantly extended relative to the Mn−P bonds in **4.3**, consistent with the lower metal oxidation state present in the former.

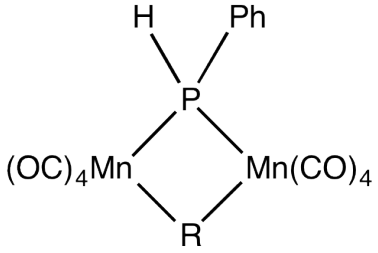

Figure 4.8: The family of Mn(I) *sec*-phosphides. R = μ−P(H)Ph, Br, μ−P(COMe)Ph.[94–96]

In terms of the metal-metal bonding present in **4.3**, a simple electron count suggests that the formation of an inter-metal single bond is plausible, and the observed internuclear distance of 2.8717(4) Å is consistent with this view. The apparently diamagnetic behaviour of **4.3** at room temperature represents an interesting contrast with previous reports of both straightforward half-sandwich Mn(II) complexes[97] as well as with **4.1** and **4.2**, and also with bimetallic $\{M_2(NCy)_4\}\{Mn(\eta^5-Cp)\}_2$ (M = Sb, As).[98] Magnetochemistry suggested high-spin paramagnetic behaviour for these latter complexes, which contain hard N-based cyclohexamide ligands, but the inclusion of softer P-based ligands as seen in **4.3** would be expected to support low-spin Mn(II) and an inter-metal interaction. Indeed, the observation of short Mn−C(Cp) distances (2.1163(8) – 2.1783(2) Å) in **4.3** is consistent with the metal centres being low spin.[99] To investigate this further, the full crystallographic structure was interrogated by quantum mechanical methods using hybrid density-functional calculations (DFT) by Prof. Kloo of the KTH Royal Institute of Technology in Stockholm, Sweden.

The geometry of **4.3** was optimised in spin states of all possible multiplicities, i.e. M = 1, 3, 5, 7, 9, and 11. The energetic spin splitting was calculated at the B3LYP/LACV3P+** and B3LYP*/LACV3P+** levels, but since decreasing the amount of Hartree-Fock exchange from the 20% incorporated in the hybrid density-functional B3LYP to the 15% used in B3LYP* has been shown to better describe complexes of first-row transition metals, the results discussed herein are based on B3LYP* calculations.[100;101] This analysis predicts the ground state to be a so-called broken-symmetry or open-shell singlet state, in which each manganese ion has one unpaired electron that are coupled antiferromagnetically. However, the closed-shell singlet state (having no unpaired electrons) lies only 9 kJ mol^{-1} higher in energy than the open-shell singlet. Considering the accuracy of the methods applied, these two singlet states should be regarded as energetically degenerate. The triplet state (having one unpaired electron on each manganese that couple ferromagnetically) lies 15 kJ mol^{-1} higher than the ground state, while the quintet state (M = 5) lies 127 kJ mol^{-1} above. In spin states of higher multiplicity, i.e. M = 7, 9, and 11, the complex is unstable with respect to metal-ligand (phosphine and cyclopentadienyl) dissociation. Thus, all high-spin states seem to be unimportant for understanding the chemical properties of the complex. It must be concluded that the DFT analysis of the energetic spin splitting predicts the ground state to be of singlet (M = 1) multiplicity, while it is unclear whether this singlet is of closed- or open-shell nature.

An analysis of the corresponding geometries sheds further light on this issue. The geometrically optimised structures of both singlets (open- and closed-shell) are superficially very similar. However, a close inspection of atom-atom distances reveals significant differences; the closed-shell singlet structure displays Mn−Mn = 2.879 Å, Mn−P(phosphido) = 2.263 and 2.286 Å, Mn−P(phosphine) = 2.250 Å, and Mn−C = 2.16 – 2.23 Å, while the corresponding distances for the open-shell singlet structure are Mn−Mn = 3.248 Å, Mn−P(phosphido) = 2.352 and 2.374 Å, Mn−P(phosphine) = 2.291 Å, and Mn−C = 2.17 – 2.28 Å. The observation that the molecular units are more closely bound in the closed-shell structure and that the Mn−Mn distance is markedly shorter (compared to 2.8717(4) Å in **4.3**), combined with the expected valence electron structure of Mn(II), suggests the presence of a direct Mn−Mn single bond in the structure. Modelling clearly points to the highest occupied molecular orbital constituting a direct d-d-mediated Mn−Mn single bond in the closed-shell structure (Figure 4.9).

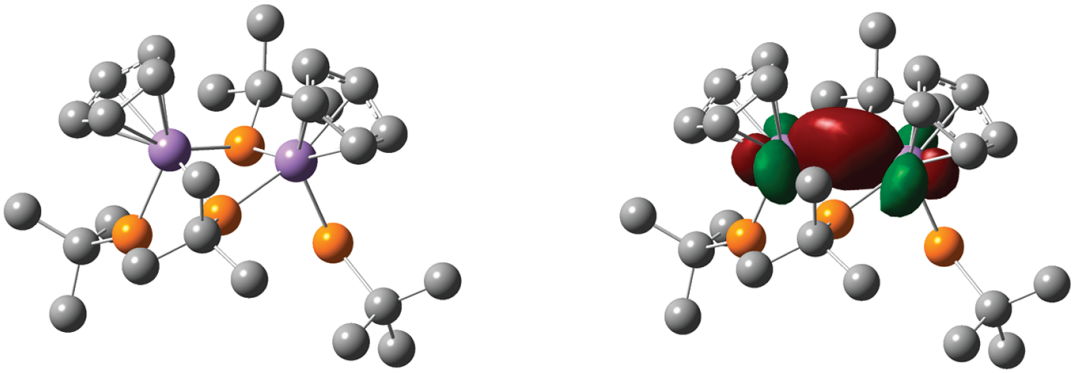

Figure 4.9: Optimised structure of **4.3** (left; Mn = purple, P = gold, C = grey) in the closed-shell singlet state, including the bonding highest occupied molecular orbital (right). H-atoms are omitted for clarity.

Due to the extremely air-sensitive nature of **4.3** and the lability of the t−BuPH$_2$ ligands, detailed magnetic measurements (4.2 – 298 K) proved inconclusive.

In summary, the isolation of **4.3** allows the direct observation of a Mn(II) phosphide complex. This complex exists as a dimer on the basis of the formulation Cp(t−BuPH)Mn · H$_2$P(t−Bu), with the crystallographic observation of an inter-metal distance of 2.8717(4) Å suggesting a direct Mn−Mn interaction. This view is reinforced by DFT studies, which strongly point to a singlet ground state stabilised by a direct Mn−Mn single bond, with support of the metal superstructure provided by two mono-deprotonated phosphide ligands that bridge the metal ions.

4.4 Conclusions

The three complexes discussed within this chapter use simple N- and P-based donor ligands to probe the reactivity of manganocene with weak organic acids. The results presented complement the findings previously demonstrated within the relevant literature, which established that the cyclopentadienyl ligands of manganocene are capable of deprotonating organic acids, although the basicity is not as strong as that of some other organometallic bases such as butyllithium. It had also been previously suggested that this type of reactivity relied heavily on the selection of suitable acidic ligands. With the weak organic acids employed in this chapter, simple manganese-based dimers were formed, and in the cases of **4.1** and **4.2** prior deprotonation of half of the available acidic protons did not alter the reaction pathway. The dimer **4.3** featured a slightly more acidic phosphorus-based ligand, which was deprotonated by manganocene although not to the fullest extent (only half of the available phosphine was singly-deprotonated, the rest remained intact and coordinated to the metal centres). Manganocene is the first-row transition metal metallocene with the most polar M−Cp bonding situation, and is therefore the most capable of behaving as a Brønsted base. The studies presented within this chapter established some of the limits of this basicity, and so provide a framework within which other syntheses could be designed, both for manganocene and for the other, less polar, transition metal metallocenes.

Chapter 5

Studies of the Formation of Transition Metal Complexes Containing Guanidinate and Amidinate Ligands

5.1 Publications Resulting from this Work

J. Haywood, F. A. Stokes, R. J. Less, M. McPartlin, A. E. H. Wheatley, D. S. Wright, "A Quadruply-Bonded $[Cr_2(guanidinate)_4]^{4-}$ Tetraanion", *Chem. Commun.*, 2011, **47**, 4120.

5.2 Introduction

The amidinate and guanidinate ligands have been widely used in reactions with transition metals, particularly in the formation of paddlewheel complexes (see Chapter 1, Section 1.3.2), which have potential applications within catalysis and materials science.[102] Amidinate complexes are known for many of the main group and transition elements, the latter of which have recently attracted interest as olefin polymerisation catalysts,[103;104] whilst metal guanidinate species have been shown to act as pre-catalysts in the dimerisation of aldehydes.[105] The development of novel amidinate and guanidinate materials is still a very active field, as the search continues for interesting molecules which may be capable of catalysis or possess unusual magnetic or structural properties.

5.3 Results and Discussion

Reactions of Transition Metal Metallocenes with *N,N′*-Dimethylformamidine

N,N′-Dimethylformamidine had previously been successfully used in reactions with metallocenes in the Wheatley and Wright groups, as discussed in Chapter 1 Section 1.3.2, with the reactions between nickelocene and manganocene with the lithiated ligand producing a classical paddlewheel structure (Compound **1.11**, Figure 1.18) and a metal cage complex with a tetrahedral oxygen core (Compound **1.12**, Figure 5.2), respectively. Although crystal structures had been obtained for these products, the research had not continued along this route, so some of the early stages of this project involved repeating these reactions and expanding them to include other metallocenes. Amidinate ligands can form either bridging or chelating interactions with metal centres, depending on the bulk of the R groups involved.[106] *N,N′*-Dimethylformamidine (Figure 5.1) was selected as a suitable ligand for metallocenes as it is sterically undemanding and so likely to coordinate in a bridging mode, which could allow for the formation of multiple bonds between metals.

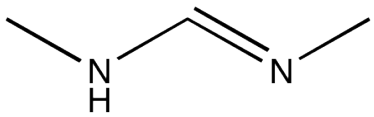

Figure 5.1: The structure of *N,N′*-dimethylformamidine.

5.3.1 $Mn_4O(N,N'-dimethylformamidinate)_6$, 5.1

The reaction between manganocene and the lithiated *N,N′*-dimethylformamidine was expected to proceed according to Scheme 5.1, producing a structure with the familiar paddlewheel motif of the type M_2L_4. Presuming that the metallocene precursor transferred the metal ions in the +2 oxidation state intact, the structure likely obtained would be neutral, with the possibility of multiple bonding between the Mn(II) centres. This work had been undertaken previously within the Wheatley and Wright groups, and was repeated in order to attempt to isolate the product shown in Scheme 5.1.

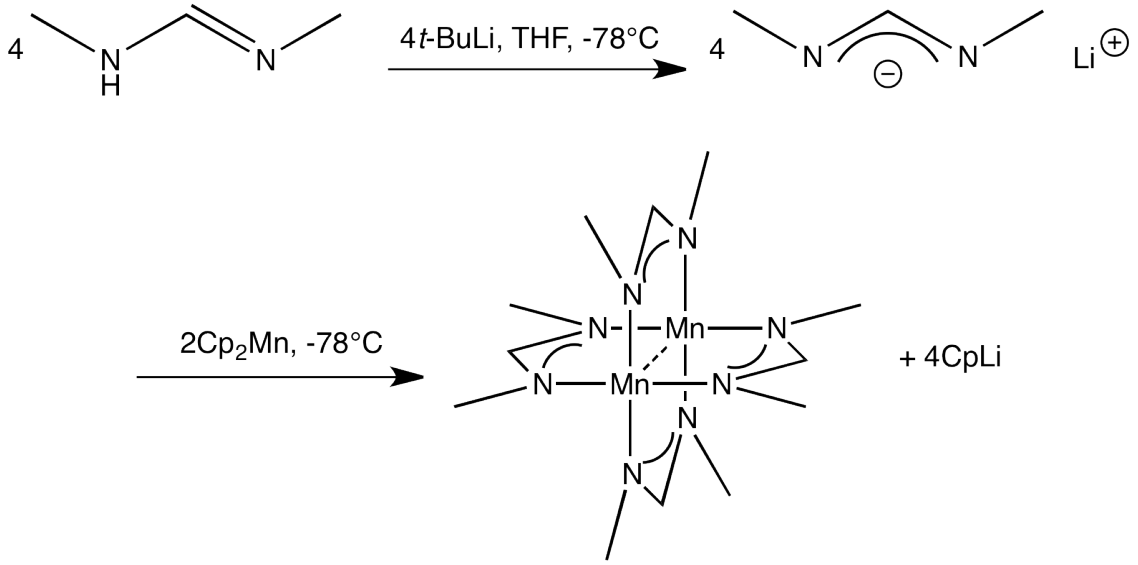

Scheme 5.1: Reaction scheme illustrating the synthetic method employed in the attempted generation of Mn_2(*N,N′*−dimethylformamidinate)$_4$.

It was found that the species targeted in Scheme 5.1 was not isolable from the reaction mixture. Instead, in cases where trace amounts of oxygen or water were presumably present, **5.1** was obtained exclusively. Crystals of **5.1** were isolated as colourless blocks in a pale pink solution in a 33% yield (with respect to Cp_2Mn) from the reaction of *N,N′*-dimethylformamidinine with one equivalent of *t*-BuLi followed by *in situ* reaction in THF with Cp_2Mn and crystallisation at -30° C. **5.1** was characterised using ^{1}H and ^{13}C NMR spectroscopy, elemental analysis and single-crystal X-ray diffraction.

^{1}H and ^{13}C NMR studies of **5.1** were undertaken using DMSO−d_6 as the solvent, as **5.1** was insoluble in deuterated THF and toluene. The ^{1}H NMR spectra showed that the *N,N′*-dimethylformamidine had been deprotonated to give a symmetrical, delocalised ligand. Single-crystal X-ray crystallographic studies of **5.1** were undertaken, which showed that the structure featured an encapsulated oxide at its core, surrounded by four Mn(II) centres, each of which were bridged by *N,N′*-dimethylformamidinate ligands (Figure 5.2).

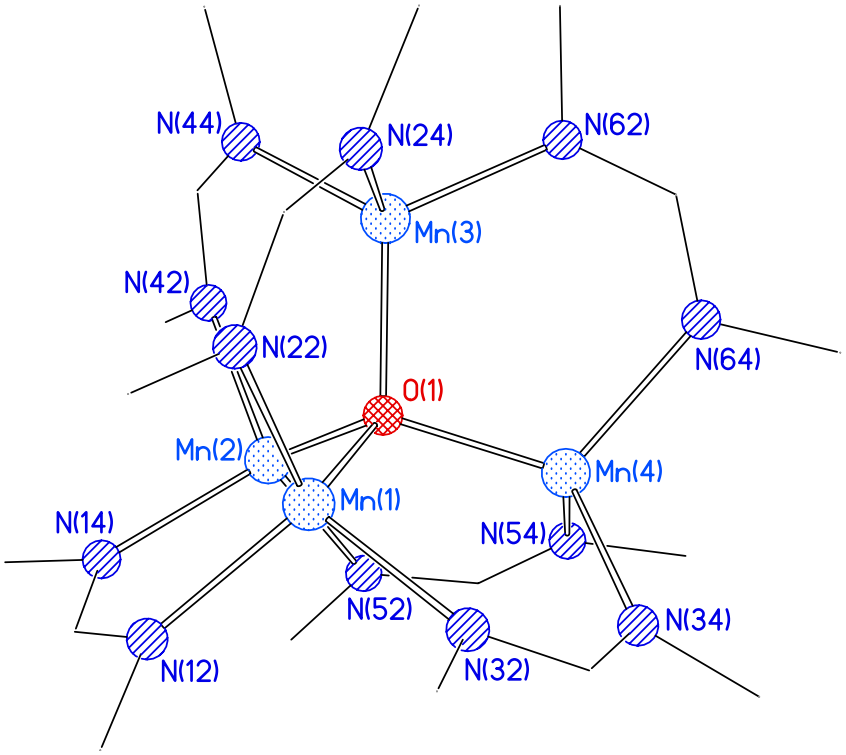

Figure 5.2: The crystal structure of $Mn_4O(N,N'-dimethylformamidinate)_6$, **5.1**. H-atoms omitted for clarity.

Atoms	**Distance (Å)**
O−Mn	2.014(2) – 2.028(2)
Mn−N	2.104(2) – 2.124(2)
	Angle (°)
Mn−O−Mn	107.7(7) – 111.6(1)
O−Mn−N	109.1(1) – 112.9(1)
C−N−Mn	115.9(2) – 128.1(2)

Table 5.1: Selected bond lengths and angles for **5.1**.

The observed structure of **5.1** does not decompose in the presence of trace amounts of oxygen or water, but incorporates oxygen into the complex whilst maintaining the metal +2 oxidation state. The encapsulation of an oxide without decomposition has been observed previously for organometallic complexes, as discussed in Chapter 1, Section 1.3.2 with reference to a relevant example from 2011, in which the reaction between Cp^*Zn and CO_2 produced the zinc oxocarboxylate $[Zn_4(\mu_4\text{-}O)(O_2CCp^*)_6]$ which featured a tetrahedral $[Zn_4O]^{6+}$ core.[48] This zinc acetate structure is relatively common,[107;108] and there are many literature examples of metal complexes with encapsulated oxides, although manganese species are not common amongst them.

The structure of **5.1** is similar to that of $Mn_4O(DPhF)_6$,[50] which also featured a μ_4-O core around which four Mn centres were observed in a tetrahedral arrangement, bridged by six of the bulky *N,N′*-diphenylformamidinate ligands. The synthesis of $Mn_4O(DPhF)_6$ involved layering the reaction solution with moist but oxygen-free hexanes, suggesting that the source of the μ_4-O in $Mn_4O(N,N'-\text{dimethylformamidinate})_6$ was likely to be trace H_2O rather than atmospheric O_2, as oxygen was excluded from the reaction. This hypothesis is also supported in **5.1** by the fact that attempts to introduce controlled amounts of O_2 from a cylinder were undertaken but led to no significant increase in product yield. The possibility also exists that the THF solvent used could be the source of the μ_4-oxide seen in **5.1**, as this product was not isolated when the reaction was attempted using alternative solvents which do not contain oxygen, such as toluene. This type of oxygen abstraction from THF was reported by Mulvey *et al.* in 2010,[109] in a study which utilised a sodium-manganese base to cleave THF bonds, giving a bimetallic species containing an oxide core. This type of reactivity may be possible with the lithium-manganese system of **5.1**, and also fits with the observation of no increase in product yield on addition of O_2 from a cylinder. In order to prove this hypothesis it would be necessary to trap the remaining THF fragments, as in the Mulvey study where crystalline bimetallated butadiene fragments were isolated from the reaction mixture. Upon further exposure to the atmosphere, **5.1** rapidly decomposed to a dark brown, oily substance, indicating that the tolerance of this species for moisture and oxygen is very limited.

5.3.2 Ni_2(*N,N′*−dimethylformamidinate)$_4$, 5.2

The reaction between nickelocene and the lithiated *N,N′*-dimethylformamidine proceeded according to the sequence shown in Scheme 5.2. This work had been undertaken previously within the Wheatley and Wright groups, but was repeated in order to obtain more data and to contribute to a more comprehensive understanding of the reactivity patterns of this *N,N′*-dimethylformamidinate ligand with the various metallocenes utilised in this project. Crystals of **5.2** were isolated as pale brown blocks in a green solution in a 33% yield (with respect to Cp_2Ni) from the reaction of *N,N′*-dimethylformamidinine with one equivalent of *t*-BuLi followed by *in situ* reaction in THF with Cp_2Ni and crystallisation at -30° C. **5.2** was characterised using ^{1}H and ^{13}C NMR spectroscopy, elemental analysis and single-crystal X-ray diffraction. DFT calculations were employed to investigate whether or not any inter-metal bonding was present in this species.

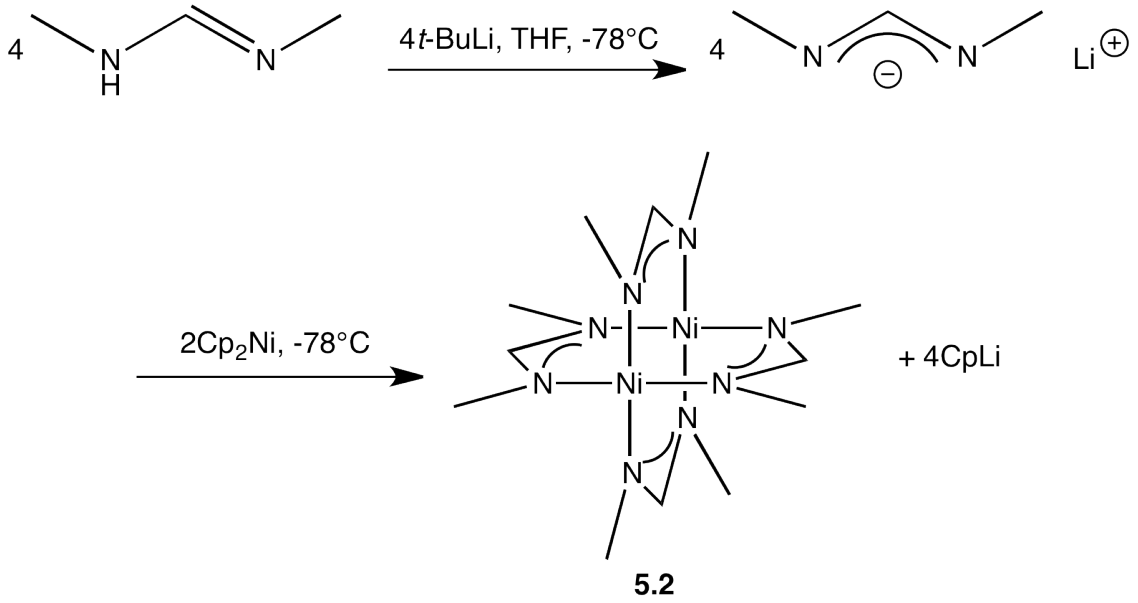

Scheme 5.2: Reaction scheme illustrating the synthetic method employed in the generation of Ni_2(*N,N′*−dimethylformamidinate)$_4$, **5.2**.

^{1}H and ^{13}C NMR studies of **5.2** showed that the *N,N′*-dimethylformamidine had been deprotonated to give a symmetrical, delocalised ligand. Single-crystal X-ray crystallographic studies of **5.2** were undertaken, which showed that the structure contained four amidinate ligands which bridged the two nickel centres in a classic paddlewheel or 'Chinese lantern' arrangement (Figure 5.3). The crystallographically observed Ni···Ni distance of 2.4846(8) Å was similar to that seen in several other reported nickel-amidinate paddlewheel complexes.[110;111]

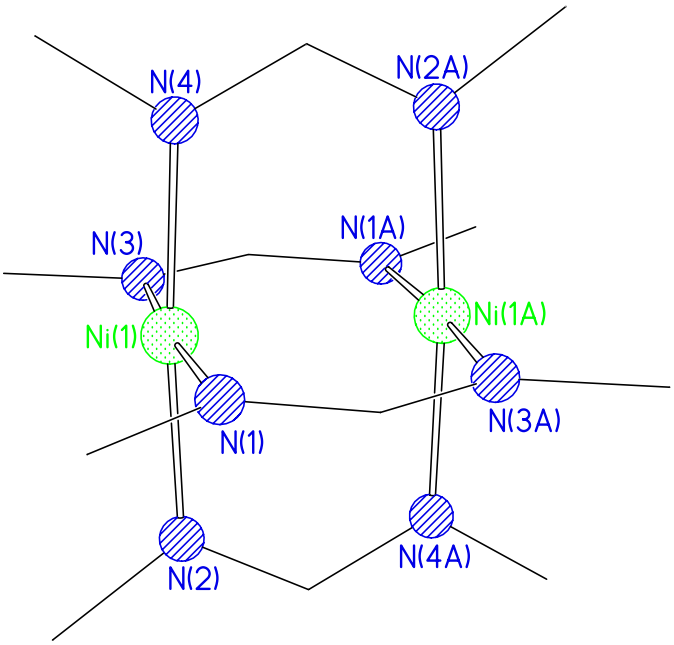

Figure 5.3: The crystal structure of $Ni_2(N,N'-dimethylformamidinate)_4$, **5.2**. H-atoms, except those attached to N, omitted for clarity.

Atoms	**Distance (Å)**
Ni(1)−Ni(1A)	2.4846(8)
Ni−N	1.903(3) – 1.907(2)
C=N	1.308(3) – 1.321(4)
	Angle (°)
N−Ni−N	89.7(1) – 90.2(1)
Ni−Ni−N	86.10(7) – 89.26(7)

Table 5.2: Selected bond lengths and angles for **5.2**.

Each d^8 nickel(II) centre in **5.2** adopted a square planar geometry to give a diamagnetic species with no bonding interaction between the metal centres. Cotton *et al.* suggested that it is impossible to have any true bonding interaction between divalent square planar species, as all bonding and antibonding MOs would be occupied in the manner $\sigma^2\pi^4\delta^2\delta^{*2}\pi^{*4}\sigma^{*2}$ giving a net bond order of zero.[34] To confirm the bond order between metals, DFT calculations were carried out by Professor Lars Kloo at the KTH Royal Institute of Technology in Stockholm, Sweden to see whether the lowest energy configuration for this species would involve any Ni−Ni bonding interaction. These calculations were performed in the D_4 point group, although the true geometrical ground state would have a lower symmetry than this due to the tendency of the methyl groups to rotate. The Ni···Ni distance was calculated to be 2.51 Å with a bond order of 0.056, so essentially zero.

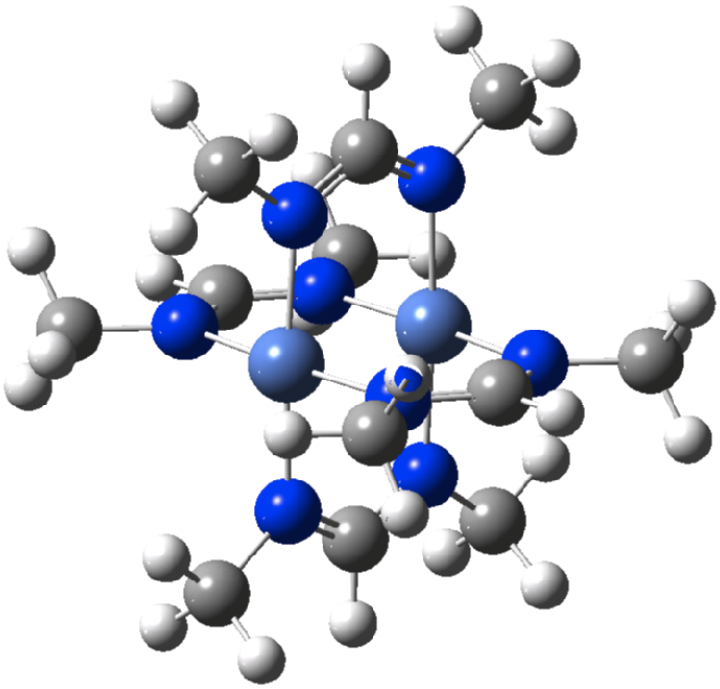

Figure 5.4: The image of the structure obtained following calculations on **5.2** (Ni - pale blue, N = dark blue, C = grey, H = white).

The lack of inter-metal bonding in **5.2** limits its potential uses as the metal centres are unlikely to bind any additional substrates for catalysis. Therefore, it was a logical progression of this research to attempt an analogous reaction with a metal that would be more likely to engage in the formation of metal-metal single or multiple bonds.

5.3.3 $Cr_2(N,N'-dimethylformamidinate)_4$, 5.3

The reaction that led to the formation of **5.1** and **5.2** was repeated with Cp_2Cr (Scheme 5.3) with the aim of synthesising a species with a similar structure to that of **5.2**, but with some degree of inter-metal bonding present. Crystals of **5.3** were isolated as yellow blocks in a brown solution in a 15% yield (with respect to Cp_2Cr) from the reaction of *N,N′*-dimethylformamidinine with one equivalent of *n*-BuLi followed by *in situ* reaction in THF with Cp_2Cr and crystallisation at -30° C. **5.3** was characterised using ^1H and ^{13}C NMR spectroscopy, elemental analysis and single-crystal X-ray diffraction.

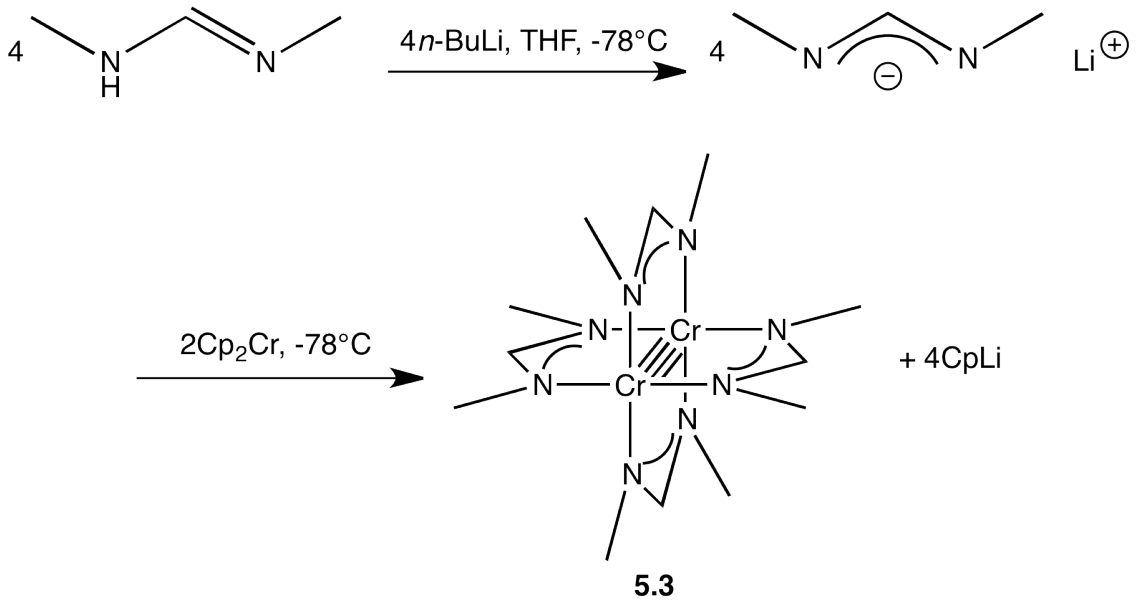

Scheme 5.3: Reaction scheme illustrating the synthetic method employed in the generation of $Cr_2(N,N'-dimethylformamidinate)_4$, **5.3**.

^1H and ^{13}C NMR studies of **5.3** showed that the *N,N′*-dimethylformamidine had been deprotonated to give a symmetrical, delocalised ligand. Single-crystal X-ray crystallographic studies of **5.3** were undertaken, which showed that the structure obtained with Cp_2Cr was analogous to the $Ni_2(N,N'-dimethylformamidinate)_4$ structure **5.2**, with four amidinate ligands bridging two chromium centres in the typical paddlewheel or 'lantern' style (Figure 5.5). The Cr···Cr distance of 1.8722(6) Å is rather short, although it is within the range of Cr···Cr distances found in formally quadruply-bonded arrangements (1.844(2) – 2.612(1) Å).[112–117]

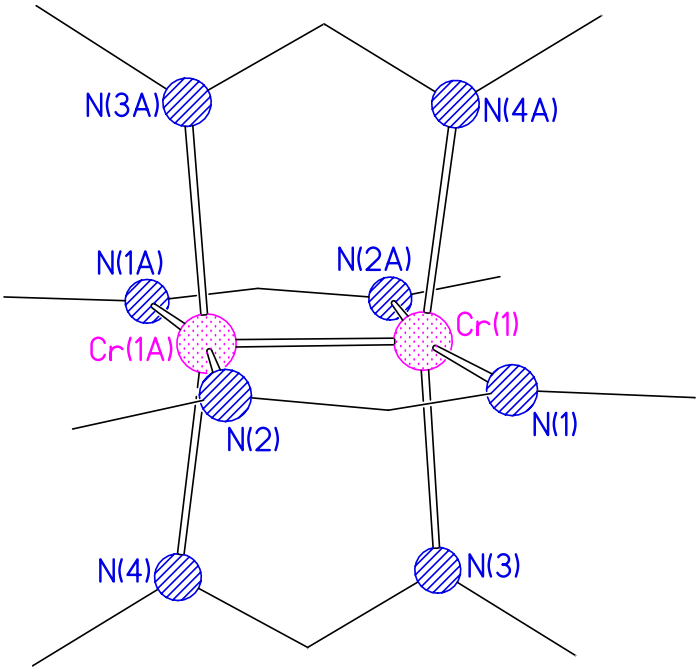

Figure 5.5: The crystal structure of $Cr_2(N,N'-dimethylformamidinate)_4$, **5.3**. H-atoms omitted for clarity.

Atoms	**Distance (Å)**
Cr(1)−Cr(1A)	1.8722(6)
Cr−N	2.033(2) – 2.042(2)
C=N	1.312(3) – 1.318(3)
	Angle (°)
N−Cr−N	89.03(7) – 90.09(6)
Cr−Cr−N	94.77(5) – 96.57(5)

Table 5.3: Selected bond lengths and angles for **5.3**.

Compound **5.3** is similar to many other neutral dinuclear Cr−Cr bonded compounds which have been structurally characterised and which have the general formula $[Cr_2L_4]$ (where L = bidentate ligand). These species all contain two quadruply-bonded Cr(II) centres bridged by four chelating N-ligands and feature metal-metal bonding involving $\sigma, 2\,\pi$ and δ orbitals. **5.3** is very unusual within this class of compounds as it incorporates a particularly sterically unhindered amidinate ligand, giving a kinetically unprotected structure which could potentially be of interest for further research into the coordination and 'trapping' of small molecules. Recent work by Murray *et al.* used Cr_2 units in the trapping of O_2,[118] a desirable process within industry where oxygen is separated from air on a scale of 100 Mtons/year.[119] This area is one in which this research into multiply-bonded paddlewheel species could be developed, as it is possible to obtain a high level of control over the steric and electronic properties of the dimetal products by tuning the donor ligands appropriately (see Chapter 8).

Reactions of Transition Metal Metallocenes with Guanidinates

Guanidinates are structurally similar to the amidinate ligands used in this project, but with the potential to further delocalise and stabilise a negative charge across three nitrogen atoms. As with the amidinate ligands,[102] guanidinate metal complexes are established for many elements of the periodic table,[43] and diverse applications within the fields of catalysis and materials science are emerging.[120;121]

5.3.4 $Li_2[Mn\{NC(N(CH_3)_2)_2\}_4 \cdot 3\,THF]$, 5.4

1,1,3,3-Tetramethylguanidine was selected as a potentially interesting ligand for metallocenes on the basis that it has a slightly more flexible structure than the bicyclic guanidines and is less sterically hindered than many of the popular guanidine ligands. When reacting this ligand with manganocene, the synthetic approach was based on the hypothesis that the likely product would be a paddlewheel of general structure $[Mn_2L_4]$, with two Mn(II) centres bridged by four guanidinate ligands, as outlined in Scheme 5.4. Crystals of **5.4** were isolated as brown blocks in a brown solution in a 5% yield (with respect to Cp_2Mn) from the reaction of 1,1,3,3-tetramethylguanidine with one equivalent of *n*-BuLi followed by *in situ* reaction in THF with Cp_2Mn and crystallisation at -30° C. **5.4** was characterised

using ^{1}H and ^{13}C NMR spectroscopy, elemental analysis and single-crystal X-ray diffraction.

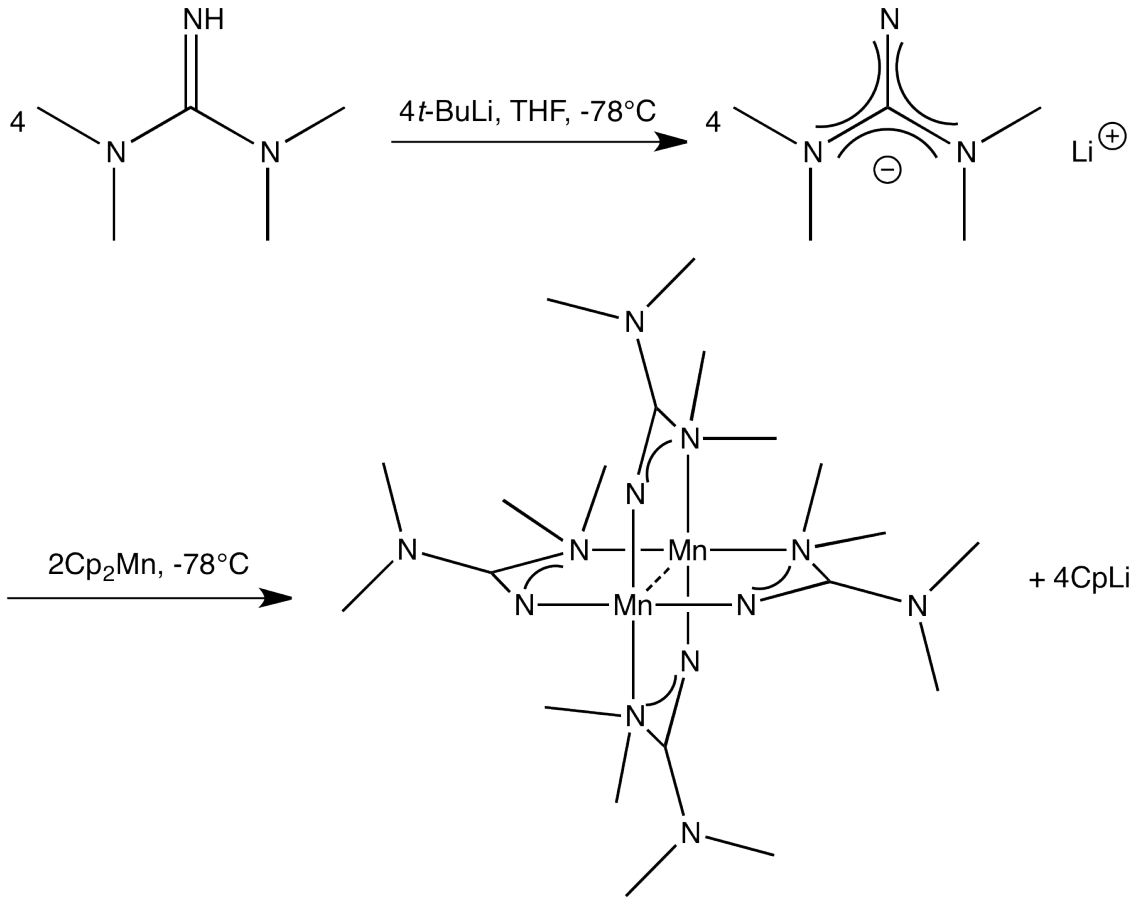

Scheme 5.4: Reaction scheme illustrating the synthetic method employed in the attempted generation of $Mn_2(1,1,3,3-$tetramethylguanidinate$)_4$, **5.4**.

^{1}H and ^{13}C NMR studies showed that the 1,1,3,3-tetramethylguanidine ligand had been deprotonated, with the only ^{1}H signal visible being those of the methyl protons at 2.6 ppm (the starting material contains a very broad NH signal at 5.1 ppm). In order to elucidate the solid-state structure of **5.4** single-crystal X-ray crystallographic studies were undertaken, which showed that rather than adopting the expected paddlewheel configuration, **5.4** featured a spirocyclic $MnLi_2$ core bridged by four guanidinate ligands in a monodentate fashion utilising coordination through the deprotonated central nitrogen (Figure 5.6). In contrast to all of the other novel species reported within this chapter, **5.4** is not a transition metal dimer, but instead has an asymmetric bimetallic arrangement.

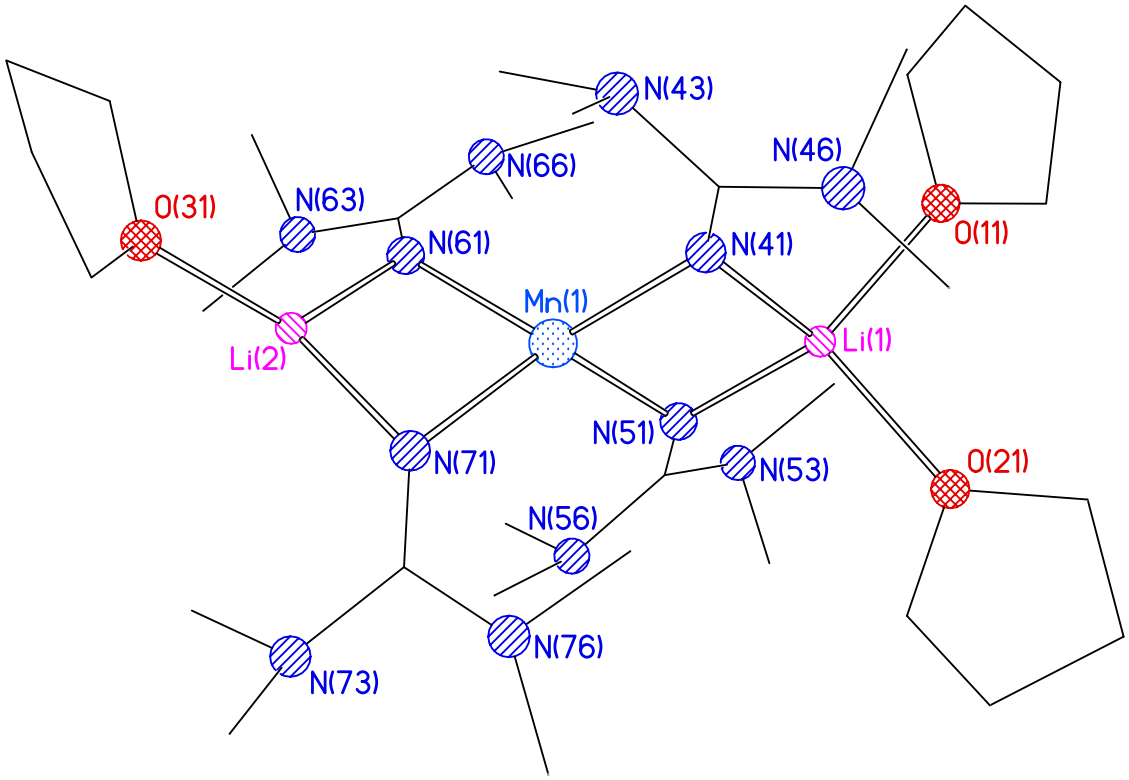

Figure 5.6: The crystal structure of $Li_2[Mn\{NC(N(CH_3)_2)_2\}_4 \cdot 3\,THF]$, **5.4**. H-atoms omitted for clarity.

Atoms	**Distance (Å)**
Mn−N	2.094(2) – 2.119(2)
Mn−Li	2.724(5) – 2.816(5)
Li−N	1.927(5) – 2.036(5)
Li(1)−O	2.046(4) – 2.056(4)
Li(2)−O	1.942(5)
	Angle (°)
Mn−N−Li	47.9(1) – 50.7(1)
N−Mn−N (Li-bridged)	88.8(7) – 91.8(7)
N−Mn−N	127.6(7) – 125.1(7)

Table 5.4: Selected bond lengths and angles for **5.4**.

The observed structure of **5.4** is somewhat unusual in that it adopts an asymmetrical coordination mode with regard to the THF molecules, with the lithium ion on one side of the molecule coordinated to a single THF unit, whilst the other lithium ion is bis-solvated. The reason for this is unclear, although it seems likely to be some steric consideration that arises in the solid state, such as packing constraints within the crystal lattice. There are no obvious intermolecular contacts within the lattice that would account for this asymmetric coordination, and only one other compound featuring this type of asymmetric Li···THF coordination has been reported.[122]

The monodentate guanidinate bridging mode seen in **5.4** is not particularly unusual, with several examples of this type of coordination having been reported for various transition metals.[123–125] Within **5.4**, four bridging ligands each coordinate through one nitrogen centre to give a distorted tetrahedral arrangement around the central manganese with N−Mn−N angles ranging from 88.8(7) – 127.6(7)°. Several examples of compounds featuring a structurally similar Li−Mn−Li spirocyclic core were reported by Andersen *et al.* in 1976[126] and Morris and Girolami in 1989 (Figure 5.7),[127] although these and all other relevant examples feature alkyl rather than nitrogen-based ligands.[128] The Mn···Li bond distances within the Morris and Girolami structures are, on average, 2.6 Å, so comparable to the distances within **5.4** which range from 2.724(5) – 2.816(5) Å.

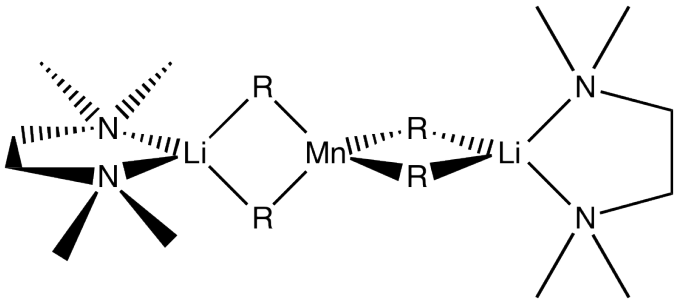

Figure 5.7: The series of $[Li_2(TMEDA)_2][MnR_4]$ complexes characterised by Morris and Girolami (R = Me, Et, CH_2CH_2-t-Bu, *n*-Bu, CH_2SiMe_3, Ph).[127]

In their investigation into thirteen-electron Mn(II) tetraalkyls, Morris and Girolami noted the unusual stability of these compounds. They reasoned that $[Li_2(TMEDA)_2][MnR_4]$ species were resistant to β-elimination up to 110° C due to a shift to the left in the equilibrium of $[MnR_4]^{2-} \rightleftharpoons [MnR_3]^{3-}$, caused by the complexation of the TMEDA to the lithium cations. This was postulated to reduce the Lewis acidity of the lithium and to inhibit the dissociation of LiR from

$Li_2[MnR_4]$. A similar effect could be in operation in the observed formation of **5.4**, through the coordination of THF rather than TMEDA to the lithium cations. This complexation could confer a greater stability to the complex, leading to the preferential formation of **5.4** over any paddlewheel-like dimer structure which would likely have a weak bonding situation between the manganese centres.

Compound **5.4** represents a different type of complex from the other transition metal amidinate and guanidinate species discussed in this chapter. The other species all feature bridging through a delocalised N=C=N moiety, whereas the bridging in **5.4** occurs through a single nitrogen donor. Also, the bridge formed in **5.4** is between two metals from different blocks of the periodic table, rather than between two transition metals to form a simple dimer of the type M_2L_4.

5.3.5 $Ni_2(hpp)_4$, 5.5

Bicyclic guanidines and guanidinates have proven popular ligand choices for transition metals in the past,[129] having a degree of structural rigidity as well as containing potential donor atoms at a suitable distance for bridging metal atoms. They have physical, electronic and chemical properties that differentiate them from their acyclic counterparts, with these characteristics imparted by their rigid framework.[129;130] The anionic guanidinate anion hpp^- has been particularly well studied.[131;132] It is well suited for bridging metal centres as the nitrogen frontier orbitals project in a parallel fashion from the molecule and it is electron-rich, due to a contribution from its zwitterionic resonance form (Figure 5.8).[129;130]

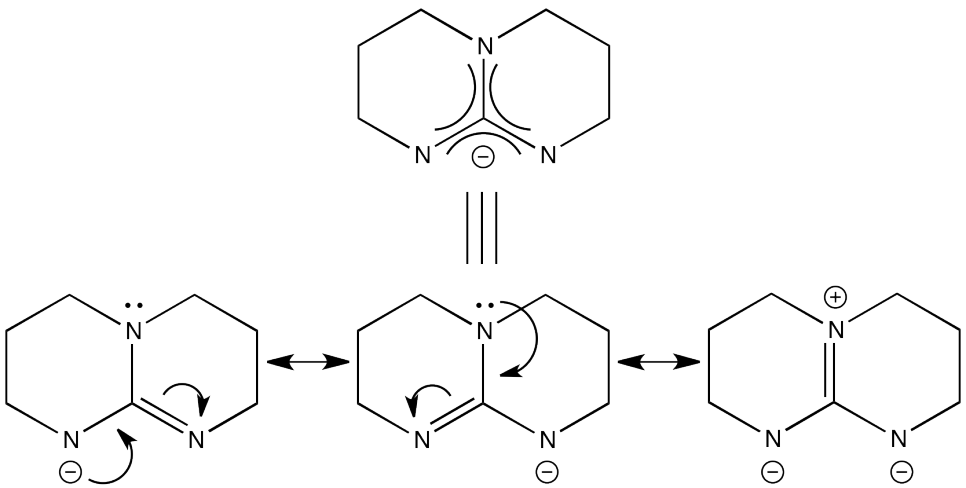

Figure 5.8: The resonance forms of the guanidinate anion hpp^-.

As discussed in Chapter 1 Section 1.2.2, hpp^- reacted with manganocene in a stepwise nucleophilic substitution reaction to give first the neutral species $[CpMn(hpp)]_2$ then the dimeric manganate species $[LiMn(hpp)_3]_2$.[11] Reaction with vanadocene gave the paddlewheel complex $[V_2(hpp)_4]$, which was capable of trapping oligomeric CpLi fragments in the solid state.[22] It was decided to extend the study of this ligand with transition metal metallocenes by attempting the reaction of hpp^- with nickelocene, Cp_2Ni, in the expectation that the reaction would proceed according to Scheme 5.5. Crystals of **5.5** were isolated as purple blocks in a dark solution in a 16% yield (with respect to Cp_2Ni) from the reaction of hppH with one equivalent of *n*-BuLi followed by *in situ* reaction in THF with Cp_2Ni and crystallisation at -30° C. **5.5** was characterised using ^1H and ^{13}C NMR spectroscopy, elemental analysis and single-crystal X-ray diffraction.

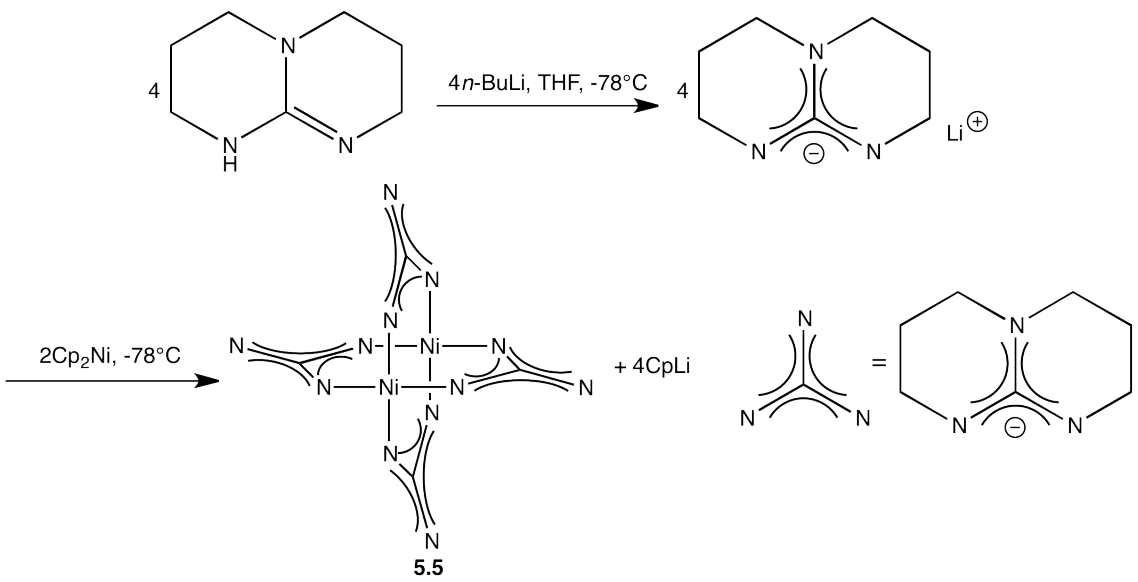

Scheme 5.5: Reaction scheme illustrating the synthetic method employed in the generation of $Ni_2(hpp)_4$, **5.5**.

^1H and ^{13}C NMR studies showed that the hppH ligand had been deprotonated to give the hpp^- anion. In order to elucidate the solid-state structure of **5.5** single-crystal X-ray crystallographic studies were undertaken, which showed that the structure adopted the anticipated paddlewheel arrangement, with two nickel centres bridged by the four guanidinate ligands (Figure 5.9).

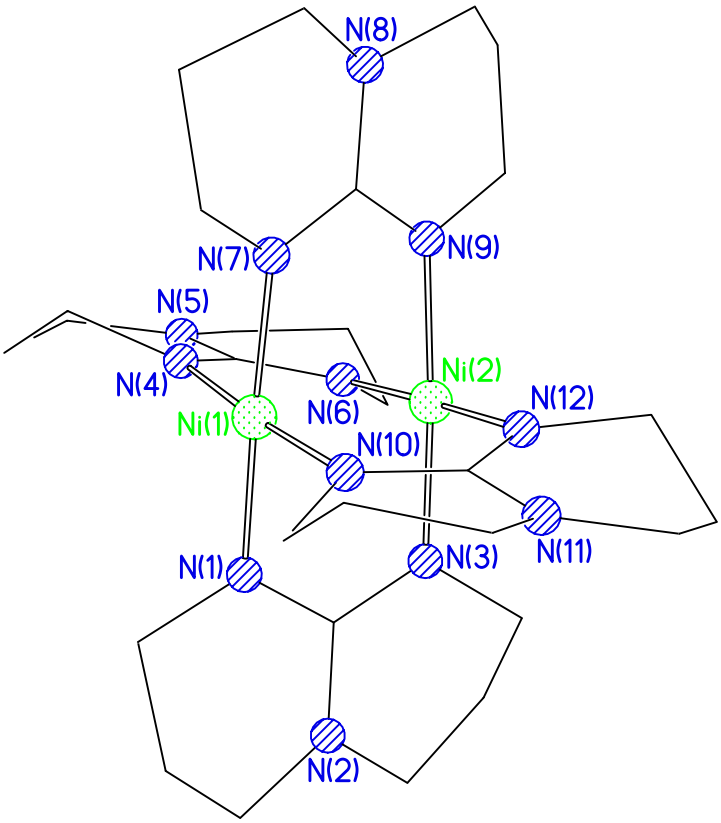

Figure 5.9: The crystal structure of $Ni_2(hpp)_4$, **5.5**. H-atoms omitted for clarity.

Atoms	**Distance (Å)**
Ni(1)–Ni(1A)	2.3753(5)
Ni–N	1.890(2) – 1.916(2)
C=N (bridging)	1.319(4) – 1.335(3)
N(1/4/7/10)···N(3/6/9/12)	mean 2.30
	Angle (°)
N–Ni–N	88.40(7) – 91.36(1)
Ni–Ni–N	86.76(7) – 90.08(7)

Table 5.5: Selected bond lengths and angles for **5.5**.

In contrast to the analogous vanadium complex, this species does not trap oligomeric CpLi fragments in the solid state, which may be due to the fact that replacing the vanadium centres with nickel altered the structure enough to prevent this from occurring. The Ni···Ni distance of 2.3753(5) Å in **5.5** is significantly larger than that seen in the V≡V species (1.933(1) Å) as there is no inter-metal bonding present in the former, and this in turn leads to the nitrogen centres responsible for coordinating the CpLi fragments being further apart (mean 2.30 Å in **5.5** compared to mean 2.63 Å in **1.13**) ,and therefore not having the required ligand bite for Li^+ coordination.

The Ni···Ni distance of 2.3753(5) Å is shorter than that seen in **5.2** (2.4846(8) Å), probably due to the greater rigidity of the ligand used in **5.5** forcing the metal centres slightly closer together in the latter compound. The bonding motif is the same in both of these compounds, with two Ni(II) centres of square planar geometry, each bonded to four nitrogen centres, giving a classical paddlewheel structure. The argument made by Cotton *et al.* against the possibility of forming bonds between two Ni(II) centres (discussed in Section 5.3.2) is also valid for **5.5** and this, coupled with the large inter-metal distance seen in **5.5**, strongly indicates that there is no formal bonding interaction between the nickel centres in this structure.

The synthesis of **5.5** complements the previously reported findings relating to the reactions of first-row transition metal metallocenes with the anion hpp^-. The electronic structure of the metals involved (and therefore their ability to form inter-metal bonds) seems to play an important role in determining the nature of the species formed, as can be seen from the two structurally similar paddlewheel species originating from the reactions with vanadocene and nickelocene, in which only the former has the ability to trap oligomeric CpLi fragments. This observation informs future synthetic decisions by providing more information as to how various metallocenes interact with the same ligand to form fundamentally different species. The products formed vary structurally, as can be seen from the comparison of these vanadium- and nickel-based paddlewheels (Compounds **1.13** and **5.5** respectively) with the $[LiMn(hpp)_3]_2$ species formed from the reaction with manganocene (Compound **1.5**).

5.3.6 $[Cr_2\{HNC(NPh)_2\}_4](Li \cdot 2\,THF)_4(LiCp)_2$, 5.6

Following the successful reaction with a lithiated amidine resulting in **5.3**, the reaction of chromocene with lithiated 1,3-diphenylguanidine was attempted according to Scheme 5.6 with the intention of using a more complex ligand containing more metal coordination sites in the form of phenyl groups. Crystals of **5.6** were isolated as orange blocks in a dark solution in an 11% yield (with respect to Cp_2Cr) from the reaction of 1,3-diphenylguanidine with one equivalent of *n*-BuLi followed by *in situ* reaction in THF with Cp_2Cr and crystallisation at -30° C. **5.6** was characterised using ^1H and ^{13}C NMR spectroscopy, elemental analysis and single-crystal X-ray diffraction.

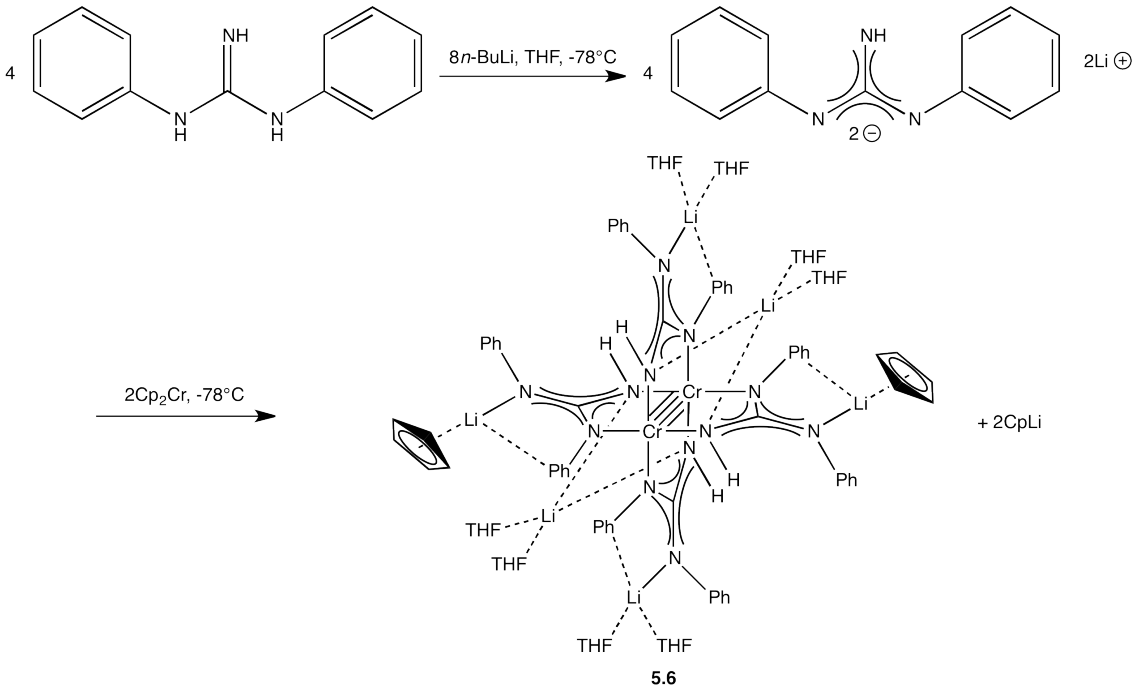

Scheme 5.6: Reaction scheme illustrating the synthetic method employed in the generation of $\{Cr_2(HNC(NPh)_2)_4\}(Li{\cdot}2\,THF)_4(LiCp)_2$, **5.6**. This scheme reflects the stoichiometry of the products, although in fact the best yields of **5.6** were obtained with a 3:3:1 ratio of 1,3-diphenylguanidine:*n*-BuLi:Cp_2Cr (discussed below).

^1H and ^{13}C NMR studies of **5.6** were ambiguous regarding the charge of the 1,3-diphenylguanidinate ligand itself as no NH signal was observed. The shifts indicated that metal coordination had taken place, and in order to elucidate the solid-state structure of **5.6** and therefore be better able to interpret the NMR data, single-crystal X-ray crystallographic studies were undertaken. These showed that the product **5.6** was highly unusual, being the first example of a tetraanionic, quadruply-bonded Cr(II) compound (Figure 5.10).

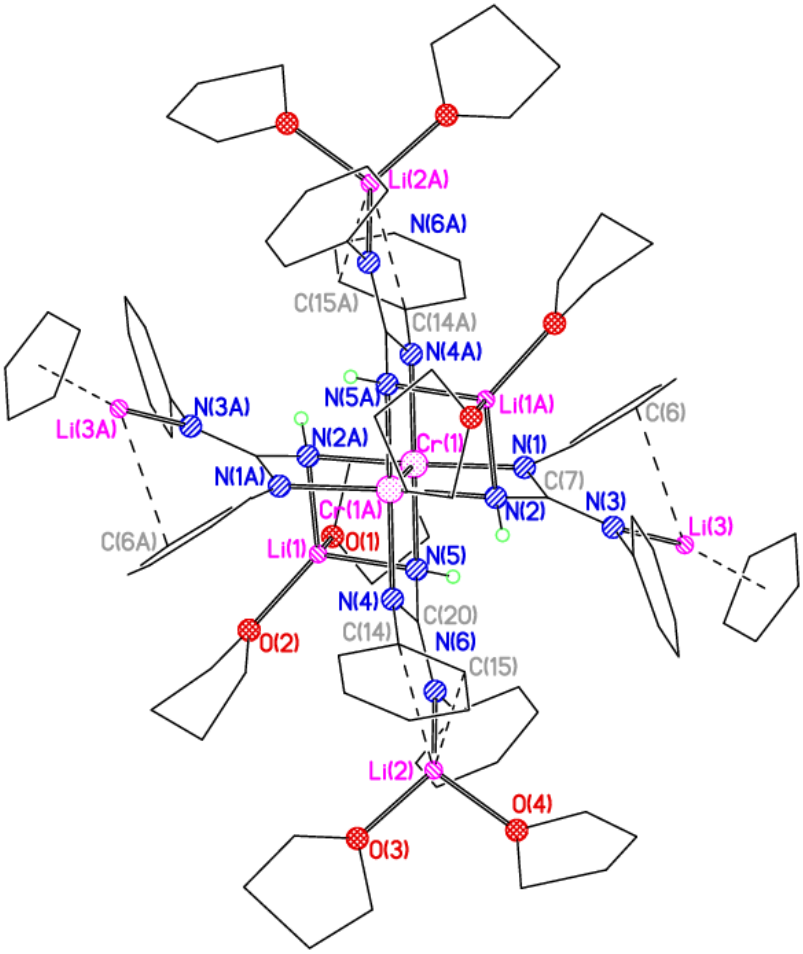

Figure 5.10: The crystal structure of $[Cr_2\{HNC(NPh)_2\}_4](Li \cdot 2\,THF)_4(LiCp)_2$, **5.6**. H-atoms, except those attached to N, omitted for clarity.

Atoms	**Distance (Å)**
Cr(1)−Cr(1A)	1.873(1)
Cr−N	2.060(3) – 2.073(3)
C=N	1.342(4) – 1.367(4)
Li(1)−N(5/2A)	2.024(6) – 2.033(7)
Li(2)−N(6)	1.942(7)
Li(2)···N(15)	2.558(8)
Li(2)···N(14)	2.744(8)
Li(3)−N(3)	2.007(8)
Li(3)−C(Cp)	2.250(9) – 2.261(9)
Li(3)···$Cp_{centroid}$	1.922(9)
Li(3)···C(6)	2.767(8)
	Angle (°)
N−Cr−N	86.9(1) – 92.2(2)
Cr−Cr−N	93.86(9) – 97.05(8)

Table 5.6: Selected bond lengths and angles for **5.6**.

The product **5.6** was obtained reproducibly from the reaction even when the stoichiometry was altered, with alternative syntheses including 1,3-diphenylguanidine:*n*-BuLi:Cp_2Cr ratios of 1:2:1, 2:4:1 and 2:3:1 (the latter being the ratio observed in **5.6**). The best results were obtained when 1,3-diphenylguanidine was used with *n*-BuLi and Cp_2Cr in a 3:3:1 ratio in THF, so an excess of lithiated guanidinate was present. The crystal structure shows a core that resembles a paddlewheel structure with two chromium centres bridged by four guanidinate ligands. The core exists as a tetraanion $[Cr_2(LH)_4]^{4-}$ where L = $[(PhN)_2C{=}NH]$ (Figure 5.11). This forms an ion-pair with four bis-THF solvated Li^+ cations. This arrangement then forms a co-complex with two CpLi monomer units, presumably generated as a by-product of the reaction between Cp_2Cr and the lithiated diphenylguanidine ligand. The product **5.6** does not seem to remain intact in the solution state - ^{1}H NMR shows the presence of several Cp environments (δ 5.5 – 4.7 ppm) as well as a complicated series of aromatic resonances (δ 6.0 – 7.4 ppm), which suggests some disintegration of the solid structure. This is possibly due to the fact that the product was insoluble in toluene, a less polar solvent, so THF was used which may have contributed to the degradation of the material. This is supported by the elemental analysis obtained, which suggests that the THF ligands coordinating the lithium ions are labile and may be easily lost by placing **5.6** under vacuum prior to isolation (10 minutes, 10^{-1} bar).

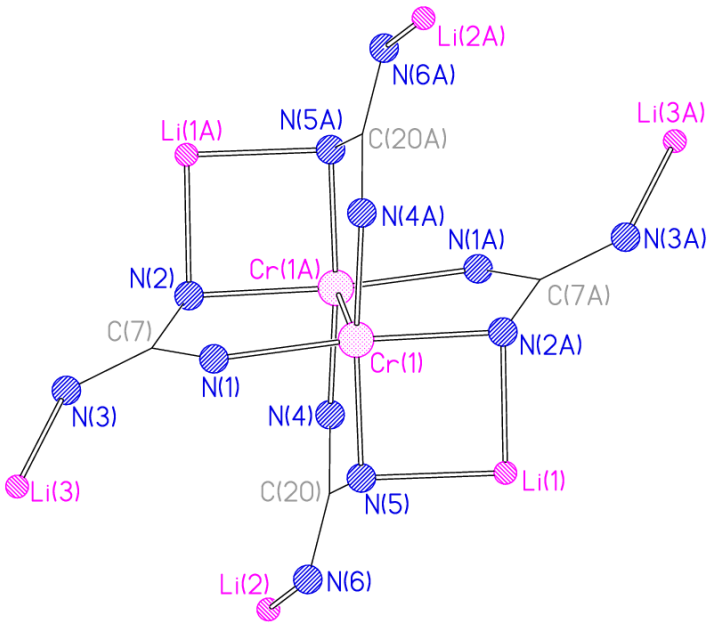

Figure 5.11: The core of $[Cr_2\{HNC(NPh)_2\}_4](Li \cdot 2\,THF)_4(LiCp)_2$, **5.6**.

Recent interest in the area of metal-metal multiple bonds has been largely focused on the formation of quintuple bonds, which have been observed between metal centres in chromium species of the type $[Cr_2L_2]$, where L is a bulky bidentate ligand (such as terphenyl). This work is discussed in Section 1.3.1, but all previously reported examples of such species involve Cr^I centres bridged by bidentate ligands and inclusion of an additional δ orbital in the Cr−Cr bond. These compounds have very short Cr−Cr bond lengths, in the range 1.7395(7) – 1.8028(9) Å. In contrast, the Cr−Cr bond length in **5.6** is 1.873(1) Å, which is similar to that observed in **5.3** and falls within the normal range for a quadruple bond. This value is consistent with the metal ions being in the +2 oxidation state. This is in contrast to the only other anionic Cr_2 amidinate-bridged species reported in the literature (Figure 5.12), which is based on a triply-bridged anion $[\{(1,2{-}Me_2C_6H_3N{=})_2CH\}_3Cr_2]^-$ which contains two Cr^I centres and a quintuple bond measuring 1.7397(9) Å.[40]

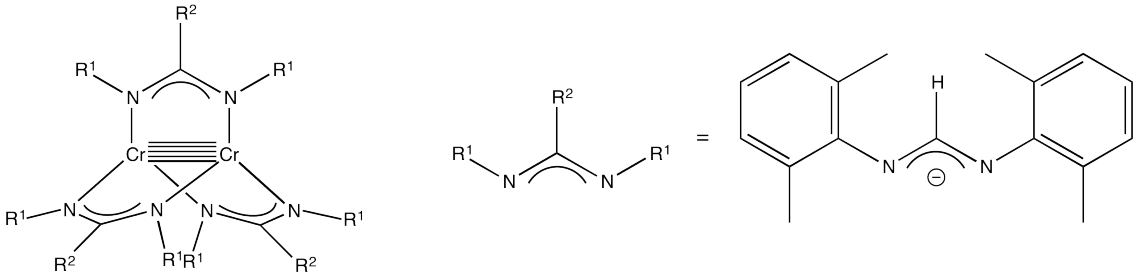

Figure 5.12: The only previously reported anionic Cr−Cr species, featuring a quintuple bond and Cr(I) centres.

There are no other reported cases in the literature of quadruply-bonded compounds of this type in which an overall, ligand-based charge is maintained, making the $[Cr_2(LH)_4]^{4-}$ tetraanion of **5.6** unprecedented within this area. It should be noted that a similar bonding situation to that of **5.6** is found in other quadruply-bonded Cr_2 compounds containing organometallic ligands, such as the $[Cr_2Me_8]^{4-}$ compound seen in Figure 5.13.[133] However, in this structure a $Li \cdot THF$ cation is closely positioned between the Me groups on adjacent metals, the organic ligands eclipsing each other.[34]

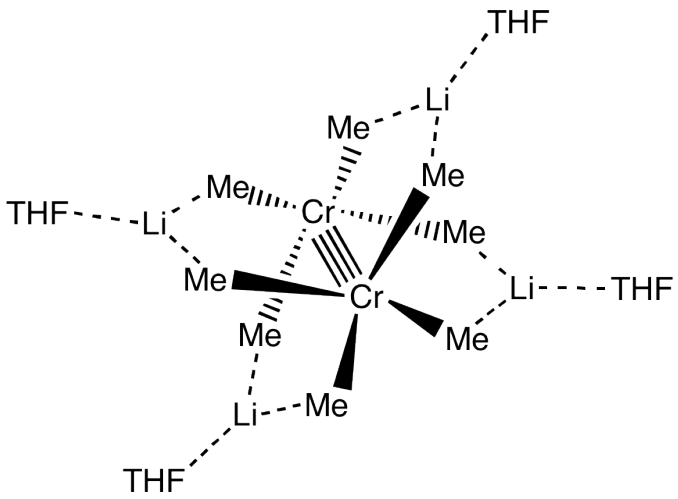

Figure 5.13: The structure of $Li_4(THF)_4[Cr_2Me_8]$.

The bonding situation seen in Figure 5.13 (involving only weak, electrostatic Li···C interactions) differs significantly from the situation within **5.6**, which contains three distinct lithium environments. The symmetry-related bis-solvated Li^+ cations positioned at either side of the $[Cr_2(LH)_4]^{4-}$ tetraanion are coordinated by two N centres from separate guanidinate ligands. This results in the formation of $Cr(\mu{-}N)_2Li$ metallocycles, with the Li^+ cations exhibiting typical tetrahedral geometry. The formation of this metallocycle seems to have little effect on the N−Cr−N angles, which are all close to 90°, as in similar structures such as **5.3**. The remaining counter-cations reside on the periphery of the structure, and are solvated by THF molecules whilst also bonding to a lone guanidinate N centre. The lack of guanidinate coordination is compensated for by short-range π-arene C···Li interactions (2.558(8) – 2.744(8) Å),[134;135] with the lithium cation adopting a distinctly distorted, pseudo-tetrahedral coordination environment.

The crystal structure of **5.6** also features metal centres associated with the co-complexing CpLi units which decorate the periphery of the molecule. These adopt a similar coordination mode to those of the previous example, interacting with a single guanidinate N centre. In order to compensate for the lack of guanidinate stabilisation and the absence of solvating THF molecules, these metal ions again form π-arene interactions with nearby phenyl groups associated with the guanidinate ligands (C···Li 2.767(8) Å), avoiding what would otherwise be a two-coordinate geometry for the metal. These π-arene C···Li interactions are typical of those found in organolithium compounds [typically 2.40 – 2.80 Å].*

*Based on a search of the CSD (March 2013), returning 60 results

The formation of a co-complex in **5.6** incorporating an alkali metal cyclopentadienyl species is similar in concept to that previously observed in the structure of the V^{III} cation $[(V_2)Li(\mu{-}Cp)Li(\mu{-}Cp)Li(V_2)]^+$ discussed in Chapter 1, Section 1.3.2.[22] In the case of **5.6**, however, neutral monomeric units rather than charged fragments of the parent lattice $(CpLi)_\infty$ are intercepted.[55]

In summary, it has been shown for the first time that Cp_2Cr is a convenient precursor for multiply-bonded Cr(II) compounds (in both **5.3** and **5.6**). The methodology employed also allowed access to a completely new representative of the most common class of quadruply-bonded Cr(II) compounds, a highly charged tetraanion of the type $[Cr_2L_4]^{4-}$. Species of this type could provide new opportunities for the construction of a range of magnetic materials and supramolecular networks.

5.4 Conclusions

The research presented within this chapter demonstrates the versatility of the transition metal metallocenes as starting materials for the preparation of new organometallic species. The products obtained range from simple paddlewheels such as **5.2**, to the asymmetric bimetallic complex **5.4**, the tetrahedral oxo-cage **5.1** and the quadruply-bonded chromium species **5.3** and **5.6** (the latter being capable of binding CpLi fragments at its periphery). Having established the ability of the first-row transition metal metallocenes in this capacity, further research could focus on the development of the reported species and analogues thereof, particularly with regards to potential uses in catalysis or small-molecule trapping (see Chapter 8).

Chapter 6

Studies of the Formation of Transition Metal Complexes Containing Redox-Active Aromatic Diamines

6.1 Publications Resulting from this Work

F. A. Stokes, L. Kloo, Y. Lv, P. J. Harford, A. E. H. Wheatley and D. S. Wright, "The Redox Effect of the $[1,2-(NH)_2C_6H_4]^{2-}$ Ligand in the Formation of Transition Metal Compounds", *Chem. Commun.*, 2012, **48**, 11298.

F. A. Stokes, M. A. Vincent, I. H. Hillier, T. K. Ronson, A. Steiner, A. E. H. Wheatley, P. T. Wood and D. S. Wright, "Reactions of Cp_2M (M = Ni, V) with Dilithium Diamido-aryl Reagents; Retention and Oxidation of the Transition Metal Ions", *Dalton Trans.*, DOI:10.1039/C3DT51632F.

6.2 Introduction

It has been seen in Chapters 4 and 5 that transition metal metallocenes are capable of transferring metal ions in their +2 oxidation state, so that this state is retained in the product. This property has been successfully utilised in the synthetic examples discussed in this project thus far, with all of the structures including metal centres in the +2 oxidation state. However, in order to broaden the scope of this project, it was decided to investigate the reaction of the relevant metallocenes

with ligands known for engaging in redox behaviour, so called 'non-innocent' ligands.

Throughout this chapter LH_2 will be used to denote the doubly-deprotonated 1,2-benzenediamine ligand $[C_6H_4(NH)_2]^{2-}$ that is involved in all of the structures discussed in Sections 6.3.1 - 6.3.3, whilst $L'H_2$ will be used to denote the doubly-deprotonated 1,8-diaminonaphthalene ligand $[C_{10}H_6(NH)_2]^{2-}$ involved in Sections 6.3.4 - 6.3.5.

6.3 Results and Discussion

Reactions of Transition Metal Metallocenes with 1,2-Benzenediamine

1,2-Benzenediamine was originally selected as a suitable starting material for exploring the reactivity of metallocenes with redox-active ligands due to its relative simplicity, the fact that it has two donor atoms which are capable of bridging metal centres, and its proven ability to engage in 'non-innocent' ligand behaviour.[136;137] It has also been observed to behave in a redox-active manner within the area of main group chemistry, as discussed in Chapter 1, Section 1.3.4. This redox activity provides the potential for the formation of higher- or mixed-oxidation state arrangements. Figure 6.1 shows the forms that this ligand can adopt and the reduction and oxidation steps involved in their formation.

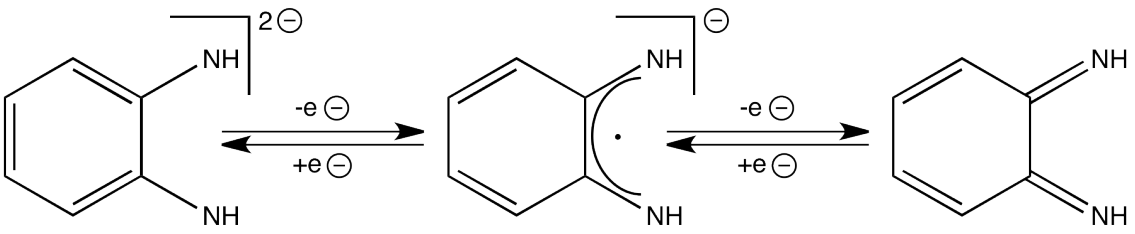

Figure 6.1: The three forms of doubly-deprotonated 1,2-benzenediamine. *Left*, the *o*-phenylenediamine dianion (opda; LH_2); *centre*, *o*-benzosemiquinone diimine radical anion (sbqdi); *right*, neutral *o*-benzoquinone diimine (bqdi).

6.3.1 $Mn_6(LH_2)_6(\mu_6{-}O) \cdot 4\,THF$, 6.1

The synthetic strategy employed in the generation of **6.1** can be seen in Scheme 6.1. Crystals of **6.1** were isolated as pink blocks in a dark pink solution in a 39% yield (with respect to Cp_2Mn) from the reaction of 1,2-benzenediamine with two equivalents of *n*-BuLi followed by *in situ* reaction in THF with Cp_2Mn and crystallisation at room temperature. **6.1** was characterised using ^1H and ^{13}C NMR spectroscopy, elemental analysis (C, H, N), and by single-crystal X-ray diffraction.

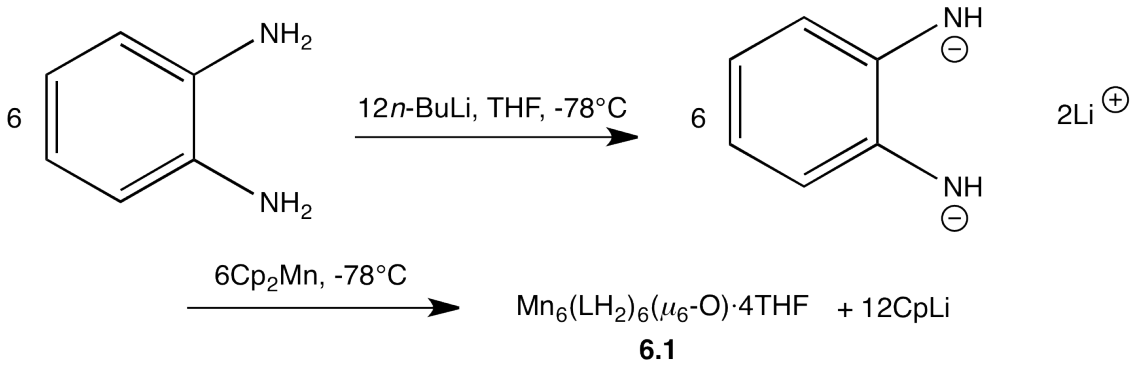

Scheme 6.1: Reaction scheme illustrating the synthetic method employed in the generation of $Mn_6(LH_2)_6(\mu_6{-}O) \cdot 4THF$, **6.1**.

Compound **6.1** was only sparingly soluble in THF and benzene, so ^1H and ^{13}C NMR spectroscopy were performed in DMSO-d_6. The ^1H NMR studies showed resonances that were apparently paramagnetically broadened, including an NH signal at δ 4.35 ppm and aromatic signals at 6.46 – 6.34 ppm which confirmed that the 1,2-benzenediamine ligand had been doubly-deprotonated to give $[C_6H_4(NH)_2]^{2-}$. Crystallographic studies of **6.1** were undertaken in order to elucidate the solid-state structure of this species. The structure revealed was a hexanuclear $Mn_6(\mu_6{-}O)$ cage, $Mn_6(LH_2)_6(\mu_6{-}O) \cdot 4THF$ (Figure 6.2). This is reminiscent of **5.1** in that it features an interstitial oxide at its centre, but the $Mn_6(\mu_6{-}O)$ motif seen here is much more unusual than the $Mn_4(\mu_4{-}O)$ core observed in that species.* The unexpected $\mu_6{-}$oxide ion at the centre of the Mn_6 core probably arises from trace H_2O and/or O_2 present in the reaction, although it could also arise from abstraction of oxygen from the THF solvent, discussed in Chapter 5, Section 5.3.1.[109] **6.1** was not always reproducibly obtained from this reaction, which often yielded no isolable products, suggesting that trace H_2O or O_2 contamination was necessary for the formation of the $Mn_6(\mu_6{-}O)$ cage.

*Based on a search of the CSD (March 2013), returning 11 results for $Mn_6(\mu_6{-}O)$ and 206 results for $Mn_4(\mu_4{-}O)$

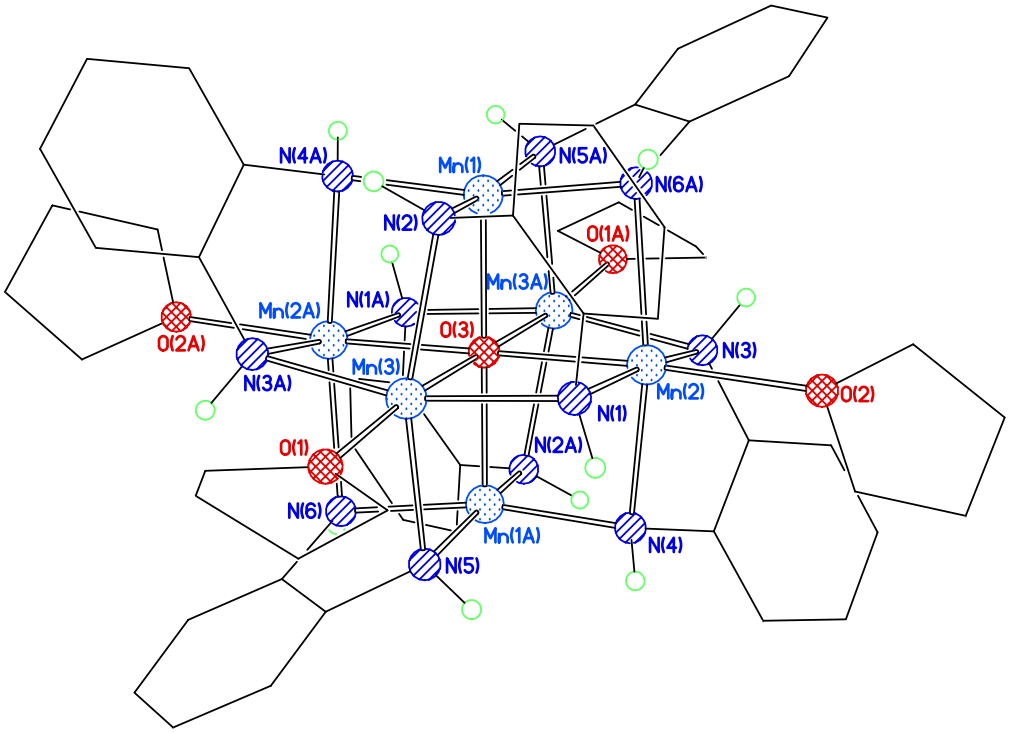

Figure 6.2: The crystal structure of $Mn_6(LH_2)_6(\mu_6{-}O) \cdot 4THF$, **6.1**. Four lattice THF molecules and H-atoms (excluding NH) omitted for clarity.

Atoms	**Distance (Å)**
Mn(1)−O(3)	2.1064(5)
Mn(2)−O(3)	2.2484(5)
Mn(3)−O(3)	2.2716(5)
Mn(1)−N	1.993(2) – 2.008(3)
Mn(2)−N(1)	2.199(3)
Mn(2)−N(3)	2.209(3)
Mn(2)−N(6)	2.308(3)
Mn(2)−N(4)	2.312(3)
Mn(3)−N(1)	2.207(3)
Mn(3)−N(3)	2.200(3)
Mn(3)−N(2)	2.294(3)
Mn(3)−N(5)	2.300(3)
Mn(2/3)−O(THF)	2.2716(5) – 2.322(3)
	Angle (°)
Mn−N−Mn	88.4(1) – 94.5(1)
Mn−μ_6-O−Mn	87.24(2) – 91.81(2)

Table 6.1: Selected bond lengths and angles for **6.1**.

Other oxo-compounds have been reported in the literature from reactions of Cp_2Mn with a range of amide and amidinate ligands, although in all prior cases the metal +2 oxidation state was retained.[138] Consideration of the charges of the ligand set present suggests that the cage contains two Mn(III) and four Mn(II) centres, so a partial oxidation of the manganese has taken place. The six LH_2 ligands of the cage adopt a μ_2-N, μ_2-N' bonding mode with each N atom spanning one of the twelve Mn···Mn edges of the Mn_6 octahedron. The coordination numbers of the Mn centres vary, with only the four equatorial metal ions being solvated by THF ligands and possessing distorted octahedral geometries, and the axial Mn centres being five-coordinate and square-based pyramidal. This arrangement seems to be consistent with the location of the Mn(II) ions within the equatorial sites and the Mn(III) ions within the axial sites, with the μ_6-O ion lying on a crystallographic inversion centre.

The pattern of $Mn-O_{oxo}$ bonds within the core of **6.1** supports the aforementioned postulated arrangement of the Mn(II) and Mn(III) ions, as the axial Mn−O bond lengths are significantly shorter, at 2.1064(5) Å, than the equatorial equivalents, at 2.2484(5) Å and 2.2716(5) Å. Similar observations can be made about the pattern of Mn−N bonds, which are noticeably shorter to the axial metal centres [range 1.993(2) – 2.008(3) Å] than to the equatorial ones [range 2.199(3) – 2.312(3) Å]. The absence of solvation by THF of the Mn(III) ions in this structure is partly accounted for by the greater steric congestion at these positions as a result of the smaller size of Mn(III). However, the strong *trans*-influence of the O_{oxo}-ligand combined with the effect of high-spin (d^4) Jahn-Teller distortion also likely plays a role in the weakening of potential additional donor bonding with the Mn(III) ions.

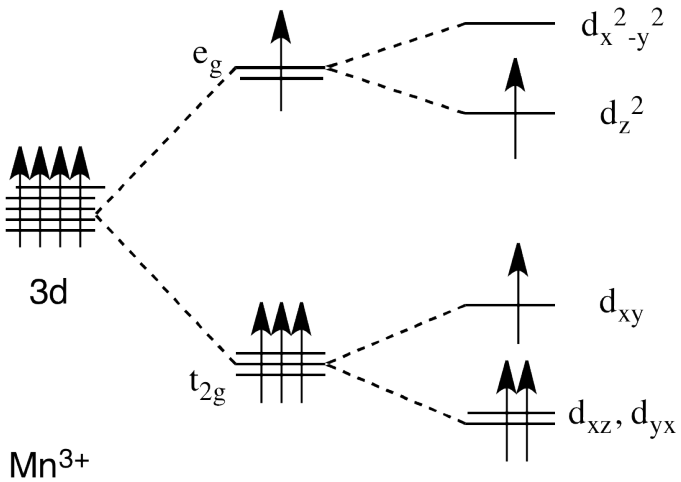

Figure 6.3: Diagram to show the effect of Jahn-Teller distortion in a d^4 Mn^{3+} species.

There are only four related $Mn_6(\mu_6{-}O)$ complexes previously reported in the literature. Although these share the same structural motif as **6.1**, a range of oxidation states are present; $Mn^{II}{}_2Mn^{III}{}_4$,[139] $Mn^{II}Mn^{III}{}_5$,[140] $Mn^{III}{}_6$[141] and $Mn^{II}Mn^{III}{}_2Mn^{IV}{}_3$.[142] There are no examples with the same mixed-oxidation state $Mn^{II}{}_4Mn^{III}{}_2$ composition as **6.1**. In addition, all of these prior examples contain carboxylate and/or alkoxide ligand sets as opposed to the softer nitrogen-based donors seen in **6.1**, and all contain six-coordinate metal ions.

It is unlikely that the redox-active ligand employed in this synthesis was responsible for the manganese oxidation seen in **6.1**, as in its doubly-deprotonated form it acts as a reducing rather than an oxidising agent. The likely cause of the oxidation is a disproportionation taking place in solution to give some reduced manganese species which was not isolated from the reaction mixture. However, the formation of **6.1** shows that this ligand set is structurally suitable for the formation of transition metal clusters, and is capable of stabilising higher- and mixed-oxidation state complexes.

6.1 would be a suitable candidate for variable-temperature magnetic studies, as it has some features in common with the "Mn_6" SMMs currently generating interest within the field. However, in order for magnetic studies to be useful, some alterations would have to be made to **6.1**, including optimisation of the reaction conditions to increase the yield obtained. It may also be necessary to alter the compound itself, by introducing bulkier ligands in order to decrease the air- and moisture-sensitivity of the product as this limits its usefulness in any future applications. These challenges are discussed further in Chapter 8.

6.3.2 $(\eta^5{-}\mathbf{Cp})(\mathbf{LH_2})\mathbf{VV}(\mathbf{LH_2})(\mathbf{Li\cdot 4\,THF})$, 6.2

The synthetic strategy employed in the generation of **6.2** was based upon that of **6.1**, and can be seen in Scheme 6.2. Crystals of **6.2** were isolated as green blocks in a dark green solution in an 8% yield (with respect to Cp_2V) from the reaction of 1,2-benzenediamine with two equivalents of *n*-BuLi followed by *in situ* reaction in THF with Cp_2V and crystallisation at room temperature. This yield was increased to 36% once the product was fully characterised and the synthesis was altered to reflect the 2:3 Cp_2V-to-LH_2Li_2 stoichiometry observed. **6.1** was characterised using ^1H and ^{13}C NMR spectroscopy, elemental analysis (C, H, N), and by single-crystal X-ray diffraction.

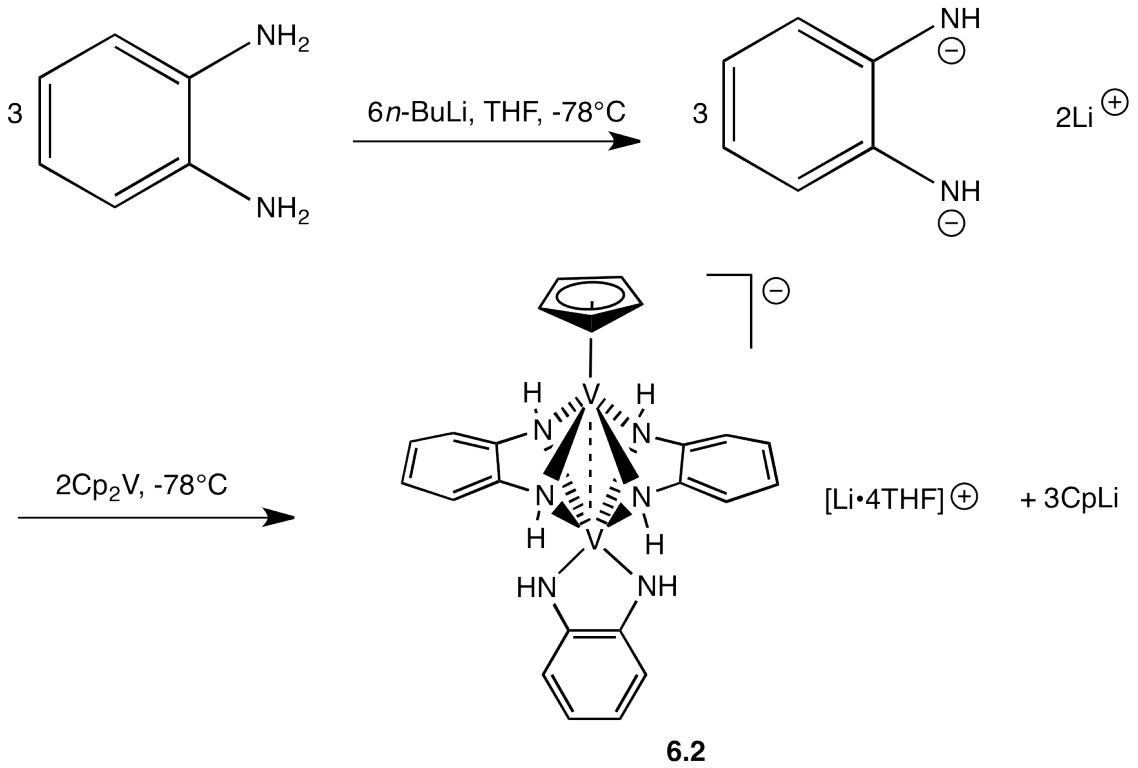

Scheme 6.2: Reaction scheme illustrating the synthetic method employed in the generation of $(\eta^5{-}\mathrm{Cp})(\mathrm{LH_2})\mathrm{VV}(\mathrm{LH_2})(\mathrm{Li}\cdot 4\mathrm{THF})$, **6.2**.

Compound **6.2** was only sparingly soluble in THF and benzene, so ^{1}H and ^{13}C NMR spectroscopy were performed in DMSO-d_6. The ^{1}H NMR studies showed sharp resonances that suggested that the species was diamagnetic. As with **6.1**, the NH resonance appeared at δ 4.36 ppm and showed by integration that the ligand had again been doubly-deprotonated to give $[\mathrm{C_6H_4(NH)_2}]^{2-}$. The ^{1}H and ^{13}C NMR spectra were assigned as seen in Figure 6.4, although in order to fully elucidate the structure of **6.2** crystallographic studies had to be undertaken. The X-ray single-crystal analysis of **6.2** showed that it has an ion-separated structure $[(\eta^5{-}\mathrm{Cp})(\mathrm{LH_2})\mathrm{VV}(\mathrm{LH_2})]\cdot[\mathrm{Li}\cdot 4\mathrm{THF}]$, with the dinuclear anion shown in Figure 6.5.

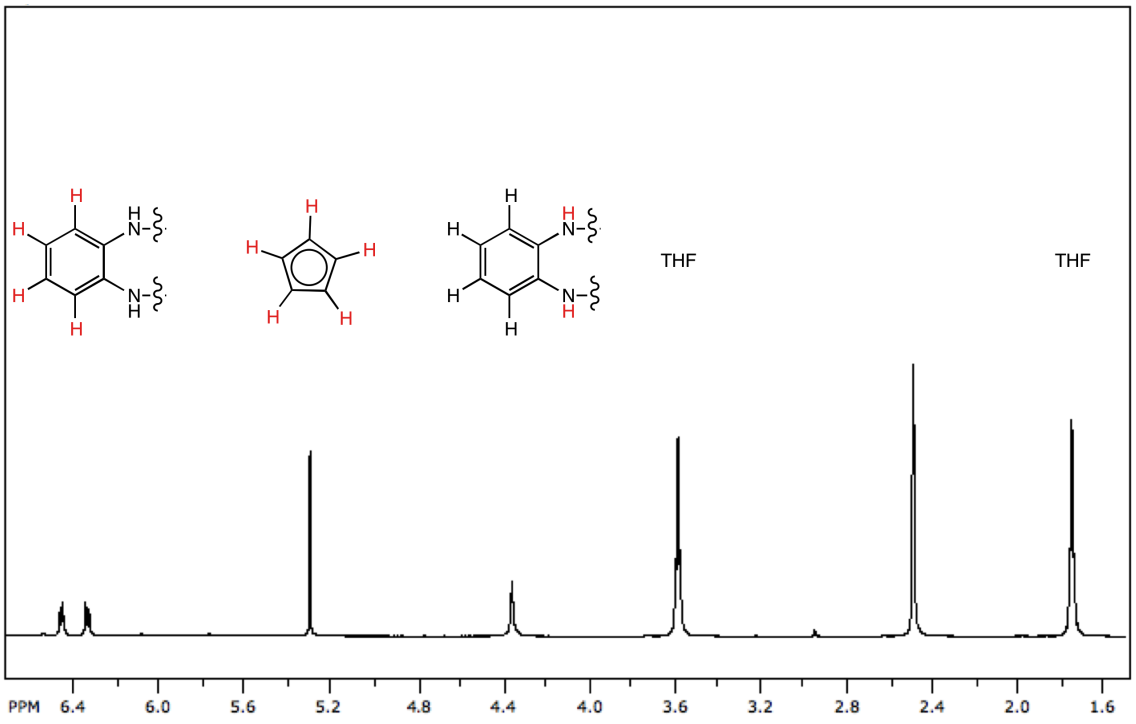

Figure 6.4: The ^{1}H NMR spectrum of **6.2**.

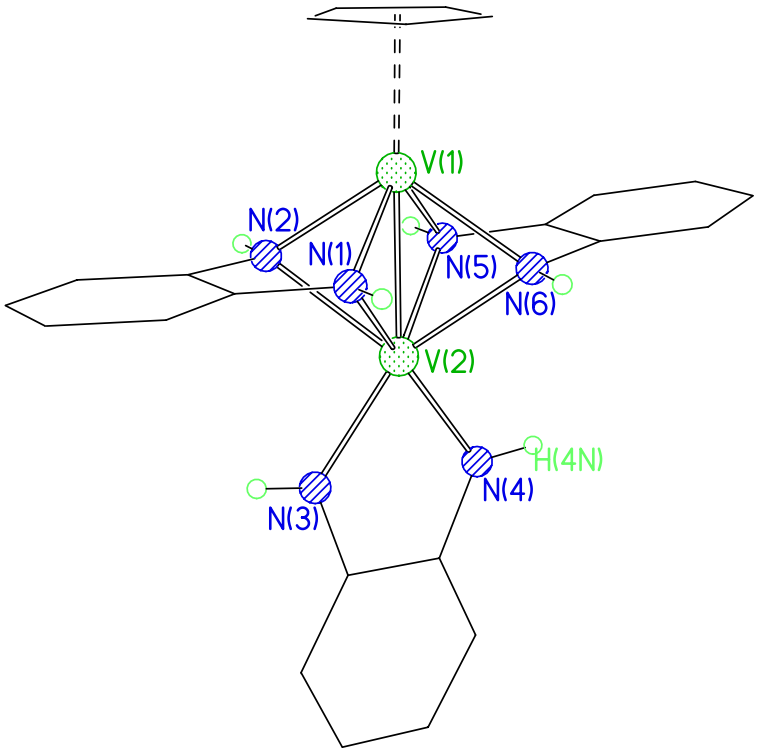

Figure 6.5: The crystal structure of the anion of (η^5−Cp)(LH_2)VV(LH_2)(Li·4THF), **6.2** with H-atoms (except NH) omitted for clarity.

Atoms	**Distance (Å)**
V(1)−C(Cp)	2.290(2) – 2.316(2)
V(1)···$C_{centroid}$	1.9703(7)
V(1)−V(2)	2.3742(9)
V(1)−N(1)	2.076(2)
V(1)−N(2)	2.091(2)
V(1)−N(6)	2.099(2)
V(1)−N(5)	2.104(2)
V(2)−N(3)	2.005(2)
V(2)−N(5)	2.151(2)
V(2)−N(6)	2.127(2)
	Angle (°)
N−V(1)−N	69.51(7) – 76.03(7)
N(3)−V(2)−N(4)	76.94(8)
N−V(2)−N	67.87(6) – 97.24(7)
V(1)−N−V(2)	67.80(6) – 68.37(5)

Table 6.2: Selected bond lengths and angles for **6.2**.

The anion in **6.2** has an asymmetrical arrangement in which the two chemically distinct vanadium centres have different coordination environments. These two V centres, V(1) and V(2) as seen in the crystal structure in Figure 6.5, are bridged by two LH_2 ligands, each of which adopts the same μ_2-N, μ_2-N' bonding mode. Whilst the nominally square-based pyramidal geometry of V(1) is completed by an axial η^5-Cp ligand, V(2) is bonded to another LH_2 ligand, this one terminal and imposing a highly distorted six-coordinate geometry on the metal atom. This arrangement results in a formal electron count of 16e for V(1) and 14e for V(2). Inspection of the ligand charges, however, indicates that both V centres have been oxidised and are present in the +3 oxidation state. As with **6.1**, it is likely that this metal oxidation stems from a disproportionation reaction taking place. The very short V(1)···V(2) distance observed [2.3742(9) Å] seemed at first to indicate the presence of a V=V double bond between the d^2 metal centres. As such, the overall arrangement of the anion of **6.2** can be regarded as a unique hybrid between organometallic V=V bonded compounds like $[(CO)_4V^{II}(\mu-PMe_2)]_2$ (containing 16e V centres)[143] and V=V bonded coordination compounds like $V^{III}{}_2(\mu-\text{salophen})_2(Na \cdot 6THF)$ (which also contains d^2 V(III) ions).[144]

Following the elucidation of the structure of **6.2**, further reaction was attempted by heating the reaction mixture to reflux, with the expectation that it would undergo a further intramolecular nucleophilic displacement of CpLi to give the neutral paddlewheel-like species $V_2(LH_2)_3$, but this reactivity was not observed, with **6.2** still being the only isolable product (Figure 6.6).

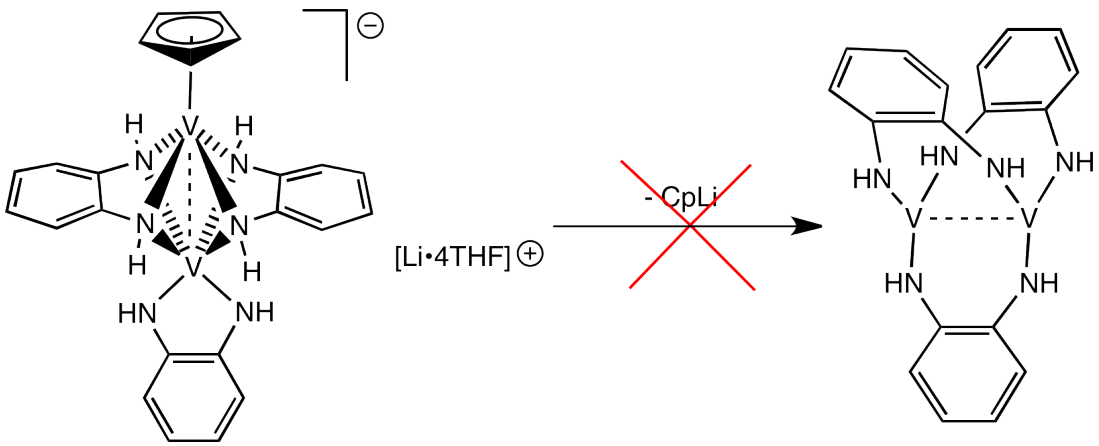

6.2

Figure 6.6: Reaction scheme illustrating the attempted further reaction of **6.2** to give a neutral paddlewheel species.

To probe the V···V interaction in **6.2** further, a quantum chemical study of the anion was undertaken by Prof. Kloo of the KTH Royal Institute of Technology in Stockholm, Sweden. All possible closed-shell singlet state, triplet and pentet states, as well as open-shell singlet states derived from antiferromagnetic coupling of the non-paired electrons in the singlet, triplet and pentet states were investigated. The closed-shell singlet state offered the best correlation with the experimentally-observed structure, bond lengths and magnetic behaviour. However, optimisation of the open-shell pentet state (maximum spin state of the compound) using a broken symmetry approach converged to an open-shell singlet state with the lowest observed total energy for the system studied. At the level of calculation used, the antiferromagnetically coupled open-shell singlet within the pentet electronic state was as much as 206 kJ mol^{-1} lower in energy, and therefore more stable, than the closed-shell singlet state. The resulting spin on the two V atoms was two (in a molecular fragment analysis the spins were 2.04 and 2.08), and the V···V distance was significantly longer than the experimental value, at 2.622 Å. Calculations on the open-shell singlet and triplet states strived towards the same open-shell singlet state.

The structure of the optimised closed-shell singlet state with C_s symmetry closely resembles that of the anion of **6.2** that is observed crystallographically. The Wiberg bond index for the 2.354 Å V···V distance is 0.69, indicating a bond order of $\leq$1. The NBO analysis further indicated the presence of only one V−V bonding molecular orbital, heavily dominated by d orbital interaction (>90%). Equatorial V−N bonding (2.135 and 2.138 Å) is composed of an s-p-d-mixed orbital on V and s-p-mixed orbitals on N, whereas the V−N bonding to the single axial LH_2 ligand (1.929 Å) is almost completely of d orbital type on V and p orbital type on N. A survey of the molecular orbitals indicates that all bonding is primarily of sigma type. An AIM analysis clearly displays a bond critical point midway between the two V atoms, with an electron density of about 0.074 - almost the same as that for the critical points between the V atoms and the N atoms of the equatorial LH_2 ligands. The HOMO-3 orbital is shown in Figure 6.7 and represents topologically the only clear bonding molecular orbital, indicating that the anion contains a direct single V−V bond rather than a V=V double bond.

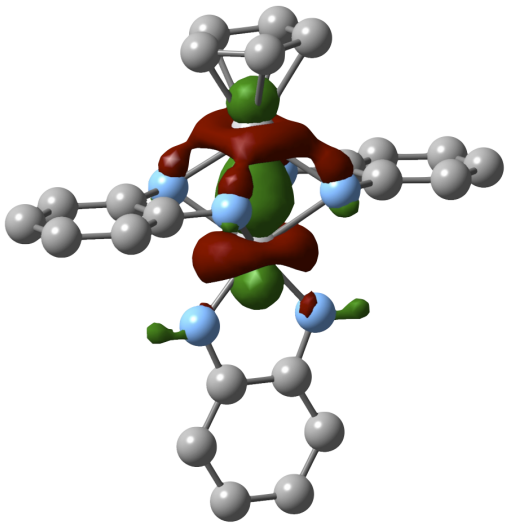

Figure 6.7: Bonding molecular orbital (HOMO-3) of the mono-anion of **6.2** with H-atoms omitted.

These conclusions regarding the nature of the metal-metal bond in **6.2** are noteworthy in that they have connotations concerning other purported examples of V=V bonded compounds. These examples have cited double bond character based solely on the crystallographic observation of short inter-metal distances and the diamagnetic behaviours of the materials involved.[143–148] Although the metal-metal distance in **6.2** is significantly shorter than in any other previously claimed V=V bonded species [range 2.42 – 2.73 Å][143–148] (for reference, the bond distances found in V≡V triply-bonded compounds are in the range 1.92 – 2.54 Å),[149;150] the first high-level calculations on such a system, which have been discussed here, emphasise that a far more complicated metal-metal bonding picture may be present in all of these cases.

Variable-temperature magnetic measurements were carried out on **6.2**, both in Cambridge and by Dr. Eichhöfer at the Karlsruhe Institut für Technologie in Germany, although the results of these studies were not straightforward to interpret. However, the results obtained were repeatable as the same trends were observed in both data sets, which used different batches of material from different syntheses of **6.2**. The purity of the product was ascertained by microanalysis before each study was undertaken. The samples exhibited a much larger magnetic response than the maximum calculated value, with temperature-independent paramagnetism also observed.

According to the spin-only formula, the presence of two V(III) (S = 1) ions could produce a maximum effective magnetic moment of 5.66 μB, with the expectation being that the magnetic susceptibility would increase with increasing temperature until reaching magnetic saturation, a limiting state in which all magnetic domains are aligned. However, this state was never reached by **6.2**. Instead, the magnetic response was observed to continue to rise. It can be tentatively suggested that this may have been due to some temperature-independent paramagnetic contribution to the magnetic susceptibility of the sample. TIP occurs due to a quantum-mechanical coupling of the non-thermally populated excited state of a material into the ground magnetic state, and has been previously observed in transition metal complexes.[151] A well known example of a compound which exhibits this effect is $[Co(NH_3)_6]^{3+}$, which one would expect to be diamagnetic, but which was shown to have a significant temperature-independent paramagnetic component to its magnetic behaviour.[152] To overcome this effect, a large external magnetic field (0.1 T) can be applied to the sample in order to energetically separate the states and limit coupling between them, allowing the ground state magnetic measurements to be taken. However, in the case of **6.2**, applying a larger field did not alter the results obtained, with magnetic susceptibility still increasing without ever reaching saturation.

The magnetic data obtained for **6.2** does not fit any known model for magnetic behaviour, and cannot be explained by assuming that the sample was exposed to air and had undergone decomposition, as any oxidation of the vanadium centres would be expected to lower rather than raise the magnetic susceptibility as V(IV) and V(V) contain fewer unpaired electrons than V(III) (one and zero respectively). Based on these preliminary findings, no satisfactory interpretation of the magnetic behaviour of **6.2** has been made, although some suggestions have been advanced as to how to progress with these studies (see Chapter 8).

6.3.3 $[Ni_6(LH_2)_6][Ni_6(LH_2)_3(LH)_3(Li \cdot THF)][2(Li \cdot 4\,THF)]$, 6.3

The synthetic strategy employed in the generation of **6.3** can be seen in Scheme 6.3. Crystals of **6.3** were isolated as purple blocks in a dark solution in a 67% yield (with respect to Cp_2Ni) from the reaction of 1,2-benzenediamine with two equivalents of *n*-BuLi followed by *in situ* reaction in THF with Cp_2Ni and crystallisation at room temperature. **6.3** was characterised using ^1H, ^{13}C and ^7Li NMR spectroscopy,

elemental analysis (C, H, N), and by single-crystal X-ray diffraction.

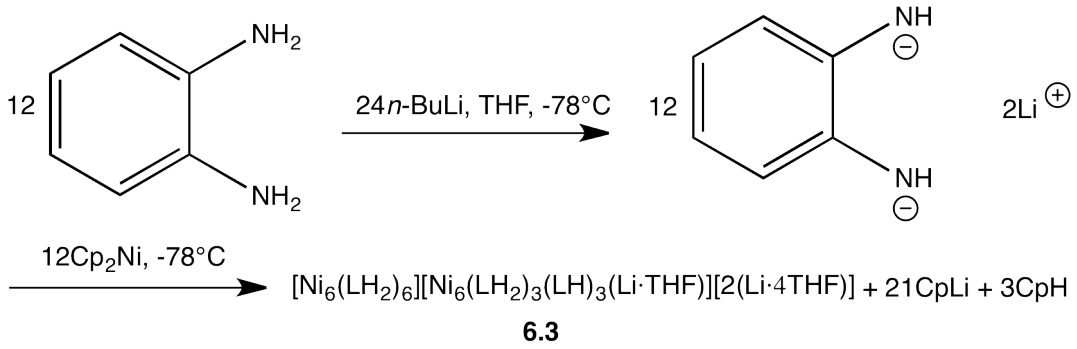

Scheme 6.3: Reaction scheme illustrating the synthetic method employed in the generation of $[Ni_6(LH_2)_6][Ni_6(LH_2)_3(LH)_3(Li \cdot THF)][2(Li \cdot 4THF)]$, **6.3**.

The ^1H and ^{13}C NMR spectra of the material obtained on dissolution of **6.3** showed three distinct ligand environments, both in the aromatic region and the NH region, the signals for which appear at relatively high-field shifts for this compound. These results suggested a lack of symmetry within the structure of **6.3**, particularly as there were six individual NH signals observable. X-ray crystallographic studies were attempted in order to further rationalise these results.

The crystals obtained of **6.3** were of low quality and did not produce useful data when single-crystal X-ray crystallography was first attempted. Repeated attempts to crystallise from different solvents and using various methods failed to improve the crystallinity, but a single-crystal X-ray structure was obtained with the use of the synchrotron facility at the Diamond Light Source in Oxfordshire. The structure at first appeared to be very similar to that of **6.1**, with a hexanuclear structure featuring six metal centres bridged by six LH_2 ligands, although in this case without the μ_6-oxide at the centre. However, the nickel structure varied significantly from the manganese example in that it contained a $[Li \cdot 4THF]^+$ cation in the lattice for each hexanuclear cage and so obviously was not a neutral system. Further refinement of the structure suggested that there were in fact two distinct nickel cages present in the solid state, in an approximately 1:1 ratio. The neutral species $Ni_6(LH_2)_6$ was observed alongside a trianionic species, $[Ni_6(LH_2)_3(LH)_3]^{3-}$, in which three of the LH_2 ligands had been deprotonated further to give three anionic ligands (LH), which were capped in the structure by a THF-solvated lithium ion to give the dianionic $[Ni_6(LH_2)_3(LH)_3(Li \cdot THF)]^{2-}$ (Figure 6.8). The remaining ligand-based 2^- charge is balanced by the $[Li \cdot 4\,THF]^+$ cations present in the crystal lattice, with one $[Li \cdot 4THF]^+$ cation observed per cage.

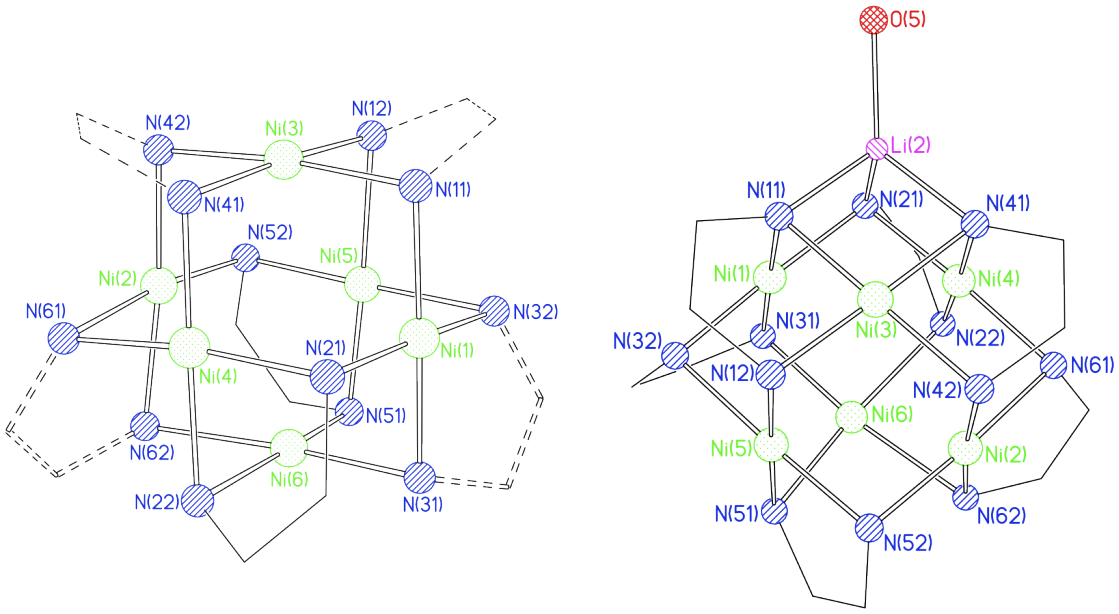

Figure 6.8: The crystal structure of the core of $[Ni_6(LH_2)_6][Ni_6(LH_2)_3(LH)_3(Li \cdot THF)][2(Li \cdot 4THF)]$. *Left*, the core of the neutral species $Ni_6(LH_2)_6$, **6.3a**; *right*, the core of the dianionic species $[Ni_6(LH_2)_3(LH)_3(Li \cdot THF)]^{2-}$, **6.3b**. Both shown with H-atoms omitted and only the O-atoms of THF and the 1,2-positions of the aromatic rings shown for clarity. Lattice counterions also omitted.

Atoms	**Distance (Å)**
Ni–Ni	2.579(6) – 2.821(4)
Ni–N	1.76(1) – 2.16(2)
N–C	1.38(1) – 1.43(1)
Li(1)···O(THF)	1.73(6) – 2.32(7)
N(11/21/41)–Li(2)	1.85(2)
Li(2)···O(5)	1.85(1)
	Angle (°)
Ni(1)–N(11/21/41)–Li(2)	83.6(8) – 90.0(8)
N(11/21/31/41/51/61)–Ni(2)–N(12/22/32/42/52/62)	83.0(5) – 88.0(5)
Ni–Ni–Ni	55.9(1) – 95.6(2)

Table 6.3: Selected bond lengths and angles for **6.3**.

The existence of these two broadly similar structures which occupy the same crystallographic position generates an intrinsic difficulty when it comes to crystallographic structural refinement, as the slight differences in bond lengths and angles between the neutral and charged cages leads to disorder and large anisotropic parameters. The bond distances and angles given in Table 6.3 represent average values across the two distinct structures, except when atom labels relating to **6.3b** are explicitly given. X-Ray diffraction data collected on **6.3** suggests an extensively disordered structure based on non-bonded octahedral arrangements of six Ni(II) centres at the core of a $[1,2{-}C_6H_4(NH)_2]_6Ni_6$ cage (Figure 6.8).

The extreme air- and moisture-sensitive nature of the material is inconsistent with this formulation alone, and the observation of $[Li \cdot 4\,THF]^+$ cations within the crystal lattice suggested a mixture of species in the same lattice, both of which are based on this Ni_6 motif. The $[Li \cdot 4\,THF]^+$ species provided the clearest evidence of a second species in the lattice, but partial occupancy of sites can also be detected associated with the Ni_6 octahedra themselves. The structures **6.3a** and **6.3b** (Figure 6.8) were lastly freely refined based on multiple data acquisitions. This made it possible to state with confidence that $[Li \cdot 4THF]^+$ and $[Li \cdot THF]^+$ exhibit 100 and 50% occupancies respectively and therefore to conclude that the species **6.3a** and **6.3b** can reproducibly co-exist within the same lattice and that they do so in an approximately 1:1 ratio. Subtle structural variations between the two species account for the relatively high $R1$ value of 14%, and the *wR2* value of 36%. Regardless, the identity and essential connectivity of the components of **6.3** are not in doubt. Unfortunately it is unlikely that it will be possible to reduce the $R1$ value relating to **6.3** as the disorder is an intrinsic quality resulting from the two separate cage species occupying the same lattice.

The bonds between nitrogen and lithium are relatively short at 1.87 Å, even when compared to previously characterised geminally *N,N*-dimetallated amides, whilst Ni−N bonds (range 1.85 – 2.20 Å) show significant variability but are within the normal range for such interactions [1.577 – 3.094 Å, mean 2.037Å]†. In contrast to the alkali metals, which are strongly bonded to their solvating THF molecules (O−Li(1) = 1.84 – 2.06 Å, O(5)−Li(2) = 1.87 Å), that interacting with Ni(5) does so only very weakly (O(6)−Ni(5) = 2.55 Å). Despite the variability of these bond distances, they all lie within the normal ranges for such interactions. Li−O distances when Li is solvated by THF have been reported in the range 1.536 – 2.787

†Based on a search of the CSD (March 2013), returning 55,177 results

Å (mean 1.942 Å),[‡] and Ni−O distances in the range 1.662 – 2.916 Å (mean 2.052 Å).[§] With regards to the structure of **6.3b**, it can be seen that due to the ligand arrangement observed in the neutral species **6.3a** there is one position that seems the most likely site for Li^+ to occupy in the metallated derivative. This site can be viewed as a face of three N-dianions that undergoes μ^3-capping by the metal ion, with the *syn* orientation of the two diamide ligands bonded to Ni(3) (with respect to the square planar coordination geometry of that metal ion) leading to the formation of a pocket within which the Li^+ ion can reside when it caps N(11)/(21)/(41) in **6.3b** (see Figure 6.8, *left* - the solid dashed lines represent the *syn* arranged ligands).

With the structure of **6.3** determined, it was then possible to fully assign the ^{1}H and ^{13}C NMR spectra for this material. At first it seemed that these three sets of signals could be attributed to the three different ligand environments observed within the solid-state structure of the product, although it seemed unlikely that the trianionic lithium-capped cage would be preserved in solution. On closer inspection, this latter hypothesis was strengthened by the fact that the proton signals integrated with a ratio of 1:1:1 rather than the 2:1:1 expected if the two distinct cages were both present. The ^{1}H NMR also contained six NH resonances (δ 0.63 – -2.10 ppm) rather than five, suggesting that in solution the trianionic ligands were mono-protonated to reform LH_2, resulting in only one species being present in the solution-state, the neutral $Ni_6(LH_2)_6$ cage **6.3a**. When examined closely, in can be seen that this structure actually contains three symmetry-related pairs of ligands rather than six ligands in identical environments as might at first be assumed (these ligand pairs can be clearly seen in Figure 6.9). As noted above, this feature prevents the need for a substantial reorganisation energy of the ligand set upon lithiation to form **6.3b**.

[‡]Based on a search of the CSD (March 2013), returning 6,115 results
[§]Based on a search of the CSD (March 2013), returning 36,752 results

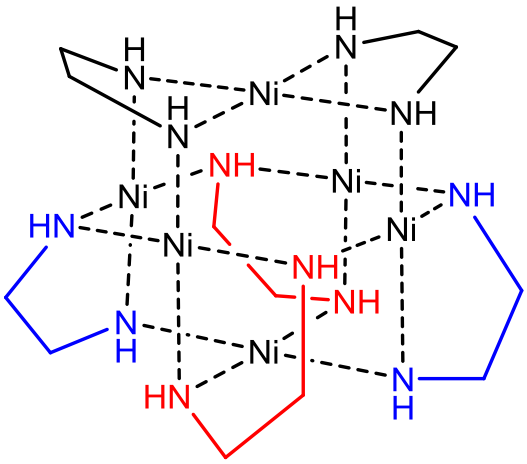

Figure 6.9: The symmetry-related ligand pairs observable within the structure of **6.3a**.

The ^{1}H and ^{13}C NMR spectra were assigned based on this hypothesis that the three ligand sets spectroscopically observed are due to the mono-protonation of the geminally dianionic N-centres observed in **6.3b** due to the solvent sensitivity of this species, resulting in **6.3a** being the only observed structure in solution (Figures 6.10 and 6.11). The six NH signals observed in the ^{1}H NMR spectra support this interpretation as this observation is consistent with the proposed asymmetry of **6.3a**. The high-field position of these NH signals was surprising, in particular the existence of a hydride-type resonance at δ -2.10 ppm. It was observed using HMBC NMR spectroscopy that the NH peaks show 4-bond correlations with aromatic ring protons (δ 0.58(s)/6.45(m) and 0.43(s)/6.34 – 6.28(m) ppm, δ 0.63(s)/6.32(d) and -0.05(s)/5.51(d) ppm, δ 0.29(s)/5.45(d) and -2.10(s)/5.65(d) ppm) which allowed for unambiguous assignment of the ligand pairs.

The ^{7}Li NMR spectrum of **6.3** showed two signals at δ -3.20 and -1.21 ppm, in a 2:3 ratio. The ^{1}H NMR indicated that only **6.3a** was present in solution, in which case only one lithium environment, that of solvated Li^{+} would be present. The signals observed cannot be rationalised in terms of the crystal structure either, as if the two species were to persist in solution the peaks should integrate 1:2, so it is not possible to state conclusively which lithium species are present in solution. ^{7}Li has a medium quadrupole moment (Q = -0.04 b, I = $^{3}/_{2}$), with narrow peaks usually indicating symmetric (tetrahedral) environments,[153] and the range in which these signals fall is consistent with solvated lithium cations,[154;155] so it may be that there are different solvation environments manifest due to the presence of both THF and DMSO.

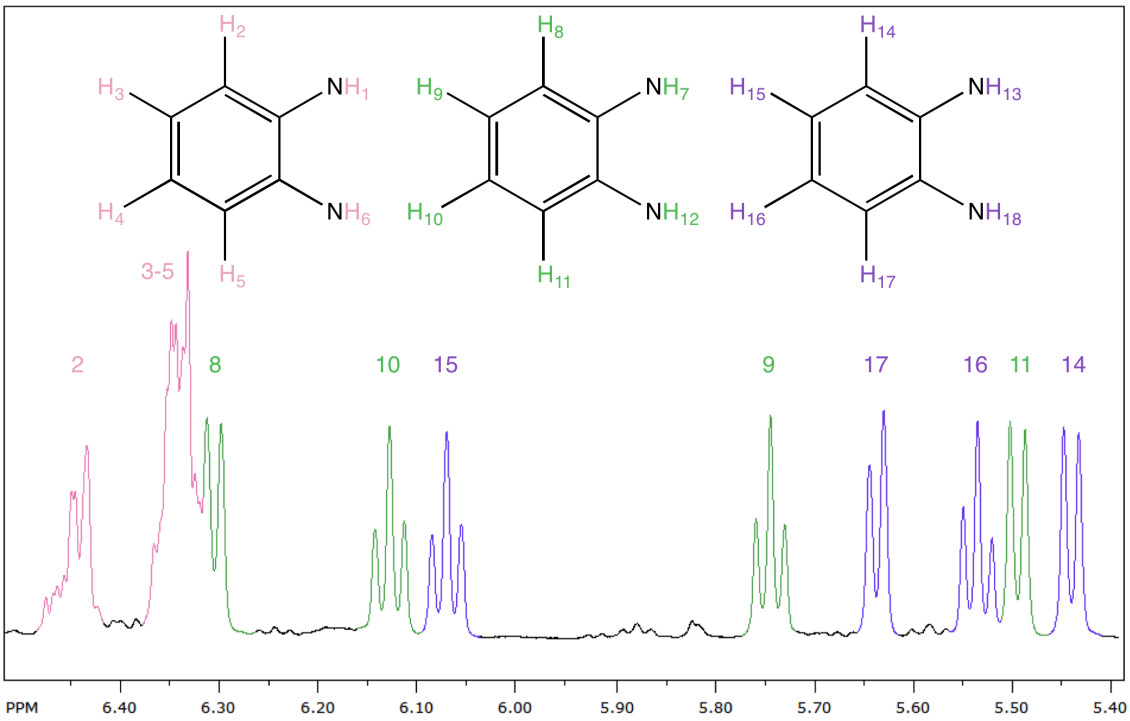

Figure 6.10: The ^{1}H NMR spectrum of **6.3**, showing the assigned aromatic region.

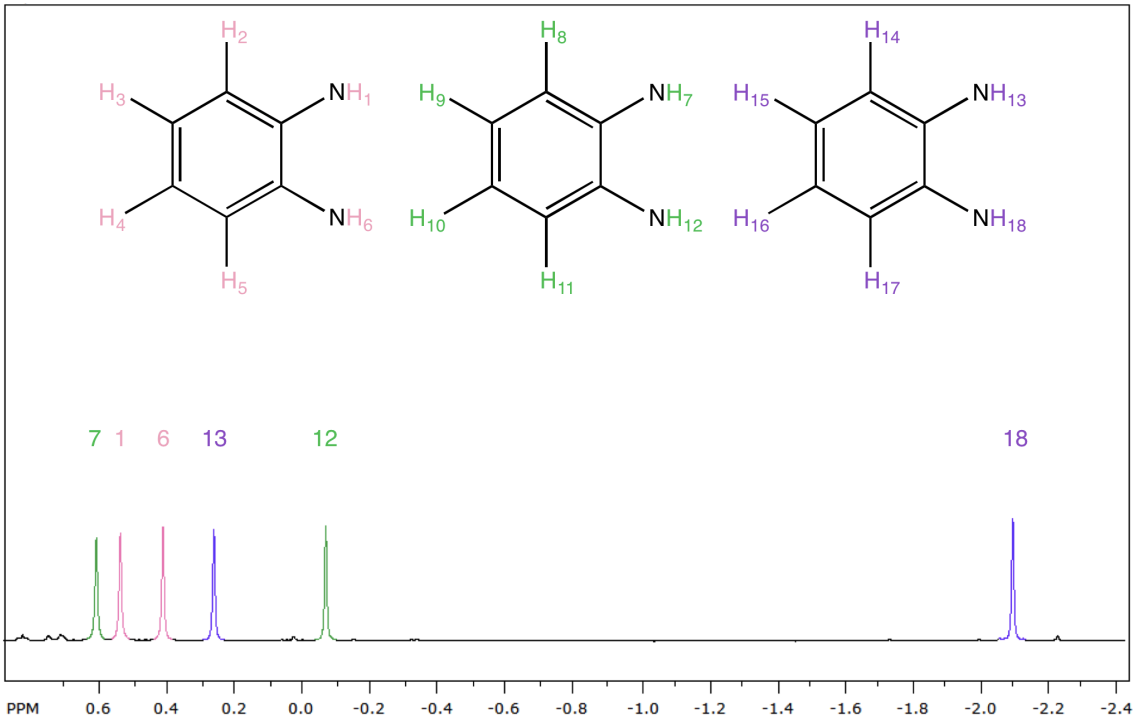

Figure 6.11: The ^{1}H NMR spectrum of **6.3**, showing the assigned amine region.

In order to probe the structure of **6.3** more fully, DFT studies were conducted by Dr Vincent at the University of Manchester, with the aim of rationalising the ^{1}H NMR shifts observed for this material. Calculations relating to the neutral **6.3a** were performed at three calculated levels [6-311++G(2DF,2PD) basis], originally using a 'fast' M06L functional then using the B3LYP functional, and finally the PBE1PBE functional which has been suggested as a method suitable for dealing with magnetic materials. All of these calculations produced six high-field NH resonances which, although not exactly concordant with the experimental data, showed the same trends. All three levels showed aromatic peaks between δ 6.0 – 8.0 ppm and high-field NH resonances. Although the predicted values did not correspond exactly with the experimental results, all calculations predicted a similar range of shifts in this NH region, around 1.5 ppm (experimentally the range seen is 1.6 ppm), with the M0L6 values being somewhat too low-field at δ 1.0 – -0.5 ppm and the B3LYP and PBE1PBE values being slightly too high-field at δ -1.7 – -3.1 ppm and -2.0 – -4.0 ppm respectively (experimental values were δ 0.63 – -2.10 ppm).

In order to simplify the calculations a relatively small basis set was used, and the inclusion of transition metals complicated the situation further, so given these caveats the results of the calculations reflect the experimental data for the **6.3a** system rather well, with the B3LYP level of theory giving the best results (Figure 6.12, Table 6.4). Similar M06L calculations were performed on the **6.3b** system, using the same basis set, which did not reflect the experimental data so closely. The results of this calculation showed proton shifts which were less well separated than those predicted from the calculations on **6.3a**, appearing more as a continuous spectrum, although high-field NH resonances were still present. The DFT calculations presented here support the hypothesis that only one species, **6.3a** is present in solution, as the calculations on this model fit the experimental data much more closely than those relating to **6.3b**.

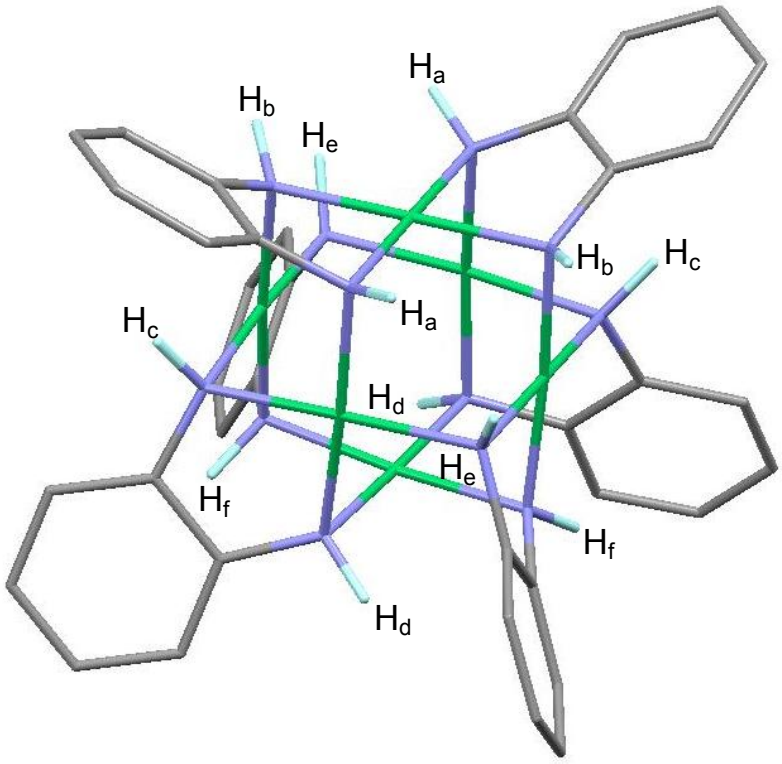

Figure 6.12: The structure of **6.3a** optimised at the B3LYP/6- 311++G(2df,2pd) level of theory (aromatic H-atoms omitted for clarity).

	$\mathbf{H}_a$	$\mathbf{H}_b$	$\mathbf{H}_c$	$\mathbf{H}_d$	$\mathbf{H}_e$	$\mathbf{H}_f$
δ **/ ppm (Calculated)**	-1.98	-1.73	-3.12	-2.71	-2.14	-2.91
	H	**H**	**H**	**H**	**H**	**H**
δ **/ ppm (Observed)**	0.58	0.63	-2.10	0.29	0.43	-0.05

Table 6.4: Calculated and observed ^{1}H NMR spectroscopic shifts (ppm) for **6.3a**. The structure was optimised at the B3LYP/6-311++G(2df,2pd) level of theory.

6.3 shared some common structural features with **6.1**, as both **6.1** and **6.3a** are hexanuclear cage structures. However, **6.3** proved to be a much more complicated system than **6.1**, containing two similar cage species, which caused difficulties in the initial characterisation of the material. Both the neutral and the heterometallic dianionic cage present within **6.3** (as **6.3a** and **6.3b** respectively) are examples of metallic cluster arrangements generated using a transition metal metallocene starting material. In this case it may be of interest to probe the magnetic properties of **6.3** in future studies as nickel(II) species have shown promise in the area of single-molecule magnets,[156] as have heterometallic nickel/lanthanum complexes.[157] It has been shown that the heterometallic cage Cu_6Na can be converted to $Cu_{12}La_8$

using metal salts.[158] It may be possible to adapt this technique in order to synthesise novel polynuclear metal complexes using **6.3** as a starting material, focusing on nickel/lanthanum species as potential magnetically interesting materials. **6.3** is also interesting in that it provides further evidence of the broad range of products accessible using metallocene starting materials and redox-active ligands, as **6.1** – **6.3** all employ identical methodology and yet produce significantly different molecular species.

Reactions of Transition Metal Metallocenes with 1,8-Diaminonaphthalene

Following the success of the reactions of the metallocenes with 1,2-benzenediamine it was decided to expand the research by investigating similar reactions using a related ligand. 1,8-Diaminonaphthalene was the logical choice as it is structurally more complex than the 1,2-benzenediamine ligand whilst being in the same family and likely to behave in a similar fashion. The 1,8-diaminonaphthalene ligand has been reported in several literature examples to be capable of bridging metal centres with the same $\mu_2{-}\mathrm{N}, \mu_2{-}\mathrm{N}'$ bonding mode adopted by the bridging LH_2 ligands in **6.2**.[159–161] However, there are only two known examples of the 1,8-diaminonaphthalene ligand adopting a chelating bonding mode (as seen in the terminal LH_2 ligands in **6.2**),[162;163] both of which feature the neutral ligand rather than the dianion $L'H_2$. As with 1,2-benzenediamine, the 1,8-diaminonaphthalene ligand was initially doubly-deprotonated by two equivalents of *n*-butyllithium to give the dianion (Scheme 6.4), which was then reacted with the metallocenes.

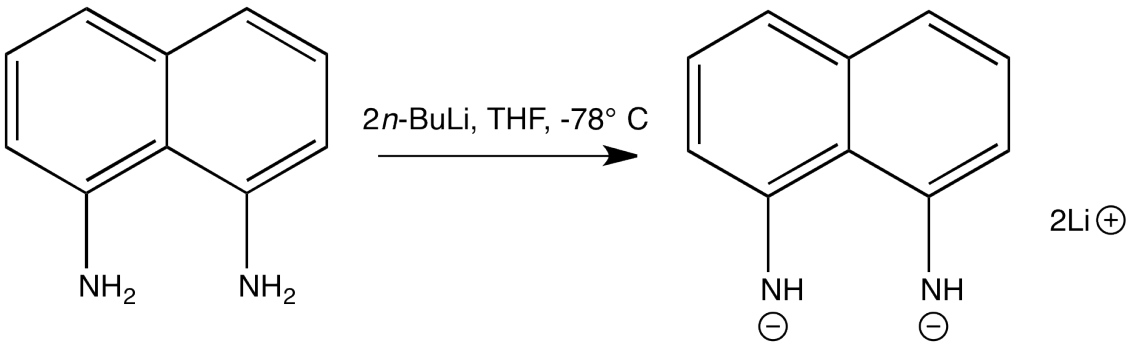

Scheme 6.4: Reaction scheme depicting 1,8-diaminonaphthalene being deprotonated to give the dianionic species used in the syntheses of **6.4** and **6.5**.

6.3.4 $(L'H_2)_3V(Li \cdot 2THF)_3$, 6.4

The synthetic strategy employed in the generation of **6.4** was modelled on that of **6.2**, with the intention being to increase the structural complexity of the ligand involved in the reaction and to observe the effect of this on the product formed (Scheme 6.5).[160] Crystals of **6.4** were isolated as brown blocks in a dark solution in a 6% yield (with respect to Cp_2V) from the reaction of 1,8-diaminonaphthalene with two equivalents of *n*-BuLi followed by *in situ* reaction in THF with Cp_2V and crystallisation at 5° C. **6.4** was characterised using ^1H and ^{13}C NMR spectroscopy, elemental analysis (C, H, N), and by single-crystal X-ray diffraction.

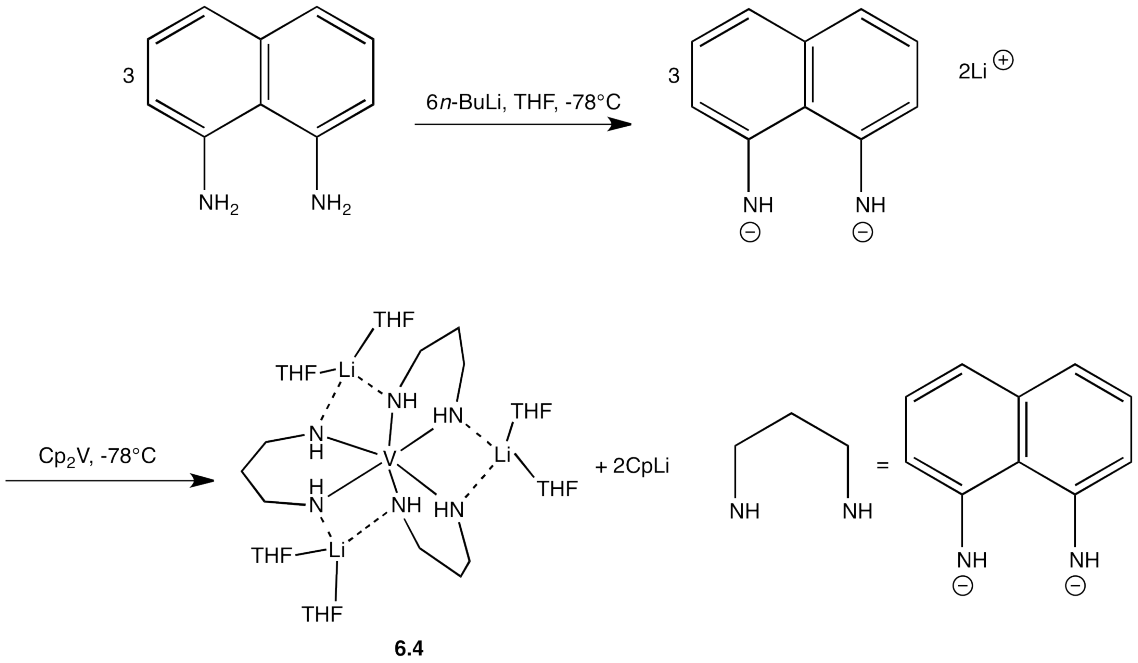

Scheme 6.5: Reaction scheme illustrating the synthetic method employed in the generation of $(L'H_2)_3V(Li \cdot 2THF)_3$, **6.4**.

NMR spectroscopy on **6.4** gives ambiguous results regarding the charge on the diaminonaphthalene ligand. A single type of aromatic ring is clearly discernible by ^1H NMR spectroscopy, but associated NH resonances are not observed. The spectroscopically observed ratio of THF to arene is 2:1. In order to elucidate the solid-state structure of **6.4**, single-crystal X-ray crystallographic studies were undertaken, which showed that the compound contains one vanadium centre complexed by three $L'H_2$ ligands. As in **6.2**, the vanadium has been oxidised to V(III). The ligand charge is balanced by three THF-solvated lithium ions which bridge the nitrogen centres of adjacent ligands (Figure 6.13).

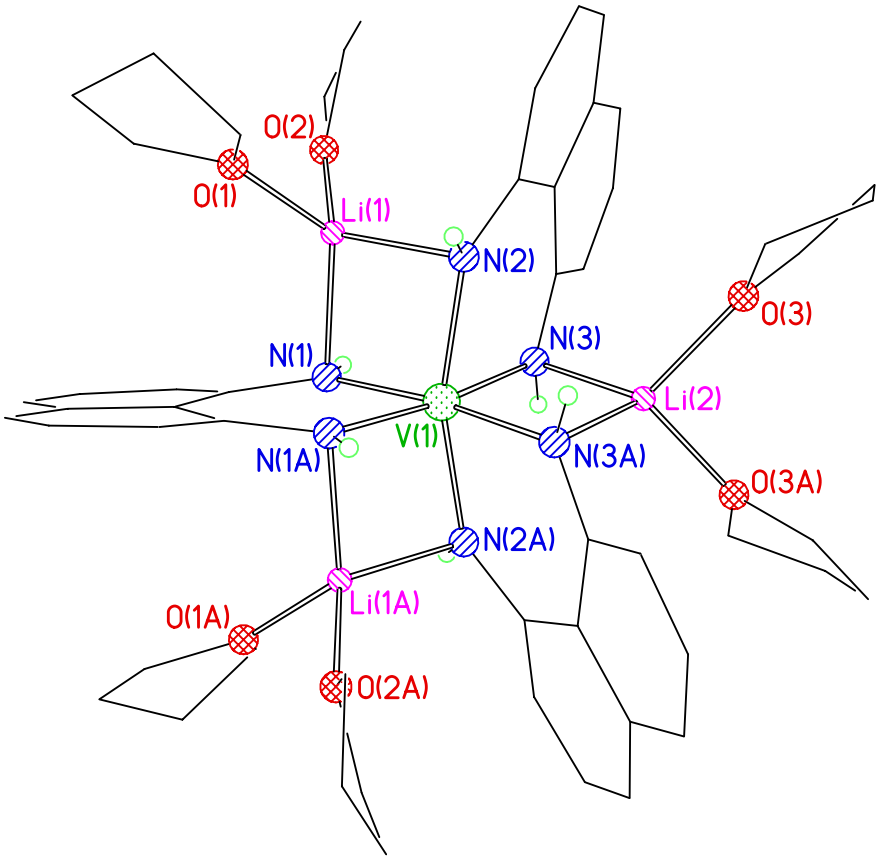

Figure 6.13: The crystal structure of $(L'H_2)_3V(Li \cdot 2THF)_3$, **6.4** with H-atoms omitted for clarity.

Atoms	**Distance (Å)**
V–N	2.047(2) – 2.094(3)
V···Li	2.741(9) – 2.792(5)
N–Li	2.068(6) – 2.117(6)
Li–O	1.931(6) – 1.959(6)
	Angle (°)
N–V–N	82.4(1) – 97.5(1)
N–Li–N	93.5(2) – 98.4(4)

Table 6.5: Selected bond lengths and angles for **6.4**.

The structure of **6.4** is unusual in that it features bridging between vanadium and an alkali metal, which is relatively uncommon. Mono-bridged species have been previously reported for vanadium(V) nitrides[164;165] and a V−V bonded vanadium(II) guanidinate,[22] but the formation of comparable $V(\mu{-}N)_2Li$ metallocycles has only been reported on two prior occasions; $(i{-}Pr_2N)_2V[\mu{-}CH_2C(=CH_2)Ni{-}Pr]Li$[166] and $Me_2V(\mu{-}NSit{-}Bu_3)_2Li$,[167] though the interstitial oxide $(Cy_2N)_4(MeC)V_2LiO$ has revealed a $V(\mu{-}N)(\mu{-}O)Li$ motif.[168]

The formation of this mono-vanadium complex contrasts with the previously reported ability of bis-nitrogen donor ligands to stabilise triple V≡V bonds, as in complex **1.13** (Figure 1.20). The vanadium centre in **6.4** is in a distorted octahedral environment, with the ligands bonded symmetrically (V−N bond distances range from 2.047(2) – 2.094(3) Å). The coordination of the ligand to lithium results in the formation of 4-membered metallocycles, which lie essentially flat, with the lithium residing only 0.24 Å out of the N−V−N plane. Vanadium(III) octahedral species have been noted previously, most often in the form of aquo-complexed[169;170] or otherwise solvated[171] tricationic metal centres, although the neutral species $V[PS_2(OEt)_2]_3$[172], $(acac)_3V$[173] and the mono-cationic $[L_6V]^+$ (L_6 = tetramethylenediamine-*N,N,N,N*-tetraacetate) have been reported.[174]

The prior synthesis of **6.2** led to the design of the synthetic strategy employed in the generation of **6.4**, with the aim of assessing the effect of the ligand changes involved. In both **6.2** and **6.4**, the vanadium centres are oxidised from V(II) to V(III), most likely by a disproportionation reaction. However, the product formed as a result of substituting 1,2-benzenediamine for 1,8-diaminonaphthalene was significantly different from **6.2**, with the observed structure of **6.4** containing one vanadium centre chelated by three dianionic $L'H_2$ ligands, with the nitrogen centres of adjacent ligands bridged by solvated lithium cations. This result shows the dramatic structural effects that changing the ligand can have. **6.2** also retained a cyclopentadienyl ligand from the metallocene starting material, a further indication that the chemistry of these materials is complex and that predicting the composition, structures and properties of the resultant species is non-trivial, an issue which is discussed further in Chapter 8.

6.3.5 $[(L'H_2)_2Ni(Li \cdot 2\,THF)]_2$, 6.5

The synthetic strategy employed in the generation of **6.5** was the same as that used in the synthesis of **6.4** (Scheme 6.6), and was modelled on that used in the prior syntheses of compounds **6.1** – **6.3**. Crystals of **6.5** were isolated as orange-red blocks in a dark red solution in a 34% yield (with respect to Cp_2Ni) from the reaction of 1,8-diaminonaphthalene with two equivalents of *n*-BuLi followed by *in situ* reaction in THF with Cp_2Ni and crystallisation at -30° C. **6.5** was characterised using ^1H and ^{13}C NMR spectroscopy, elemental analysis (C, H, N), and by single-crystal X-ray diffraction.

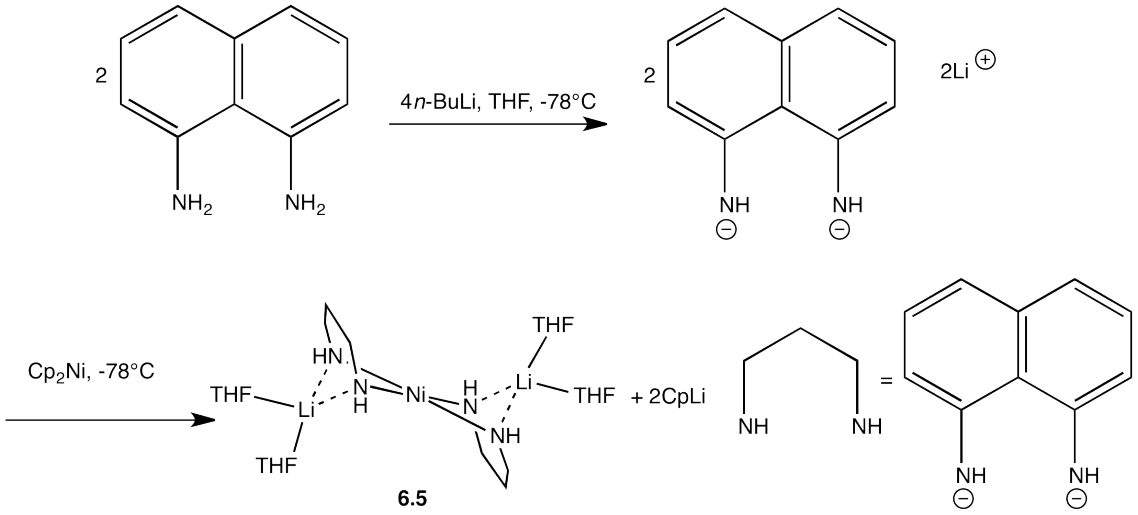

Scheme 6.6: Reaction scheme illustrating the synthetic method employed in the generation of $[(L'H_2)_2Ni(Li \cdot 2\,THF)]_2$, **6.5**.

^1H and ^{13}C NMR spectroscopy of **6.5** revealed that a single type of 1,8-diaminonaphthalene ring was present within this species, with the ^1H NMR spectrum containing a single NH resonance at δ 1.36 ppm. The signal integration indicated that the ligand had been vicinally doubly-deprotonated. The crystals of **6.5** used in these NMR studies were grown in a 1:1 solvent mixture of THF and toluene, with signals for both solvents observable in the ^1H and ^{13}C NMR spectra of the material. Toluene was only observed in trace amounts, whereas the ^1H resonances for THF were more considerable, with the diaminonaphthalene ring signals and the THF signals existing in a 1:2 ratio. This suggested that the crystallographic structure of **6.5** contained significant amounts of THF, either as part of the structure or trapped within the crystal lattice.

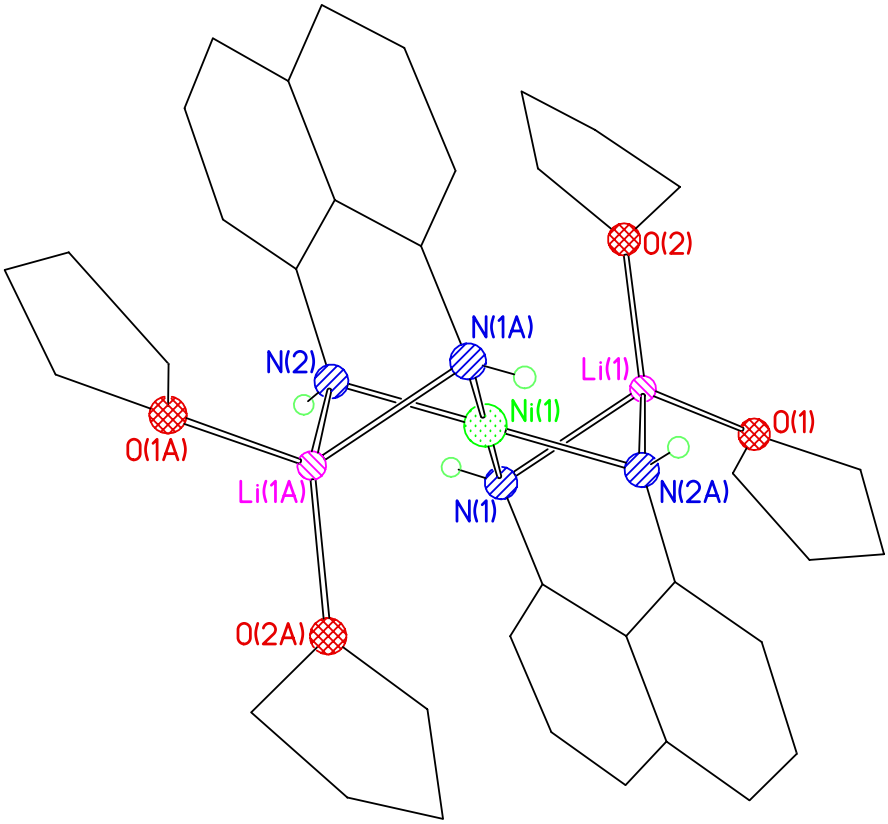

Figure 6.14: The crystal structure of $[(L'H_2)_2Ni(Li \cdot 2\,THF)]_2$, **6.5** with H-atoms and lattice toluene solvent omitted.

Atoms	**Distance (Å)**
Ni–N	1.877(2) – 1.901(2)
Ni···Li	2.552(4)
N–Li	2.089(5) – 2.101(5)
Li–O	1.927(4) – 1.933(5)
	Angle (°)
N–Ni–N	85.57(9) – 94.43(9)
Ni–N–Li	53.7(1) – 53.9(1)

Table 6.6: Selected bond lengths and angles for **6.5**.

The synthetic strategy employed in the generation of **6.5** was modelled on that of **6.3**, with the intention being to change the ligand involved in the reaction and to observe the effect of this on the product formed. 1,8-Diaminonaphthalene is more sterically demanding than 1,2-benzenediamine but is still capable of bridging metal centres.[160;175] However, the product formed as a result of substituting 1,2-benzenediamine with 1,8-diaminonaphthalene was significantly different from **6.3**, with the observed structure of **6.5** containing one nickel centre and two lithium centres bridged by the two dianionic 1,8-diaminonaphthalene ligands. Crystallographic studies show **6.5** to be a dilithium nickelate containing one Ni(II) centre complexed by two $L'H_2$ ligands and two bis-solvated lithium ions (Figure 6.14). The crystals were grown in a 1:1 solvent mixture of THF and toluene, and the crystallographic structure showed both THF molecules (solvating the lithium cations) and toluene molecules trapped within the lattice. The distorted square planar Ni^{II} centre is bound to four donor N-centres of the doubly-deprotonated organic ligand, giving the nickelate dianion. The inclusion of lithium in this structure leads to the formation of 4-membered metallocycles similar to those seen in **6.4**, although in this case rather than being flat these rings are puckered and distorted (the N-atoms lie on average 1.52 Å above or below the Li···Ni···Li plane).

The Ni−(μ−L)−Li motif seen in this structure is observed very rarely in the solid-state. In fact, aside from nickel porphyryns,[176;177] such η^2-N bridging of nickel and lithium has only been reported once previously, in the structure of the dinitrogen complex $(PhLi)_6Ni_2(N_2) \cdot 2\,(OEt_2)$[178] where dinitrogen is bonded 'edge-on' to a Ni−Ni moiety and simultaneously interacts with a lithium centre, increasing the N−N distance to 1.35 Å. This interaction does not result in a LiN_2Ni metallocycle of the type observed in **6.5**. More common are bridging interactions in which oxygen is the donor rather than nitrogen, although again in contrast to the $(L_4Ni^{II})Li_2$ scenario seen in **6.5**, these oxygen-bridged systems have generally taken the form $(L_3Ni^{II})Li$ with alkoxides,[179;180] quinolates,[181] carboxylates,[182;183] acetonates[184] and salen[185] derivatives all capable of acting as η^2-O inter-metal bridges. In the cases of salen systems and the alkoxide ligand $[Me_2NCH_2CHMeO]^-$ the formation of LiL_2Ni metallocycles is observed, and these are comparable to those seen in **6.5**.[179;185]

Of the two previously reported examples of the 1,8-diaminonaphthalene ligand adopting a chelating rather than bridging bonding mode,[162;163] one of these features a nickel(II) centre and two chelating ligands in a similar motif to **6.5**

(Figure 6.15). However, the structure of $[Ni(1,8{-}dan)_2(DMF)Cl]_2 \cdot 3\,H_2O$ (where 1,8-dan = 1,8-diaminonaphthalene) varies significantly from **6.5** in that the 1,8-diaminonaphthalene ligands coordinating the nickel centre are neutral, rather than doubly-deprotonated as the ligands seen in **6.5**. The asymmetric unit of $[Ni(1,8{-}dan)_2(DMF)Cl]_2 \cdot 3\,H_2O$ shows two $[Ni(1,8{-}dan)_2(DMF)]^+$ cations, charge-balanced by two chloride anions, with three water molecules present in the lattice. The observed Ni−N distances range from 2.070(2) – 2.108(2) Å, and are longer than those seen in **6.5** [range 1.877(2) – 1.901(2) Å], as is expected considering that the neutral ligand is less capable of electron donation to the metal than the doubly-deprotonated system.

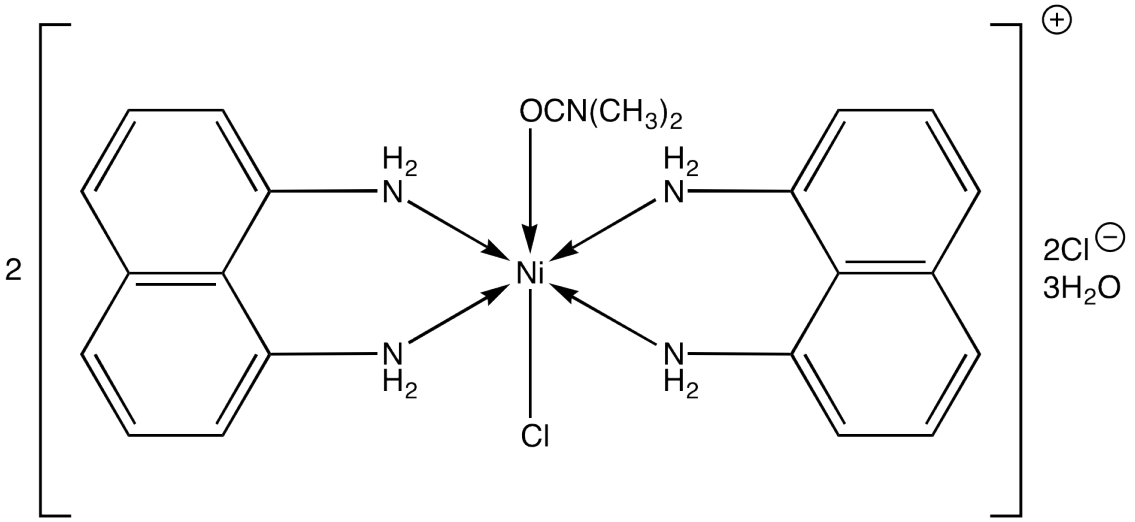

Figure 6.15: The structure of $[Ni(1,8{-}dan)_2(DMF)Cl]_2 \cdot 3\,H_2O$.

The complex $[Ni(1,8{-}dan)_2(DMF)Cl]_2 \cdot 3\,H_2O$ was tested as a 'green catalyst' (in this case meaning phosphorus-free) for the hydrogenation of acetophenone. The material showed some promise in the presence of KOH when H_2 gas was used as a hydrogen source, with a conversion of 72.1% and a turnover number of 721, although the conditions of 80° C and 50 atm pressure of H_2 used were fairly harsh. The development of phosphorus-free hydrogenation catalysts for practical applications is highly desirable for environmental reasons,[186;187] as is the replacement of precious metals such as ruthenium and iridium in such catalysts with cheaper alternatives, for economic reasons. Nickel is particularly suitable for preliminary studies due to it being relatively inexpensive, and the promising early results from the investigations into the catalytic properties of $[Ni(1,8{-}dan)_2(DMF)Cl]_2 \cdot 3\,H_2O$ suggest that the synthesis of materials such as **6.5** could be developed in this interesting and stimulating area.[188–190]

6.4 Conclusions

The study of the reactions of transition metal metallocenes with redox-active ligands was motivated by the observation that these metallocenes are capable of forming highly-charged multiply-bonded species such as **5.6**. This, combined with the redox effects of the ligands, provided the potential for the formation of higher- or mixed-oxidation state arrangements. The resulting complexes represent a diverse class of materials, from mixed-oxidation state clusters to metal-metal bonded species with novel magnetic properties. This area of research is particularly ripe for further development as the chemistry of these materials is still largely unknown, in particular in relation to their potential applications with regard to catalysis and magnetic data storage. These preliminary studies also demonstrate the versatility of metallocenes in these syntheses as well as illuminating the research possibilities related to this area, as interest in single-molecule magnets and organometallic catalysis continues to grow. Ligand choice played an important role in these studies, with this preliminary work focusing on structurally simple molecules, investigating 1,2-benzenediamine first as it had shown promise as ligand for main group and transition metal species. The study was then extended to a related system, that of 1,8-diaminonaphthalene, and the results obtained demonstrated that these changes have a profound effect on the properties of the products isolated.

Chapter 7

General Conclusions

The aims of this project, as described in the Introduction (Section 1.4) were as follows -

- To synthesise and characterise a range of transition metal-containing complexes and materials using transition metal metallocenes as starting materials.
- To develop the synthetic chemistry of the transition metal metallocenes, using their known reactivity patterns and versatility to design novel reaction pathways, and to fully investigate the properties of any resulting materials.
- To investigate the reactivity of transition metal metallocenes with nitrogen-based redox-active ligands.
- To study the variable-temperature magnetic behaviour of products formed, where relevant.
- To study any inter-metal bonding interactions (in particular any multiple bonds) of products formed where relevant, including by computational methods.

The research presented within this project concentrated on the first of these aims, as a range of novel transition metal-containing species were synthesised and characterised. These successful syntheses also contributed to the existing field of transition metal metallocene chemistry, adding to and developing what is already known about the use of these materials as starting materials within organometallic synthesis. The obvious conclusion to draw from these studies is that first-row transition metal metallocenes are suitable starting materials for a range of organometallic products, and can be used as versatile synthetic precursors for metal-containing materials.

It can also be concluded that the metallocenes utilised in this study offer access to materials that would not be obtained easily or at all with the more commonly used transition metal halides as starting materials. These products include the multiply-bonded chromium paddlewheel **5.6**, which is peripherally functionalised by units of CpLi originating from the metallocene starting material. In several of the characterised products cyclopentadienyl ligands remained coordinated to the metal centre to which they are bound in the reagent Cp_2M. All of the compounds presented in Chapter 4 are dimeric molecules featuring two metal centres and two cyclopentadienyl ligands amongst their components, although they differ significantly in their structures and properties. In all of these cases the retention of the cyclopentadienyl ligand is a result of the limited ability of metallocenes to fully deprotonate organic acids, a subtle reactivity that leads to the isolation of interesting and varied solid-state structures.

Another conclusion that can be drawn from the research presented is that there is great potential for metallocene starting materials to be used in the generation of magnetic materials which could conceivably have applications in data storage or other areas. The preliminary research into this area discussed in Chapter 6 shows that when magnetic measurements were undertaken on the vanadium dimer **6.2**, the results were not straightforward and will require further investigation to enable a full understanding of the behaviour of these materials. Although the magnetic behaviour of this molecule is not fully understood it is certainly interesting, as it has a much higher than anticipated magnetic response along with some temperature-independent paramagnetic contribution. The mixed-oxidation state manganese cage **6.1** is a representative of a class of materials that are currently highly desirable; manganese-based clusters with the potential to be developed into single-molecule magnets through tuning of the coordinated ligands. The formation of this species and other transition metal structures containing redox-active ligands from reactions with metallocene precursors is promising with regards to the development of novel magnetic materials.

Some of the manganese chemistry presented herein bears similarities to magnesium chemistry described within the literature. A magnesium analogue of **6.1**, minus the oxide core, was reported by Clegg *et al.* in 1994 as the first octahedral Mg_6 cluster.[191] The structure differs slightly from that of **6.1** as every magnesium centre is solvated by a THF molecule, giving each a five-coordinate square-pyramidal geometry with all of the metal centres in the +2 oxidation state, although the

essential connectivity is very similar. There are also examples of magnesium species which share key structural characteristics with **5.4**, namely the classical 'Weiss motif'[192] arrangement whereby linear Li···M···Li centres are connected by four anionic ligands. Of the published examples of lithium magnesiates, several structures feature amido ligands,[193–195] and the recently published tetraorganomagnesiate $[(TMEDA)Li_2Mg(CH_2SiMe_3)_4]$ has a very similar structural arrangement to that seen in **5.4**.[196] This relationship between magnesium and manganese is worth noting, as the body of existing literature pertaining to magnesium coordination chemistry provides a useful insight into the formation of related manganese species, and could be used to inform and direct further study.

One of the established aims of this projects was to investigate any inter-metal bonding within the products obtained, wherever relevant. This was achieved largely through DFT calculations and inference from similar compounds, and also by taking into account the electronic configurations of the materials in question. It was thus established that, for example, **4.3** had a single Mn−Mn bond, **5.3** and **5.6** contained quadruple Cr−Cr bonds, and that **5.2** and **5.5** showed no degree of inter-metal bonding between nickel centres. Other examples are discussed in the relevant chapters, but it can be seen that the aim set out at the beginning of the project, to assess the degree of inter-metal bonding within relevant compounds, was achieved through a combination of methods. This aspect of the work was important as it established the materials most likely to be suitable for further reactions, or to possess some catalytic capabilities. Multiply-bonded metal centres can be used to trap small molecules, act as catalytic sites, and be exploited synthetically, for example as precursors to supramolecular networks. Therefore, the establishment of the bonding situations within the molecules discussed in this project was a vital aspect of the research, and one which was managed successfully. The information yielded by these investigations will assist in directing future study into these structures and related materials.

The research presented throughout this project serves as an illustration of how metallocene starting materials can be deployed in the generation of novel products. These products provide new opportunities for the construction of magnetic materials and supramolecular networks, areas which are currently being pursued within the groups. The aims set out at the beginning of the project were largely achieved, although to different extents as more emphasis was placed on the synthetic goals of the project than on the more materials-based aspects, such as the research into the

magnetic properties of some of the species characterised herein. The synthetic goal of producing a range of novel metal-containing materials was particularly successful, as several of the species discussed within this project differ significantly from each other, even in cases where similar methodologies and indeed ligands were employed in the syntheses. An example of this can be seen within Chapter 6, where three metallocenes (Cp_2Mn, Cp_2V and Cp_2Ni) were reacted with the same ligand to give three products that differed both structurally and in terms of their properties. However, this can also be viewed as a drawback in that it is extremely difficult to predict the outcomes of these reactions, limiting the degree of control it is possible to exert and making synthetic design problematic. The yields also tended to be variable, and the air- and moisture-sensitivity of both the starting materials and the products renders handling and isolating them non-trivial.

In summary, this research furthers our collective understanding of metallocene reactivity and contributes to the field of synthetic inorganic chemistry related to metallocene chemistry. The ways in which this research could be used to direct further studies are discussed at length in Chapter 8.

Chapter 8

Future Work

The scope of this project was very broad, and the results obtained are suitable for development in several different ways. The main aim of the project, the synthesis of novel organometallic compounds using first-row transition metal metallocenes as starting materials, lends itself to almost infinite further study as long as suitable ligands can be obtained for syntheses. More generally, the complexes structurally characterised within this work can be seen as proof-of-concept as to the viability and versatility of using the metallocenes as starting materials, and can be used as a basis for designing other, similar reactions and making informed choices as to appropriate ligands, solvents and reaction conditions. Although synthesis is the most obvious route along which this research can be developed, there are other areas into which it can be seen as a logical progression from this research to explore. In terms of future synthetic work, more specific examples of how to build on the results already obtained are discussed below, with the understanding that any future work would be less broad in nature and would instead focus more closely on the individual synthetic challenges presented by this research.

The structurally analogous compounds **4.1** and **4.2** discussed in Chapter 4, along with similar examples previously reported in the literature, offer an insight into the extent to which manganocene can be used as a Brønsted base to deprotonate organic acids. This could be developed into a study of the precise boundaries of this type of reactivity, if a range of acids of known pK_a were reacted with manganocene in order to assess exactly how strong an acid has to be in order to be singly- or doubly-deprotonated by the metallocene reagent. If this study were successful, it could be expanded to the other first-row transition metal metallocenes in order to establish more comprehensive guidelines relating to the ability of these materials to deprotonate organic acids, aiding future syntheses and contributing

further knowledge to the field of synthetic metallocene chemistry. Further work could also focus on expanding the family of materials related to **4.1** and **4.2** and on analysis of materials obtained, for example in relation to their magnetic behaviour.

The manganese phosphine/phosphide dimer **4.3** discussed in Chapter 4, Section 4.3.3 was novel in its ligand arrangement, but disintegrated easily on exposure to vacuum and in solution. One area in which this research project could be developed is that of phosphorus-donor transition metal clusters and paddlewheel complexes, as these are still relatively rare compared with their oxygen- and nitrogen-donor counterparts. The use of phosphorus-based ligands allows access to compounds with different electronic properties from the oxygen- and nitrogen-based analogues. The original synthetic strategy behind **4.3** was directed toward the potential formation of analogues of the amido/imido manganese clusters discussed in Chapter 1, Section 1.3.3, using primary phosphine ligands capable of bridging metal centres. Although this was not the direction in which the research evolved, phosphorus-ligated manganese clusters remain a desirable synthetic target, and further work relating to this field would be a rational continuation of the research presented within this project. The initial focus would likely be directed at ligand choice, with an obvious first step being the synthesis of direct phosphorus analogues of the nitrogen-containing 2-aminopyrimidine ligands successfully used by Bond *et al.* in the generation of amido/imido clusters.[16] If this approach proved successful, further ligand manipulations could be undertaken in order to create a family of related compounds, which could then undergo variable-temperature magnetic studies in order to screen them for any unusual or interesting magnetic behaviour.

In terms of synthetic developments, some of the compounds reported within Chapter 5 are highly interesting, whereas some are unlikely to elicit much further study. The simple paddlewheel complexes **5.2** and **5.5** both contain two nickel centres and four bridging N-donor ligands in the familiar M_2L_4 conformation, with no inter-metal bonding between the nickel centres evident. As such, they are unlikely to be active as catalysts or have any immediately obvious applications, so although they contribute to the field of transition metal paddlewheel chemistry and have some interesting structural features, it is unlikely that further research would focus particularly on developing this chemistry. The vanadium analogue of **5.2** is a potential synthetic target, as it would complete the family of *N,N′*-dimethylformamidinate paddlewheels obtained from the metallocenes employed within this project, and would likely contain a triple bond, and so be more likely to

possess catalytic activity than its nickel counterpart. This could then be developed into a study in which the ligands were systematically substituted for related ligands, in order to build a more comprehensive picture of the ligand effects on the sterics and electronics of these systems. The aim of this would be to obtain results for all of the relevant transition metal metallocenes and compare them, as well as to observe how ligand choice affects factors such as inter-metal distance. The manganese analogue of **5.2** and **5.3** has also yet to be obtained, with the only isolable product from the reaction thus far being the manganese-oxo complex **5.1**. In order to obtain the oxygen-free version, some modification of the synthesis would be required, such as carrying out the entire preparation within a glovebox environment.

The tetrahedral manganese-oxo cage **5.1** could be a subject for further study on its own merit, particularly in conjunction with the related octahedral manganese-oxo cage **6.1**. The initial research would likely focus on establishing where the interstitial oxide in each species originates from, and how to make these materials in a more controlled manner, possibly through the considered introduction of a limited amount of water at some point during synthesis. The introduction of oxygen into organometallic complexes is discussed in Chapter 1, Section 1.3.2, with one method being the layering of the dry reaction solution with wet hexanes to produce crystals with the desired encapsulated oxide ion. The ability of **5.1** to trap oxygen in this manner without more substantial decomposition occurring and the oxygen-scavenging nature of the manganese ions could potentially lead to applications within organometallic chemistry, removing oxygen from systems. Development of this exact system into a practical method of oxygen removal may not be possible but research into related materials could lead to the furthering of this idea and the potential development of suitable materials for oxygen removal within syntheses.

With regards to specific compounds, one obvious direction into which to take this research would be to investigate the catalytic potential of the multiply bonded chromium species from Chapter 5, in particular **5.3**, $Cr_2(N,N'-\text{dimethylformamidinate})_4$. As mentioned within the discussion of this compound, Cr_2 units have recently been utilised in oxygen binding studies as part of the complex $Cr_3(1,3,5-\text{benzenetricarboxylate})_2$.[118] This material features paddlewheel-type arrangements of quadruply-bonded Cr^{II} centres connected *via* triangular BTC^{3-} ligands to give a porous three-dimensional framework. This is known to be capable of reversible binding of O_2 across the Cr−Cr bond although the dissociation conditions, which require heating to 50° C under vacuum for 48 hours, are as yet too

energy-intensive for practical purposes. However, this research, presented by Long, has potential implications for materials such as **5.3**, in which the *N,N′*-ligands allow for tight control of the steric and electronic properties of the product obtained, and the paddlewheels formed are similar to $Cr_3(1,3,5-\text{benzenetricarboxylate})_2$, with open structures that expose the metal centres which are therefore available for small-molecule coordination. A collaboration with the Long group on this research would potentially be beneficial. It would also be expedient to develop the materials aspect of this research, in particular probing possible ways in which molecular compounds such as **5.3** could be isolated and mounted in order to render them more practical for use as catalysts or for the binding of small molecules. For example, solid-state catalysts are often used in the form of thin films deposited onto the internal surfaces of a vessel, a process which has not been attempted with **5.3**, and the viability of which would need to first be established before pursuing any catalytic studies.

Compounds **5.4** and **5.6** are similar in that they both contain lithium as well as one or more transition metal centres in their solid-state structures. Compound **5.4** is not obviously related to any of the other species reported within this project, featuring as it does one manganese centre and two lithium centres bridged by monodentate guanidinates to give a spirocyclic molecule that is then asymmetrically coordinated by THF. It is unlikely that much future work would be focused around this particular species, as it is improbable that this or related compounds would exhibit any desirable catalytic or magnetic behaviour. Compound **5.6**, however, is particularly interesting and it is likely that some further work would be directed towards extending this result by creating a family of such structures, with suitable aromatic ligands chosen for their ability to assist in stabilising the CpLi units that, in the case of **5.6**, decorate the periphery of the molecular structure. It may be possible to develop this into the synthesis of supramolecular arrangements, using bridging ligands to support an extended network of structures with the potential capability of trapping CpLi or other small molecule fragments within this network. Trapping of fragments that are not otherwise accessible can increase knowledge about rare systems and aid in the development of further syntheses and materials. The isolation and characterisation of **5.6** can be seen as further proof that metallocenes are valuable starting materials for research focused on the synthesis of complex molecular structures with the capability to trap or form co-complexes with other molecular fragments.

The synthetic possibilities relating to the novel complexes presented in Chapter 6 are myriad, as research into reactions of transition metal metallocenes with redox-active ligands is an area which has only recently begun to be investigated in a systematic and meaningful way. The complexes **6.1** - **6.5** utilise structurally simple ligands, although this leads to a diverse range of products - developing this chemistry through the use of more complex ligands could lead to any number of notable results, with materials produced likely to possess interesting magnetic properties. Similarly, using analogues of the ligands already investigated but replacing the N-donor ligands with O-, S-, or P-donor atoms may provide further information as to the nature of the products formed, as tuning the electronic properties of the ligands may lead to formation of products with different material properties. Developing a family of related molecules based on such ligands is likely to yield more structurally and magnetically novel complexes and is an area into which future work related to this project is likely to enter, with an emphasis on mixed-oxidation state clusters that may be capable of magnetic data storage.

The magnetism studies presented within this project constitute the first foray into expanding the synthetic aspect of the research into materials-based analysis of the properties of the reported compounds. This is an area into which it would be logical to develop, particularly with regard to the species presented within Chapter 6. These materials utilise redox-active ligands to promote the formation of various metal-based compounds, including heterometallic species, polynuclear clusters and asymmetric transition metal coordination species. The latter of these, the ion-separated species **6.2**, has already shown unique magnetic behaviour which would benefit from further study since, as yet, the data collected does not fit any proposed models. One suggestion as to how to progress with regards to magnetic measurements on this compound is to synthesise a fully deuterated version of **6.2** and undertake a neutron diffraction study. This poses some problems due to the expense and potential difficulty involved in the synthesis of a deuterated analogue of the product. However, it is one route which could be explored if research were to continue on this particular material. It has also been suggested that the magnetic behaviour of **6.2** may be due to a phase change occurring within the material at a certain temperature, in which case variable-temperature X-ray crystallography could be employed to elucidate this. A collaboration with magnetism specialists would perhaps facilitate this work, particularly if they are able to offer advice on mounting and handling extremely air-sensitive magnetic materials, as that was one of the major difficulties when undertaking the original studies.

The manganese-oxo mixed-oxidation state cage **6.1** would also be suitable for magnetic studies. As discussed in Chapter 6, Section 6.3.1, the field of manganese-based single-molecule magnets is one which is attracting much interest currently, with advancements being made towards the creation of magnetic materials suitable for use in a data storage capacity, for example within hard drives. Other uses for SMMs have also been posited, including applications within quantum computing and magnetic refrigeration.[74] Recent developments in this area include the synthesis of a molecular material with the highest energy barrier to magnetisation of any compound reported thus far; 86.4 K ($[Mn_6O_2(sao)_6(O_2CPh)_2 \cdot 4\,EtOH]$, **1.17**).[80] A high energy barrier is desirable as it means that the material remains magnetised for longer, and the molecule that achieved this record value was an "Mn_6" cluster featuring Mn^{III} ions and bulky oxygen-donor salicylaldoxime ligands. This species is structurally quite similar to **6.2**, as they are both clusters based around six manganese centres bridged by ligands, although in the case of **1.17** the ligands are oxygen- rather than nitrogen-based and the manganese ions are all in the +3 oxidation state. In order to move the research presented in this project into this area, some further proof-of-concept work would need to be undertaken in order to establish suitable ligands and reaction conditions for generating materials likely to display this type of magnetic behaviour. It would also be necessary to optimise said reactions in order to give sufficiently high yields for extensive magnetic studies. One of the limiting factors in undertaking magnetic analysis of **6.1** was the extremely air-sensitive nature of the material, so the use of bulkier N-donor ligands to reduce this and to structurally mimic molecules with established desirable magnetic behaviour such as $Mn^{III}{}_6O_2(sao)_6(O_2CPh)_2 \cdot 4\,EtOH$ provides a rational way in which to initiate this research.

There are several more specific ways in which this research could be developed. The issue of low yields, mentioned briefly in Chapter 7, would need to be addressed before this work could be extended into other areas. The yields obtained for many of the products were highly variable and unpredictable, so optimisation of reaction conditions and investigation into alternate methodologies to improve yields would be a logical next step in developing this research, particularly if the eventual aim is to make commercial use of these species where they will need to be produced consistently on a viable scale. One aspect that was not within the scope of this project but which would be valuable is the investigation into scaling-up these reactions, although this would only be worthwhile if studies into improving

the yields had been undertaken. Most of the syntheses were carried out using approximately 100 mg of the metallocene starting material, a decision which was due to the very air- and moisture-sensitive nature of both the reactants and the products, in order to minimise the amount of material lost if the reaction should become exposed to the atmosphere. To facilitate larger scale syntheses, it would be necessary to consider alternative methodologies. Performing entire reactions within a glovebox environment would be a potential area in which to progress, as this would help eliminate atmospheric contamination during synthetic steps such as filtration, when the attachment and detachment of the filter stick make air exposure more likely. Increasing the reliability of these reactions would allow for further study of the products and would increase the likelihood of them being used in further reactions, either as reagents or as catalysts.

The research undertaken within this project also highlighted several issues with the reported reactions, largely concerning their unpredictability. In several cases the products obtained from reactions were not those expected or predicted, and had to be rationalised retroactively. As demonstrated throughout Chapter 6, making very minor changes to either the ligand or the metallocene used in reactions led to major differences in product identity and structure, which again were unpredictable. These factors may frustrate some of the further work undertaken, and may mean that some of the ideas postulated within this chapter are not in fact viable, in particular the creation of libraries of compounds closely related to those already characterised.

One way of building upon the research presented within this project would be to focus more closely on potential applications of the products already characterised, possibly in conjunction with the scaling-up research described above. This approach avoids the issues of unpredictability and lack of control related to using the reported reactions to generate more novel compounds, instead restricting further research to the compounds already obtained. The focus of this project was largely synthetic, with the main aim being the synthesis and characterisation of novel materials using first-row transition metal metallocenes as reagents. As such, there is not much research into the applications that these materials might be suited for, aside from some preliminary magnetic measurements, as this was not within the remit of the project. Future work could delve into this area, particularly with regard to catalytic applications and magnetic possibilities.

References

[1] T. J. Kealy and P. L. Pauson, "A New Type of Organo-Iron Compound", *Nature*, 1951, **168** (4285), 1039.

[2] E. O. Fischer and W. Pfab, "Zur Kristallstruktur der Di-Cyclopentadienyl-Verbindungen des Zweiwertigen Eisens, Kobalts und Nickels", *Z. Naturforsch. B 7*, 1952, 377.

[3] G. Wilkinson, M. Rosenblum, M. C. Whiting and R. B. Woodward, "The Structure of Iron Bis-Cyclopentadienyl", *J. Am. Chem. Soc.*, 1952, **74** (8), 2125.

[4] P. F. Eiland and R. Pepinsky, "X-Ray Examination of Iron Biscyclopentadienyl", *J. Am. Chem. Soc.*, 1952, **74** (19), 4971.

[5] J. D. Dunitz and L. E. Orgel, "Bis-Cyclopentadienyl Iron: A Molecular Sandwich", *Nature*, 1953, **171** (4342), 121.

[6] S. Coriani, A. Haaland, T. Helgaker and P. Jørgensen, "The Equilibrium Structure of Ferrocene", *ChemPhysChem.*, 2006, **7** (1), 245.

[7] R. B. Woodward, M. Rosenblum and M. C. Whiting, "A New Aromatic System", *J. Am. Chem. Soc.*, 1952, **74** (13), 3458.

[8] R. A. Layfield, "Manganese(II): the Black Sheep of the Organometallic Family", *Chem. Soc. Rev.*, 2008, **37** (6), 1098.

[9] A. D. Bond, R. A. Layfield, J. A. MacAllister, M. McPartlin, J. M. Rawson and D. S. Wright, "The First Observation of the $[Cp_3Mn]^-$ Anion; Structures of Hexagonal $[(\eta{-}Cp)MnK \cdot 1.5thf]$ and Ion-Separated $[(\eta{-}Cp)Mn][Mg(thf)] \cdot 2\,thf$", *Chem. Commun.*, 2001, (19), 1956.

[10] N. Feeder, A. D. Hopkins, R. A. Layfield and D. S. Wright, "Synthesis and Structure of $[Cp_2PbCp^{thf}Na] \cdot 0.5thf$; Implications to the Control of Di-

mensionality in p-Block Metallocene Anion Systems (Cp = C_5H_5, Cp^{thf} = $\{C_5H_4\}CH_2C_4H_7O$)", *J. Chem. Soc., Dalton Trans.*, 2000, (14), 2247.

[11] C. Brinkmann, F. García, J. V. Morey, M. McPartlin, S. Singh, A. E. H. Wheatley and D. S. Wright, "Stepwise Nucleophilic Substitution of Manganocene, Syntheses and Structures of the Dimer $[CpMn(hpp)]_2$ and the Unusual Manganate Cage $[LiMn(hpp)_3]_2$ (hppH = 1,3,4,6,7,8-hexahydro-2*H*-pyrimido[1,2-*a*]pyrimidine)", *Dalton Trans.*, 2007, (18), 1570.

[12] R. A. Layfield and S. M. Humphrey, "A Manganese(II) Allyl Complex: Synthesis, Structure, and Magnetic Properties of $[Li(thf)_4][Mn\{\eta^3-(Me_3Si)_2C_3H_3\}\{\eta^1-(Me_3Si)_2C_3H_3\}_2]$", *Angew. Chem., Int. Ed.*, 2004, **43** (23), 3067.

[13] C. S. Alvarez, A. Bashall, E. J. L. McInnes, R. A. Layfield, R. A. Mole, M. McPartlin, J. M. Rawson, P. T. Wood and D. S. Wright, "Structural and Magnetic Studies of the Tris(cyclopentadienyl)manganese(II) "Paddle-Wheel" Anions $[Cp_{3n}(MeCp)_nMn]$ (n = 0 – 3, MeCp = $C_5H_4CH_3$, Cp = C_5H_5)", *Chem.-Eur. J.*, 2006, **12** (11), 3053.

[14] B. D. Murray and P. P. Power, "Three-Coordinate Metal Amides of Manganese(II) and Cobalt(II): Synthesis and X-Ray Structure of the First Tris(silylamide) of Manganese and the X-Ray Crystal Structures of $[M_2(N(SiMe_3)_2)_4]$ (M = Mn, Co)", *Inorg. Chem.*, 1984, **23** (26), 4584.

[15] C. S. Alvarez, A. D. Bond, E. A. Harron, R. A. Layfield, J. A. McAllister, C. M. Pask, J. M. Rawson and D. S. Wright, "Synthesis and Structure of the Octanuclear Manganese(II) Cage $[(\eta-Cp)Mn\{2-NH(4,6-Me_2pm)\}\cdot Mn\{2-N(4,6-Me_2Pm)\}]_4$ (Cp = C_5H_5, pm = Pyrimidine)", *Organometallics*, 2001, **20** (20), 4135.

[16] C. S. Alvarez, A. Bashall, A. D. Bond, D. Cave, E. A. Harron, R. A. Layfield, M. E. G. Mosquera, M. McPartlin, J. M. Rawson, P. T. Wood and D. S. Wright, "Applications of Manganocene in the Synthesis of Mn(II) Amide and Imide Cages", *Dalton Trans.*, 2003, (15), 3002.

[17] M. A. Beswick, J. S. Palmer and D. S. Wright, "p-Block Metallocenes: The Other Side of the Coin", *Chem. Soc. Rev.*, 1998, **27** (3), 225.

[18] S. Iqbal, *Chemistry Of P-Block Elements*, Discovery Publishing House Pvt. Limited, 2003.

[19] S. Harder, "Recent Developments in Cyclopentadienyl-Alkalimetal Chemistry", *Coord. Chem. Rev.*, 1998, **176** (1), 17.

[20] D. R. Armstrong, M. J. Duer, M. G. Davidson, D. Moncrieff, C. A. Russell, C. Stourton, A. Steiner, D. Stalke and D. S. Wright, ""Paddle-Wheel" Tris(cyclopentadienyl)tin(II) and -lead(II) Complexes: Syntheses, Structures, and Model MO Calculations", *Organometallics*, 1997, **16** (15), 3340.

[21] J. Hartwig, *Organotransition Metal Chemistry: From Bonding to Catalysis*, University Science Books, 2010.

[22] C. Fernández-Cortabitarte, F. García, J. Morey, M. McPartlin, S. Singh, A. Wheatley and D. Wright, "Trapping of Oligomeric Cyclopentadienyllithium Cationic and Anionic Fragments by a V≡V-Bonded Ligand", *Angew. Chem., Int. Ed.*, 2007, **46** (28), 5425.

[23] J. Haywood, F. A. Stokes, R. J. Less, M. McPartlin, A. E. H. Wheatley and D. S. Wright, "A Quadruply-Bonded $[Cr_2(guanidinate)_4]^{4-}$ Tetraanion", *Chem. Commun.*, 2011, **47** (14), 4120.

[24] N. Sidgwick, *The Electronic Theory of Valency*, The Clarendon Press, 1927.

[25] D. Shriver, *Inorganic Chemistry*, Oxford University Press, 2006.

[26] J. Su, X.-W. Li, R. C. Crittendon and G. H. Robinson, "How Short is a −Ga≡Ga− Triple Bond? Synthesis and Molecular Structure of $Na_2[Mes^*{}_2C_6H_3{-}Ga{\equiv}Ga{-}C_6H_3Mes^*{}_2]$ (Mes^* = 2,4,6-*i*-$Pr_3C_6H_2$): The First Gallyne", *J. Am. Chem. Soc.*, 1997, **119** (23), 5471.

[27] Y. Xie, H. F. Schaefer III and G. H. Robinson, "The Gallium−Gallium Triple Bond in a Realistic Model. A Density Functional Theory Study of $Na_2[(C_6H_5)_2C_6H_3GaGaC_6H_3(C_6H_5)_2]$", *Chem. Phys. Lett.*, 2000, **317** (1-2), 174.

[28] M. M. Olmstead, R. S. Simons and P. P. Power, "Synthesis and Characterization of $[Sn_2\{C_6H_3{-}2_6(2,4,6{-}i{-}Pr_3C_6H_2)_2\}_2]^{-\cdot}$: A Singly Reduced Valence Isomer of a "Distannyne"", *J. Am. Chem. Soc.*, 1997, **119** (48), 11705.

[29] F. A. Cotton, A. H. Cowley and X. Feng, "The Use of Density Functional Theory To Understand and Predict Structures and Bonding in Main Group Compounds with Multiple Bonds", *J. Am. Chem. Soc.*, 1998, **120** (8), 1795.

[30] G. H. Robinson, "Gallanes, Gallenes, Cyclogallenes, and Gallynes: Organometallic Chemistry about the Gallium−Gallium Bond", *Acc. Chem. Res.*, 1999, **32** (9), 773.

[31] S. Aldridge and A. Downs, *The Group 13 Metals Aluminium, Gallium, Indium and Thallium: Chemical Patterns and Peculiarities*, Wiley, 2011.

[32] R. Crabtree, *The Organometallic Chemistry of the Transition Metals*, John Wiley & Sons, 2009.

[33] T. Nguyen, A. D. Sutton, M. Brynda, J. C. Fettinger, G. J. Long and P. P. Power, "Synthesis of a Stable Compound with Fivefold Bonding Between Two Chromium(I) Centers", *Science*, 2005, **310** (5749), 844.

[34] F. A. Cotton, C. A. Murillo and R. A. Walton, *Multiple Bonds between Metal Atoms*, Springer, 2005.

[35] F. A. Cotton, E. A. Hillard, C. A. Murillo and H.-C. Zhou, "After 155 Years, A Crystalline Chromium Carboxylate with a Supershort Cr−Cr Bond", *J. Am. Chem. Soc.*, 2000, **122** (2), 416.

[36] F. A. Cotton, L. M. Daniels, E. A. Hillard and C. A. Murillo, "The Lengths of Molybdenum to Molybdenum Quadruple Bonds: Correlations, Explanations, and Corrections", *Inorg. Chem.*, 2002, **41** (9), 2466.

[37] J. L. Eglin, L. T. Smith and R. J. Staples, "Tungsten to Tungsten Quadruple Bonds: Over 30 Years of Research, 50 Structurally Characterized Compounds and 100 Known Compounds", *Inorg. Chim. Acta*, 2003, **351**, 217.

[38] F. A. Cotton and C. B. Harris, "The Crystal and Molecular Structure of Dipotassium Octachlorodirhenate(III) Dihydrate, $K_2[Re_2Cl_8]_2H_2O$", *Inorg. Chem.*, 1965, **4** (3), 330.

[39] K. A. Kreisel, G. P. A. Yap, O. Dmitrenko, C. R. Landis and K. H. Theopold, "The Shortest Metal−Metal Bond Yet: Molecular and Electronic Structure of a Dinuclear Chromium Diazadiene Complex", *J. Am. Chem. Soc.*, 2007, **129** (46), 14162.

[40] Y.-C. Tsai, C.-W. Hsu, J.-S. Yu, G.-H. Lee, Y. Wang and T.-S. Kuo, "Remarkably Short Metal−Metal Bonds: A Lantern-Type Quintuply Bonded Dichromium(I) Complex", *Angew. Chem., Int. Ed.*, 2008, **47** (38), 7250.

[41] A. Noor and R. Kempe, "The Shortest Metal−Metal Bond", *Chem. Rec.*, 2010, **10** (6), 413.

[42] M. P. Coles, "Application of Neutral Amidines and Guanidines in Coordination Chemistry", *Dalton Trans.*, 2006, (8), 985.

[43] P. J. Bailey and S. Pace, "The Coordination Chemistry of Guanidines and Guanidinates", *Coord. Chem. Rev.*, 2001, **214** (1), 91.

[44] M. P. Coles and R. F. Jordan, "Cationic Aluminum Alkyl Complexes Incorporating Amidinate Ligands. Transition-Metal-Free Ethylene Polymerization Catalysts", *J. Am. Chem. Soc.*, 1997, **119** (34), 8125.

[45] S. Dagorne, I. A. Guzei, M. P. Coles and R. F. Jordan, "Synthesis and Structures of Cationic Aluminum and Gallium Amidinate Complexes", *J. Am. Chem. Soc.*, 2000, **122** (2), 274.

[46] P. Harford, Unpublished Work, 2009.

[47] F. Bottomley and L. Sutin, "Organometallic Compounds Containing Oxygen Atoms", Academic Press, volume 28 of *Advances in Organometallic Chemistry*, 1988, 339–396.

[48] S. Schulz, S. Schmidt, D. Bläser and C. Wölper, "Direct Carboxylation of Zincocene Cp^*_2Zn", *Eur. J. Inorg. Chem.*, 2011, (27), 4157.

[49] A. E. H. Wheatley, "The Oxygen Scavenging Properties of Alkali Metal-Containing Organometallic Compounds", *Chem. Soc. Rev.*, 2001, **30** (5), 265.

[50] F. A. Cotton, L. M. Daniels, L. R. Falvello, J. H. Matonic, C. A. Murillo, X. Wang and H. Zhou, "Transition Metal (Mn, Co) and Zinc Formamidinate Compounds Having the Basic Beryllium Acetate Structure, and Unique Isomeric Iron Compounds", *Inorg. Chim. Acta*, 1997, **266** (1), 91.

[51] C. Walling and S. A. Buckler, "The Reaction of Oxygen with Organometallic Compounds. A New Synthesis of Hydroperoxides", *J. Am. Chem. Soc.*, 1955, **77** (22), 6032.

[52] K. Qin, C. D. Incarvito, A. L. Rheingold and K. H. Theopold, "A Structurally Characterized Chromium(III) Superoxide Complex Features "Side-on" Bonding", *Angew. Chem., Int. Ed.*, 2002, **41** (13), 2333.

[53] F. Bottomley, C. P. Magill and B. Zhao, "Organometallic Oxides: Oxidation of $(\eta{-}C_5Me_5)_2V$ with O_2 to form $[(\mu{-}\eta^3\text{-}C_5Me_5O_3)V(O)]_2$, $[\eta{-}C_5Me_5)V]_4(\mu{-}O)_6$, and $(\eta{-}C_5Me_5)_6V_8O_{17}$", *Organometallics*, 1991, **10** (6), 1946.

[54] F. Meyer and C. Limberg, *Organometallic Oxidation Catalysis*, Topics in Organometallic Chemistry, Springer, 2007.

[55] R. E. Dinnebier, U. Behrens and F. Olbrich, "Solid State Structures of Cyclopentadienyllithium, -sodium, and -potassium. Determination by High-Resolution Powder Diffraction", *Organometallics*, 1997, **16** (17), 3855.

[56] G. R. Giesbrecht, J. C. Gordon, D. L. Clark and B. L. Scott, "Synthesis, Structure and Solution Dynamics of Lithium Salts of Superbulky Cyclopentadienyl Ligands", *Dalton Trans.*, 2003, (13), 2658.

[57] N. J. Long, *Metallocenes: An Introduction to Sandwich Complexes*, John Wiley & Sons, 1998.

[58] S. Harder, "Erratum to "Recent Developments in Cyclopentadienyl-Alkalimetal Chemistry": [Coordination Chemistry Reviews 176 (1998) 17-66]", *Coord. Chem. Rev.*, 2000, **199** (1), 331.

[59] G. Arom, S. M. J. Aubin, M. A. Bolcar, G. Christou, H. J. Eppley, K. Folting, D. N. Hendrickson, J. C. Huffman, R. C. Squire, H.-L. Tsai, S. Wang and M. W. Wemple, "Manganese Carboxylate Clusters: from Structural Aesthetics to Single-Molecule Magnets", *Polyhedron*, 1998, **17** (17), 3005.

[60] M. L. Hays, D. J. Burkey, J. S. Overby, T. P. Hanusa, S. P. Sellers, G. T. Yee and V. G. Young, "Steric Influence on the Structure, Magnetic Properties, and Reactivity of Hexa- and Octaisopropylmanganocene", *Organometallics*, 1998, **17** (25), 5521.

[61] M. E. Switzer, R. Wang, M. F. Rettig and A. H. Maki, "Electronic Ground States of Manganocene and 1,1′-Dimethylmanganocene", *J. Am. Chem. Soc.*, 1974, **96** (25), 7669.

[62] C. Jørgensen, "Differences Between the Four Halide Ligands, and Discussion Remarks on Trigonal-Bipyramidal Complexes, on Oxidation States, and on Diagonal Elements of One-Electron Energy", *Coord. Chem. Rev.*, 1966, **1**, 164.

[63] A. Davison, N. Edelstein, R. H. Holm and A. H. Maki, "E.S.R. Studies of Four-Coordinate Complexes of Nickel, Palladium and Platinum Related by Electron Transfer Reactions", *J. Am. Chem. Soc.*, 1963, **85** (13), 2029.

[64] F. Rohrscheid, A. L. Balch and R. H. Holm, "Potential Electron Transfer Complexes of the [M$-$O$_4$] Type: Synthesis and Properties of Complexes Derived from Pyrocatechol and Tetrachloropyrocatechol", *Inorg. Chem.*, 1966, **5** (9), 1542.

[65] A. L. Balch and R. H. Holm, "Complete Electron-Transfer Series of the [M$-$N$_4$] Type", *J. Am. Chem. Soc.*, 1966, **88** (22), 5201.

[66] V. Bachler, G. Olbrich, F. Neese and K. Wieghardt, "Theoretical Evidence for the Singlet Diradical Character of Square Planar Nickel Complexes Containing Two *o*-Semiquinonato Type Ligands", *Inorg. Chem.*, 2002, **41** (16), 4179.

[67] D. Herebian, E. Bothe, F. Neese, T. Weyhermüller and K. Wieghardt, "Molecular and Electronic Structures of Bis-(*o*-diiminobenzosemiquinonato)metal(II) Complexes (Ni, Pd, Pt), Their Monocations and -Anions, and of Dimeric Dications Containing Weak Metal$-$Metal Bonds", *J. Am. Chem. Soc.*, 2003, **125** (30), 9116.

[68] D. Herebian, K. E. Wieghardt and F. Neese, "Analysis and Interpretation of Metal-Radical Coupling in a Series of Square Planar Nickel Complexes: Correlated Ab Initio and Density Functional Investigation of [Ni(L$^{\mathrm{ISQ}}$)$_2$] (L$^{\mathrm{ISQ}}$=3,5-di-*tert*-butyl-*o*-diiminobenzosemiquinonate(1-))", *J. Am. Chem. Soc.*, 2003, **125** (36), 10997.

[69] S. C. Cole, M. P. Coles and P. B. Hitchcock, "Boroxide Complexes of the Group 4 Metals: A "Noninnocent" Ligand in Olefin Polymerization", *Organometallics*, 2005, **24** (13), 3279.

[70] T. W. Myers, N. Kazem, S. Stoll, R. D. Britt, M. Shanmugam and L. A. Berben, "A Redox Series of Aluminum Complexes: Characterization of Four Oxidation States Including a Ligand Biradical State Stabilized via Exchange Coupling", *J. Am. Chem. Soc.*, 2011, **133** (22), 8662.

[71] R. J. Less, V. Naseri, M. McPartlin and D. S. Wright, "Oxidative Dehydrocoupling of N-H Bonds Using a Redox-Active Main Group Superbase", *Chem. Commun.*, 2011, **47** (21), 6129.

[72] G. Christou, D. Gatteschi, D. N. Hendrickson and R. Sessoli, "Single-Molecule Magnets", *MRS Bulletin*, 2000, **25** (11), 66.

[73] M. Cavallini, M. Facchini, C. Albonetti and F. Biscarini, "Single Molecule Magnets: from Thin Films to Nano-Patterns", *Phys. Chem. Chem. Phys.*, 2008, **10** (6), 784.

[74] C. J. Milios, S. Piligkos and E. K. Brechin, "Ground State Spin-Switching *via* Targeted Structural Distortion: Twisted Single-Molecule Magnets from Derivatised Salicylaldoximes", *Dalton Trans.*, 2008, (14), 1809.

[75] T. Lis, "Preparation, Structure, and Magnetic Properties of a Dodecanuclear Mixed-Valence Manganese Carboxylate", *Acta Crystallogr., Sect. B*, 1980, **36** (9), 2042.

[76] A. Caneschi, D. Gatteschi, R. Sessoli, A.-L. Barra, L. C. Brunel and M. Guillot, "Alternating Current Susceptibility, High Field Magnetization, and Millimeter Band EPR Evidence for a Ground S = 10 State in $[Mn_{12}O_{12}(CH_3COO)_{16}(H_2O)_4]\cdot 2\,CH_3COOH\cdot 4\,H_2O$", *J. Am. Chem. Soc.*, 1991, **113** (15), 5873.

[77] P. Yang, *The Chemistry of Nanostructured Materials*, World Scientific, 2003.

[78] A. Cornia, A. C. Fabretti, R. Sessoli, L. Sorace, D. Gatteschi, A.-L. Barra, C. Daiguebonne and T. Roisnel, "Disorder Effects in Mn_{12}–acetate at 83 K", *Acta Crystallogr., Sect. C*, 2002, **58** (7), m371.

[79] E.-C. Yang, N. Harden, W. Wernsdorfer, L. Zakharov, E. K. Brechin, A. L. Rheingold, G. Christou and H. D. N., "Mn_4 Single-Molecule Magnets with a Planar Diamond Core and S = 9", *Polyhedron*, 2003, **22** (14-17), 1857.

[80] C. J. Milios, A. Vinslava, W. Wernsdorfer, S. Moggach, S. Parsons, S. P. Perlepes, G. Christou and E. K. Brechin, "A Record Anisotropy Barrier for a Single-Molecule Magnet", *J. Am. Chem. Soc.*, 2007, **129** (10), 2754.

[81] T. Kottke and D. Stalke, "Crystal Handling at Low Temperatures", *J. Appl. Cryst.*, 1993, **26** (4), 615.

[82] G. M. Sheldrick, *A Program for the Refinement of Crystal Structures*, University of Göttingen, Germany, 1997.

[83] G. Wilkinson, F. A. Cotton and J. M. Birmingham, "On Manganese Cyclopentadienide and Some Chemical Reactions of Neutral Bis-Cyclopentadienyl Metal Compounds", *J. Inorg. Nucl. Chem*, 1956, **2** (2), 95.

[84] E. C. Taylor and W. A. Ehrhart, "A Convenient Synthesis of N,N′-Disubstituted Formamidines and Acetamidines", *J. Org. Chem.*, 1963, **28** (4), 1108.

[85] A. Spek, *PLATON, A Multipurpose Crystallographic Tool*, Utrecht University, The Netherlands, 1999.

[86] A. Bashall, J. M. Cole, F. García, A. Primo, A. Rothenberger, M. McPartlin and D. S. Wright, "Primary Amido and Phosphido Complexes of Zinc: Potential Precursors to Heterometallic Arrangements", *Inorg. Chim. Acta*, 2003, **354**, 41.

[87] S. Greenberg and D. W. Stephan, "Stoichiometric and Catalytic Activation of P−H and P−P Bonds", *Chem. Soc. Rev.*, 2008, **37** (8), 1482.

[88] R. Waterman, "Metal-Phosphido and -Phosphinidene Complexes in P−E Bond-Forming Reactions", *Dalton Trans.*, 2009, (1), 18.

[89] D. R. Armstrong, N. Feeder, A. D. Hopkins, M. J. Mays, D. Moncrieff, J. A. Wood, A. D. Woods and D. S. Wright, "Electrophilic Ring-Opening of $[(RP)_nAs]^-$ Anions; a Simple Route to Functionalised Neutral Phosphines of the Type $[(Bu^tP)(Bu^tRP)_2]$", *Chem. Commun.*, 2000, (24), 2483.

[90] H. Chen, M. M. Olmstead, D. C. Pestana and P. P. Power, "Reactions of Low-Coordinate Transition-Metal Amides with Secondary Phosphanes and Arsanes: Synthesis, Structural, and Spectroscopic Studies of $[M\{N(SiMe_3)_2\}(\mu-PMes_2)]_2$ (M = Manganese, Iron), $[Mn\{N(SiMe_3)_2\}(\mu-AsMes_2)]_2$ and $Mes_2AsAsMes_2$", *Inorg. Chem.*, 1991, **30** (8), 1783.

[91] C. von Hänisch, F. Weigend and R. Clérac, "Unique Manganese Phosphorus Complex with a Mn_5P_7 Core: Synthesis, Molecular Structure, and Magnetic Properties", *Inorg. Chem.*, 2008, **47** (5), 1460.

[92] R. A. Jones, S. U. Koschmieder and C. M. Nunn, "Dinuclear Mixed Alkyl Phosphido and Alkyl Aryloxy Complexes of Manganese(II). Crystal Structures of $[Mn(CH_2CMe_3)(\mu-tert-Bu_2P)]_2$ and

[$Mn(CH_2CMe_2Ph)(\mu-O-2,4,6-(tert-Bu)_3C_6H_2)]_2$", *Inorg. Chem.*, 1988, **27** (25), 4524.

[93] S. C. Goel, M. Y. Chiang, D. J. Rauscher and W. E. Buhro, "Comparing the Properties of Homologous Phosphido and Amido Complexes: Synthesis and Characterization of the Disilylphosphido Complexes $\{M[P(SiMe_3)_2]_2\}_2$ where M = Zinc, Cadmium, Mercury, Tin, Lead and Manganese", *J. Am. Chem. Soc.*, 1993, **115** (1), 160.

[94] U. Flörke and H.-J. Haupt, "Dimanganese Octacarbonyl Compounds with Bridging Cyclohexylphosphanes", *Acta Crystallogr., Sect. C*, 1993, **49** (2), 374.

[95] U. Flörke and H.-J. Haupt, "μ−Bromo−μ−cyclohexylphosphido−bis(tetracarbonylmanganese) and μ−Bromo−μ−(pentacarbonylmanganese)phosphido−bis(tetracarbonylmanganese)", *Acta Crystallogr., Sect. C*, 1997, **53** (7), 876.

[96] L. Manojlovic-Muir, K. W. Muir, M. C. Jennings, M. J. Mays, G. A. Solan and K. W. Woulfe, "Synthesis of Dimanganese Complexes Containing Mixed Bridging Phosphido Ligands; Crystal Structures of $[Mn_2(\mu-PPh_2)\{\mu-PPhMn(CO)_5\}(CO)_8]$ and $[Mn_2(\mu-PPhH)(\mu-PPhCOMe)(CO)_8]$", *J. Organomet. Chem.*, 1995, **491** (1-2), 255.

[97] F. H. Köhler, N. Hebendanz, U. Thewalt, B. Kanellakopulos and R. Klenze, "General Entry to Novel Manganese(II) Half-Sandwich Complexes", *Angew. Chem., Int. Ed.*, 1984, **23** (9), 721.

[98] A. Bashall, M. A. Beswick, H. Ehlenberg, S. J. Kidd, M. McPartlin, J. S. Palmer, P. R. Raithby, J. M. Rawson and D. S. Wright, "The Paramagnetic, Heterometallic Manganese Cubanes [{E(NCy)}(MnCp)] (Cy = CH, Cp = CH, E = As, Sb)", *Chem. Commun.*, 2000, (9), 749.

[99] C. S. Alvarez, S. R. Boss, J. C. Burley, S. M. Humphry, R. A. Layfield, R. A. Kowenicki, M. McPartlin, J. M. Rawson, A. E. H. Wheatley, P. T. Wood and D. S. Wright, "Syntheses, Structures and Magnetic Properties of Mn(II) Dimers $[CpMn(\mu-X)]_2$ (Cp = C_5H_5; X = RNH, R^1R^2N, C≡CR)", *Dalton Trans.*, 2004, (21), 3481.

[100] M. Reiher, O. Salomon and B. A. Hess, "Reparameterization of Hybrid Functionals Based on Energy Differences of States of Different Multiplicity", *Theor. Chim. Acta*, 2001, **107** (1), 48.

[101] O. Salomon, M. Reiher and B. A. Hess, "Assertion and Validation of the Performance of the B3LYP* Functional for the First Transition Metal Row and the G2 Test Set", *J. Chem. Phys*, 2002, **117** (10), 4729.

[102] D. A. Kissounko, M. V. Zabalov, G. P. Brusova and D. A. Lemenovskii, "Principal Trends in the Chemistry of Amidinate Complexes of Main-Group and Transition Elements", *Russ. Chem. Rev.*, 2006, **75** (5), 351.

[103] V. C. Gibson and S. K. Spitzmesser, "Advances in Non-Metallocene Olefin Polymerization Catalysis", *Chem. Rev.*, 2003, **103** (1), 283.

[104] S. Collins, "Polymerization Catalysis with Transition Metal Amidinate and Related Complexes", *Coord. Chem. Rev.*, 2011, **255** (1-2), 118.

[105] B. M. Day, N. E. Mansfield, M. P. Coles and P. B. Hitchcock, "Bicyclic Guanidinate Compounds of Magnesium and their Activity as Pre-Catalysts in the Tishchenko Reaction", *Chem. Commun.*, 2011, **47** (17), 4995.

[106] D. J. Brown, M. H. Chisholm and J. C. Gallucci, "Amidinate-Carboxylate Complexes of Dimolybdenum and Ditungsten: $M_2(O_2CR)_2((N^iPr)_2CR')_2$. Preparations, Molecular and Electronic Structures and Reactions", *Dalton Trans.*, 2008, (12), 1615.

[107] J. N. van Niekerk, F. R. L. Schoening and J. H. Talbot, "The Crystal Structure of Zinc Acetate Dihydrate, $Zn(CH_3COO)_2 \cdot 2H_2O$", *Acta Cryst.*, 1953, **6** (8-9), 720.

[108] A. V. Capilla and R. A. Aranda, "Anhydrous Zinc(II) Acetate $(CH_3{-}COO)_2Zn$", *Cryst. Struct. Comms.*, 1979, **8**, 795.

[109] R. E. Mulvey, V. L. Blair, W. Clegg, A. R. Kennedy, J. Klett and L. Russo, "Cleave and Capture Chemistry Illustrated through Bimetallic-Induced Fragmentation of Tetrahydrofuran", *Nature Chem.*, 2010, **2**, 588.

[110] F. A. Cotton, M. Matusz and R. Poli, "Synthesis, Molecular Structure and Physicochemical Properties of $M_2(form)_4$ (M = Nickel, Palladium; form = *N,N′*-Di-*p*-tolylformamidinato)", *Inorg. Chem.*, 1987, **26** (10), 1472.

[111] C. Lin, J. D. Protasiewicz and T. Ren, "Electronic Tuning Using Remote Substituents in Tetrakis($\mu{-}N,N'$-diarylformamidinato)dinickel. Linear Free Energy Relationships in Dinuclear Compounds", *Inorg. Chem.*, 1996, **35** (25), 7455.

[112] F. A. Cotton and T. Ren, "Preparation and Characterization of Two New Group VI Quadruply Bonded Dinuclear Compounds: $Cr_2(DFM)_4$ and $W_2(DFM)_4$", *J. Am. Chem. Soc.*, 1992, **114** (6), 2237.

[113] F. A. Cotton, C. A. Murillo and I. Pascual, "Quadruply Bonded Dichromium Complexes with Variously Fluorinated Formamidinate Ligands", *Inorg. Chem.*, 1999, **38** (9), 2182.

[114] H. Shoukang, S. Gambarotta, C. Bensimon and J. J. Edema, "Ligand Steric Bulk: A Neglected Factor in the Formation of Cr−Cr Supershort Contacts", *Inorg. Chim. Acta*, 1993, **213**, 65.

[115] F. A. Cotton, C. A. Murillo and I. Pascual, "An Unprecedented Quadruply Bonded Compound with a Bridging Chlorine Atom: $Cr_2[(o{-}ClC_6H_4N)_2CH]_3(\mu{-}Cl)$", *Inorg. Chem. Commun.*, 1999, **2** (3), 101.

[116] F. A. Cotton, L. M. Daniels, C. A. Murillo and P. Schooler, "Chromium(II) Complexes Bearing 2,6-Substituted *N,N′*-Diarylformamidinate Ligands", *J. Chem. Soc., Dalton Trans.*, 2000, (13), 2001.

[117] F. A. Cotton, L. M. Daniels, C. A. Murillo and P. Schooler, "Chromium(II) Complexes Bearing 2-Substituted *N,N′*-Diarylformamidinate Ligands", *J. Chem. Soc., Dalton Trans.*, 2000, (13), 2007.

[118] L. J. Murray, M. Dinca, J. Yano, S. Chavan, S. Bordiga, C. M. Brown and J. R. Long, "Highly-Selective and Reversible O_2 Binding in $Cr_3(1,3,5{-}benzenetricarboxylate)_2$", *J. Am. Chem. Soc.*, 2010, **132** (23), 7856.

[119] N. N. Greenwood, *Chemistry of the Elements 2nd Ed.*, Butterworth Heinemann, Burlington, MA, 2002.

[120] M. P. Coles and P. B. Hitchcock, "Zinc Guanidinate Complexes and Their Application in Ring-Opening Polymerisation Catalysis", *Eur. J. Inorg. Chem.*, 2004, (13), 2662.

[121] C. Jones, "Bulky Guanidinates for the Stabilization of Low Oxidation State Metallacycles", *Coord. Chem. Rev.*, 2010, **254** (11-12), 1273.

[122] A. J. Wooten, P. J. Carroll and P. J. Walsh, "Evidence for Substrate Binding by the Lanthanide Centers in $[Li_3(thf)_n(binolate)_3Ln]$: Solution and Solid-State Characterization of Seven- and Eight-Coordinate

$[Li_3(sol)_n(binolate)_3Ln(S)_m]$ Adducts", *Angew. Chem., Int. Ed.*, 2006, **45** (16), 2549.

[123] J. Zhang, F. Han, Y. Han, Z. Chen and X. Zhou, "Synthesis and Structures of Titanium and Yttrium Complexes with *N,N′*-Tetramethylguanidinate Ligands: Different Reactivity of the M−N Bonds toward Phenyl Isocyanate", *Dalton Trans.*, 2009, (10), 1806.

[124] S. D. Bunge and J. L. Steele, "Synthesis and Characterization of Group 11 1,1,3,3-Tetraalkylguanidinate (TAG) Clusters: $[M_2(\mu{-}TAG)\{\mu{-}N(SiMe_3)_2\}]_2$ (M = Cu, Ag, and Au)", *Inorg. Chem.*, 2009, **48** (6), 2701.

[125] S. D. Bunge, J. A. Bertke and T. L. Cleland, "Synthesis, Structure, and Reactivity of Low-Coordinate 1,1,3,3-Tetraethylguanidinate Complexes", *Inorg. Chem.*, 2009, **48** (16), 8037.

[126] R. A. Andersen, E. Carmona-Guzman, J. F. Gibson and G. Wilkinson, "Neopentyl, Neophyl, and Trimethylsilylmethyl Compounds of Manganese. Manganese(II) Dialkyls; Manganese(II) Dialkyl Amine Adducts; Tetra-Alkylmanganate(II) Ions and Lithium Salts; Manganese(IV) Tetra-Alkyls", *J. Chem. Soc., Dalton Trans.*, 1976, (21), 2204.

[127] R. J. Morris and G. S. Girolami, "Thirteen-Electron Manganese(II) Tetraalkyls. Synthesis, Characterization, and X-Ray Crystal Structures of $[Li(tmed)]_2[MnMe_4]$ and the β-Unstable Species $[Li(tmed)]_2[MnEt_4]$ and $[Li(tmed)]_2[Mn(CH_2CH_2{-}t{-}Bu)_4]$", *Organometallics*, 1989, **8** (6), 1478.

[128] D. J. Linton, P. Schooler and A. E. H. Wheatley, "Group 12 and Heavier Group 13 Alkali Metal 'ate' Complexes", *Coord. Chem. Rev.*, 2001, **223** (1), 53.

[129] M. P. Coles, "Bicyclic-guanidines, -guanidinates and -guanidinium Salts: Wide Ranging Applications from a Simple Family of Molecules", *Chem. Commun.*, 2009, (25), 3659.

[130] M. P. Coles and P. B. Hitchcock, "Bicyclic Guanidinates in Mono- and Di-Valent Metal Complexes, Including Group 1/2 and Group 1/12 Heterometallic Systems", *Aus. J. Chem.*, 2013.

[131] M. P. Coles and P. B. Hitchcock, "A New Bonding Mode for the Bicyclic Guanidinate, $[hpp]^-$, in the Tetrametallic Yttrium Oxide Cluster, $Y_4(hpp)_8Cl_2(\mu_4{-}O)$, *Inorg. Chim. Acta*, 2004, **357** (14), 4330.

[132] M. P. Coles and P. B. Hitchcock, "Exploration of the Suitability of Bicyclic Guanidinates as Ligands in Catalytic Chemistry Mediated by Titanium", *Organometallics*, 2003, **22** (25), 5201.

[133] J. Krausse, G. Marx and G. Schödl, "Strukturuntersuchungen an Organochrom-Verbindungen I. IR-und Röntgen-Strukturanalyse des $Li_4Cr_2(CH_3)_8\ 4\,C_4H_8O$", *J. Organomet. Chem.*, 1970, **21** (1), 159.

[134] A. Malassa, C. Agthe, H. Görls, M. Podewitz, L. Yu, C. Herrmann, M. Reiher and M. Westerhausen, "Synthesis, Structures, and Magnetic Properties of *N*-Trialkylsilyl-8-amidoquinoline Complexes of Chromium, Manganese, Iron, and Cobalt as well as of Wheel-Like Hexanuclear Iron(II) and Manganese(II) Bis(8-amidoquinoline), *Eur. J. Inorg. Chem.*, 2010, (12), 1777.

[135] H. Chen, R. A. Bartlett, H. V. R. Dias, M. M. Olmstead and P. P. Power, "Synthesis and Structural Characterization of Manganese(II) Derivatives of the Bulky, Chelating Bis(amido) Ligands $[(NMes)_2SiMe_2]^{2-}$ and $[DippNCH_2CH_2NDipp]^{2-}$, Their Neutral Amine Precursors, and Their Lithium Salts (Mes = 2,4,6-$Me_3C_6H_2$; Dipp = 2,6-*i*-$Pr_2C_6H_3$)", *Inorg. Chem.*, 1991, **30** (11), 2487.

[136] L. F. Warren, "Synthesis of $[M{-}N_4]$ and $[M{-}N_6]$ Complexes Based on *o*-Benzoquinone Diimine with Cobalt, Iron, and Ruthenium", *Inorg. Chem.*, 1977, **16** (11), 2814.

[137] M. E. Gross, J. A. Ibers and W. C. Trogler, "Structural and Spectroscopic Study of Cyclopentadienylcobalt (*N*-phenyl-*o*-benzoquinone Diimines). A Case for Delocalized π Bonding, *Organometallics*, 1982, **1** (3), 530.

[138] C. S. Alvarez, A. D. Bond, D. Cave, M. E. G. Mosquera, E. A. Harron, R. A. Layfield, M. McPartlin, J. M. Rawson, P. T. Wood and D. S. Wright, "Syntheses and Magnetic Properties of Hexanuclear $[Cp_2Mn_3(L_1)_4]_2$ and Octanuclear $[Mn_8(L_2)_{12}(\mu_4{-}O)_2]$ (L_1 = 2−HNC_5H_5N, L_2 = 2−NH−3−Br−5−MeC_5H_3N, Cp = C_5H_5)", *Chem. Commun.*, 2002, (24), 2980.

[139] T. C. Stamatatos, K. A. Abboud and G. Christou, "A Family of 3-D Coordination Polymers Composed of Mixed-Valence Mn_6 Octahedra within Na_4 Tetrahedra", *J. Clust. Sci.*, 2010, **21** (3), 485.

[140] T. C. Stamatatos, K. V. Pringouri, K. A. Abboud and G. Christou, "High-Spin Molecules: A Mixed-Valence Mn_6 Octahedron with an S = 11 Ground State", *Polyhedron*, 2009, **28** (9-10), 1624.

[141] D. Liu, Q. Zhou, Y. Chen, F. Yang, Y. Yu, Z. Shi and S. Feng, "Synthesis, Structure, and Magnetic Study of Two Two-Dimensional 6^3 Honeycomb-Shaped and 4^4 Grid-Like Coordination Polymetic Networks Based on Hexa- and Dodecanuclear Manganese Cluster Units", *Cryst. Growth Des.*, 2010, **10** (6), 2661.

[142] K. C. Mondal, M. G. B. Drew and P. S. Mukherjee, "Synthesis of a Mn_6 Cluster and Its Self-Assembly of an Azido-Bridged Polymer", *Inorg. Chem.*, 2007, **46** (14), 5625.

[143] H. Vahrenkamp, "Stereochemie der Metall-Metall-Bindung Die Strukturen der Komplexe $[(CO)_4M{-}P(CH_3)_2]_2$ mit M = Mn, Cr, V Einschließlich Einer "Unmöglichen" Metall-Metall-Doppelbindung", *Chem. Ber.*, 1978, **111** (10), 3472.

[144] S. Gambarotta, M. Mazzanti, C. Floriani and M. Zehnder, "A Tetranuclear Polyfunctional Sodium-Vanadium(III) Complex containing a Vanadium(III)-Vanadium(III) Double Bond", *J. Chem. Soc., Chem. Commun.*, 1984, (16), 1116.

[145] A. M. Arif, A. H. Cowley, M. Pakulski, N. C. Norman and A. G. Orpen, "Vanadium-Phosphinidene Complex Exhibiting Vanadium-Phosphorus Multiple Bonding", *Organometallics*, 1987, **6** (1), 189.

[146] J. C. Huffman, L. N. Lewis and K. G. Caulton, "A Donor Semibridge? Molecular Structures of Dicyclopentadienyldivanadiumtetracarbonyltriphenylphosphine and Dicyclopentadienyldivanadiumpentacarbonyl", *Inorg. Chem.*, 1980, **19** (9), 2755.

[147] R. L. Bansemer, J. C. Huffman and K. G. Caulton, "A Bimetallic Vanadium(I) Polyhydride", *J. Am. Chem. Soc.*, 1983, **105** (19), 6163.

[148] F. A. Cotton, B. A. Frenz and L. Kruczynski, "Structure of Dicyclopentadienylpentacarbonyldivanadium. New Example of Grossly Unsymmetrical Carbonyl Bridging", *J. Am. Chem. Soc.*, 1973, **95** (3), 951.

[149] F. A. Cotton, E. A. Hillard, C. A. Murillo and X. Wang, "New Chemistry of the Triply Bonded Divanadium (V_2^{4+}) Unit and Reduction to an Unprecedented V_2^{3+} Core", *Inorg. Chem.*, 2003, **42** (19), 6063.

[150] S. C. Jones and D. O'Hare, "$[V(\eta^5{-}C_5H_5)]_2C_8H_6$: a Bimetallic Pentalene-Bridged Complex with Multiple Bonding between the Metal Atoms", *Chem. Commun.*, 2003, (17), 2208.

[151] R. Boca, *Theoretical Foundations of Molecular Magnetism*, Current Methods in Inorganic Chemistry, Elsevier Science, 1999.

[152] J. S. Griffith and L. E. Orgel, "The Residual Paramagnetism and Nuclear Magnetic Resonance Spectra of Cobaltic Complexes", *Trans. Faraday Soc.*, 1957, **53** (0), 601.

[153] H. J. Reich and D. P. Green, "Spectroscopic and Reactivity Studies of Lithium Reagent-HMPA Complexes", *J. Am. Chem. Soc.*, 1989, **111** (23), 8729.

[154] G. Fraenkel and M. P. Hallden-Abberton, "First Determination of the Structure of an Ion-Paired Species in Nonpolar Media: Hydrogen-1, Carbon-13, Lithium-7 NMR Spectra of Peralkylcyclohexadienyl Lithium Compounds", *J. Am. Chem. Soc.*, 1981, **103** (19), 5657.

[155] R. Cox and H. Terry Jr., "Lithium-7 NMR Studies of Aromatic Ion Pairs", *J. Magn. Reson.*, 1974, **14** (3), 317.

[156] C. Cadiou, M. Murrie, C. Paulsen, V. Villar, W. Wernsdorfer and R. E. P. Winpenny, "Studies of a Nickel-Based Single Molecule Magnet: Resonant Quantum Tunnelling in an S = 12 Molecule", *Chem. Commun.*, 2001, (24), 2666.

[157] C. G. Efthymiou, T. C. Stamatatos, C. Papatriantafyllopoulou, A. J. Tasiopoulos, W. Wernsdorfer, S. P. Perlepes and G. Christou, "Nickel/Lanthanide Single-Molecule Magnets: $\{Ni_3Ln\}$ "Stars" with a Ligand Derived from the Metal-Promoted Reduction of Di-2-pyridyl Ketone under Solvothermal Conditions", *Inorg. Chem.*, 2010, **49** (21), 9737.

[158] E. K. Brechin, A. Graham, P. E. Y. Milne, M. Murrie, S. Parsons and R. E. P. Winpenny, "New High-Spin Clusters Featuring Transition Metals", *Philosophical Transactions of the Royal Society of London. Series A: Mathematical, Physical and Engineering Sciences*, 1999, **357** (1762), 3119.

[159] M. V. Jiménez, E. Sola, J. Caballero, F. J. Lahoz and L. A. Oro, "Alkene CH Activations at Dinuclear Complexes Promoted by Oxidation", *Angew. Chem., Int. Ed.*, 2002, **41** (7), 1208.

[160] J. A. Cabeza, H. Nöth, M. d. J. Rosales-Hoz and G. Sánchez-Cabrera, "Reactivity of Triosmium Carbonyl Clusters with 1,8-Diaminonaphthalene Synthesis and Structural Characterization of Amido, Diamido, and C-Metalated Trinuclear Derivatives", *Eur. J. Inorg. Chem.*, 2000, (11), 2327.

[161] M. V. Jiménez, E. Sola, M. A. Egea, A. Huet, A. C. Francisco, F. J. Lahoz and L. A. Oro, "Key Factors Determining the Course of Methyl Iodide Oxidative Addition to Diamidonaphthalene-Bridged Diiridium(I) and Dirhodium(I) Complexes", *Inorg. Chem.*, 2000, **39** (21), 4868.

[162] Z. Chen, M. Zeng, Y. Zhang, Z. Zhang and F. Liang, "Preparation and Structures of a Series of Phosphorus-Free Nickel(II) Diamine Complexes and their Applications in Hydrogenation of Acetophenone", *Appl. Organomet. Chem.*, 2010, **24** (9), 625.

[163] C. Nachtigal, S. Al-Gharabli, K. Eichele, E. Lindner and H. A. Mayer, "Structural Studies of an Array of Mixed Diamine Phosphine Ruthenium(II) Complexes", *Organometallics*, 2002, **21** (1), 105.

[164] J.-I. Song and S. Gambarotta, "Preparation, Characterization, and Reactivity of a Diamagnetic Vanadium Nitride", *Chem.-Eur. J.*, 1996, **2** (10), 1258.

[165] R. A. Henderson, Z. Janas, L. B. Jerzykiewicz, R. L. Richards and P. Sobota, "Vanadium Phenoxide Complexes with Oxide, Nitride or Hydrazide Co-Ligands: Preparation and Crystal Structures of $[V(OC_6H_3Pr^i{}_2{-}2,6)_3NLi(C_4H_8O)_3]$, $[\{VO_2(OC_6H_3Pr^i{}_2{-}2,6)_2\}_2\{\mu{-}Li(C_4H_8O)_2\}_2]$ and $[V(NNMe_2)(OC_6H_3Pr^i{}_2{-}2,6)_3]$", *Inorg. Chim. Acta*, 1999, **285** (2), 178.

[166] J.-I. Song, P. Berno and S. Gambarotta, "Dinitrogen Fixation, Ligand Dehydrogenation, and Cyclometalation in the Chemistry of Vanadium(III) Amides", *J. Am. Chem. Soc.*, 1994, **116** (15), 6927.

[167] J. De With, A. D. Horton and A. G. Orpen, "Stable Alkylvanadium(V) Compounds Containing Bulky Imido and Amido Ligands", *Organometallics*, 1990, **9** (8), 2207.

[168] S. Gambarotta, J. J. H. Edema and R. K. Minhas, "Isolation and Characterization of a Vanadium Ethylidyne Complex. The Crystal Structure of

[$(Cy_2N)_2Li(\mu^3{-}O)(\mu^2,\eta^1{:}\eta^1CMe)$ an Unusual V_2LiO Cluster", *J. Chem. Soc., Chem. Commun.*, 1993, (19), 1503.

[169] F. A. Cotton, C. K. Fair, G. E. Lewis, G. N. Mott, F. K. Ross, A. J. Schultz and J. M. Williams, "Precise Structural Characterizations of the Hexaaquovanadium(III) and Diaquohydrogen Ions. X-ray and Neutron Diffraction Studies of $[V(H_2O)_6][H_5O_2](CF_3SO_3)_4$", *J. Am. Chem. Soc.*, 1984, **106** (18), 5319.

[170] P. L. W. Tregenna-Piggott, D. Spichiger, G. Carver, B. Frey, R. Meier, H. Weihe, J. A. Cowan, G. J. McIntyre, G. Zahn and A.-L. Barra, "Structure and Bonding of the Vanadium(III) Hexa-Aqua Cation. 1. Experimental Characterization and Ligand-Field Analysis", *Inorg. Chem.*, 2004, **43** (25), 8049.

[171] B. N. Figgis and L. G. B. Wadley, "Magnetic Properties and Structure of Hexakisureavanadium Tri-Iodide", *J. Chem. Soc., Dalton Trans.*, 1972, (10), 2182.

[172] C. Furlani, A. A. G. Tomlinson, P. Porta and A. Sgamellotti, "Preparation, Crystal Structure, and Spectroscopic Properties of Vanadium(III) Tris-(OO-diethyl phosphorodithioate), $V[PS_2(OEt)_2]_3$", *J. Chem. Soc. A*, 1970, (0), 2929.

[173] F. Sans-Ruiz, S. Martinez-Carrera and S. Garcia-Blanco, *An. R. Soc. Esp. Fis, Quim. A*, 1970, **66**, 309.

[174] K. Kanamori, A. Kyotoh, K. Fujimoto, K. Nagata, H. Suzuki and K. Okamoto, "Syntheses, Structures, and Properties of Vanadium(III) Complexes with the Hexadentate Ligand, Tetramethylenediamine-*N,N,N′,N′*-tetraacetate, *N,N′*-Bis(2-pyridylmethyl)-1,2-ethanediamine-*N,N′*-diacetate, and *N,N′*-Bis(2-pyridylmethyl)-1,3-propanediamine-*N,N′*-diacetate", *Bull. Chem. Soc. Jpn.*, 2001, **74**, 2113.

[175] J. A. Cabeza, J. M. Fernandez-Colinas, V. Riera, M. A. Pellinghelli and A. Tiripicchio, "Synthesis and Reactions with Electrophiles and Nucleophiles of the Ruthenium(I) Complex $[Ru_2(\mu{-}C_{10}H_8N_2)(CO)_6]$. Crystal Structure of $[Ru_2(\mu{-}C_{10}H_8N_2)(CO)_4\{P(OPh)_3\}_2]$($C_{10}H_{10}N_2$= 1,8-diaminonaphthalene)", *J. Chem. Soc., Dalton Trans.*, 1991, (3), 371.

[176] L. Bonomo, E. Solari, M. Latronico, R. Scopelliti and C. Floriani, "*meso*-Octaethylporphyrinogen Displaying Site Selectivity in the Stepwise Synthesis

of Polymetallic Aggregates with Interesting Redox Properties: The π-Binding Ability of Metalla-Porphyrinogens", *Chem.-Eur. J.*, 1999, **5** (7), 2040.

[177] L. Bonomo, E. Solari, R. Scopelliti, C. Floriani and N. Re, "The Porphyrinogen-Porphodimethene Relationship Leading to Novel Synthetic Methodologies Focused on the Modification and Functionalization of the Porphyrinogen and Porphodimethene Skeletons", *J. Am. Chem. Soc.*, 2000, **122** (22), 5312.

[178] C. Krüger and Y.-H. Tsay, "Molecular Structure of a π-Dinitrogen-Nickel-Lithium Complex", *Angew. Chem., Int. Ed.*, 1973, **12** (12), 998.

[179] L. G. Hubert-Pfalzgraf, V. G. Kessler and J. Vaissermann, "Soluble Ni^{II} Alkoxides Based on Dimethylaminoisopropoxide Ligands: Molecular Structure of $[Li(Pr^iOH)Ni\ (\eta^2{-}OR)_2Cl]_2$ and of *cis*-$NiCl_2(ROH)_2$ ($R = CHMeCH_2NMe_2$)", *Polyhedron*, 1997, **16** (24), 4197.

[180] S. Deeken, S. Proch, E. Casini, H. F. Braun, C. Mechtler, C. Marschner, G. Motz and R. Kempe, "Group 10 Metal Aminopyridinato Complexes: Synthesis, Structure, and Application as Aryl-Cl Activation and Hydrosilane Polymerization Catalysts", *Inorg. Chem.*, 2006, **45** (4), 1871.

[181] M. Albrecht, M. Fiege, M. Baumert, M. de Groot, R. Fröhlich, L. Russo and K. Rissanen, "Hierarchical, Lithium-Templated Assembly of Helicate-Type Complexes: How Versatile Is This Reaction?", *Eur. J. Inorg. Chem.*, 2007, (4), 609.

[182] G. Aromí, A. R. Bell, M. Helliwell, J. Raftery, S. J. Teat, G. A. Timco, O. Roubeau and R. E. P. Winpenny, "A Systematic Exploration of Nickel–Pyrazolinato Chemistry with Alkali Metals: New Cages From Serendipitous Assembly", *Chem.-Eur. J.*, 2003, **9** (13), 3024.

[183] G. Nirmala, A. K. Rahiman, S. Sreedaran, R. Jegadeesh, N. Raaman and V. Narayanan, "Synthesis, Characterization, Crystal Structure and Antimicrobial Activities of New *transN,N*-substituted Macrocyclic Dioxocyclam and their Copper(II) and Nickel(II) Complexes", *Polyhedron*, 2011, **30** (1), 106.

[184] R. Saalfrank, C. Spitzlei, A. Scheurer, H. Maid, F. Heinemann and F. Hampel, "Enantiospecific Syntheses of Copper Cubanes, Double-Stranded Copper/Palladium Helicates, and a (Dilithium)–Dinickel Coronate from Enantiomerically Pure Bis-1,3-diketones - Solid-State Self-Organization Towards Wirelike Copper/Palladium Strands", *Chem.-Eur. J.*, 2008, **14** (5), 1472.

[185] S. Gambarotta, F. Urso, C. Floriani, A. Chiesi-Villa and C. Guastini, "Carbon−Carbon Bond Forming and Breaking by a Metal-Assisted Redox Process in a Nickel(II)-Schiff Base Complex", *Inorg. Chem.*, 1983, **22** (26), 3966.

[186] H. Zhou, Z. Li, Z. Wang, T. Wang, L. Xu, Y. He, Q.-H. Fan, J. Pan, L. Gu and A. Chan, "Hydrogenation of Quinolines Using a Recyclable Phosphine-Free Chiral Cationic Ruthenium Catalyst: Enhancement of Catalyst Stability and Selectivity in an Ionic Liquid", *Angew. Chem., Int. Ed.*, 2008, **47** (44), 8464.

[187] C. Hedberg, K. Källström, P. I. Arvidsson, P. Brandt and P. G. Andersson, "Mechanistic Insights into the Phosphine-Free RuCp*-Diamine-Catalyzed Hydrogenation of Aryl Ketones: Experimental and Theoretical Evidence for an Alcohol-Mediated Dihydrogen Activation", *J. Am. Chem. Soc.*, 2005, **127** (43), 15083.

[188] P. Zerecero-Silva, I. Jimenez-Solar, M. G. Crestani, A. Arévalo, R. Barrios-Francisco and J. J. García, "Catalytic Hydrogenation of Aromatic Nitriles and Dinitriles with Nickel Compounds", *Appl. Cat. A: Gen.*, 2009, **363** (1-2), 230.

[189] A. L. Iglesias and J. J. García, "Homogeneous Hydrogenation of Fluoroaromatic Imines with Ni Compounds, Evidence for η^2−C=N Intermediate in the Catalytic Cycle", *J. Mol. Catal. A: Chem.*, 2009, **298** (1-2), 51.

[190] F. Négrier, E. Marceau, M. Che, J.-M. Giraudon, L. Gengembre and A. Löfberg, "From Al_2O_3-Supported Ni(II)-Ethylenediamine Complexes to CO Hydrogenation Catalysts: Importance of the Hydrogen Post-Treatment Evidenced by XPS", *Catal. Lett.*, 2008, **124** (1-2), 18.

[191] W. Clegg, M. Frank, R. E. Mulvey and P. A. O'Neil, "Synthesis and X-Ray Crystallographic Characterisation of σ−Phenylenediamidomagnesium · tetrahydrofuran: The First Octahedral Mg_6 Cluster", *J. Chem. Soc., Chem. Commun.*, 1994, (1), 97.

[192] E. Weiss, "Structures of Organo Alkali Metal Complexes and Related Compounds", *Angew. Chem., Int. Ed.*, 1993, **32** (11), 1501.

[193] W. Clegg, K. W. Henderson, R. E. Mulvey and P. A. O'Neil, "Synthesis and Structural Characterisation of the Mixed Lithium-Magnesium Amide, $[\{PhCH_2(Me_2NCH_2CH_2)N\}_4Li_2Mg]$: A New Type of Magnesiate Complex

Free of a Donor Solvent as Ligand, *J. Chem. Soc., Chem. Commun.*, 1993, (11), 969.

[194] W. Clegg, K. W. Henderson, R. E. Mulvey and P. A. O'Neil, "Model Structural Types for Rationalising Stoichiometries and Coordination Numbers in Lithium Amidomagnesiates: Syntheses and X-Ray Diffraction Studies of $[\{Mg(NR_2)_2\}_2]$, $[Li_2Mg(NR_2)_4]$ and $[LiMg(NR_2)_3 \cdot py]$ (R = benzyl, py = pyridine)", *J. Chem. Soc., Chem. Commun.*, 1994, (6), 769.

[195] R. E. Mulvey, "s-Block Metal Inverse Crowns: Synthetic and Structural Synergism in Mixed Alkali Metal−Magnesium (or Zinc) Amide Chemistry, *Chem. Commun.*, 2001, (12), 1049.

[196] S. E. Baillie, W. Clegg, P. Garca-Álvarez, E. Hevia, A. R. Kennedy, J. Klett and L. Russo, "Synthesis, Structural Elucidation, and Diffusion-Ordered NMR Studies of Homoleptic Alkyllithium Magnesiates: Donor-Controlled Structural Variations in Mixed-Metal Chemistry", *Organometallics*, 2012, **31** (14), 5131.